THIS FILE IS MADE AVAILABLE THROUGH THE DECLASSIFICATION EFFORTS AND RESEARCH OF:

THE BLACK VAULT

THE BLACK VAULT IS THE LARGEST ONLINE FREEDOM OF INFORMATION ACT / GOVERNMENT RECORD CLEARING HOUSE IN THE WORLD. THE RESEARCH EFFORTS HERE ARE RESPONSIBLE FOR THE DECLASSIFICATION OF THOUSANDS OF DOCUMENTS THROUGHOUT THE U.S. GOVERNMENT, AND ALL CAN BE DOWNLOADED BY VISITING:

HTTP://WWW.BLACKVAULT.COM

YOU ARE ENCOURAGED TO FORWARD THIS DOCUMENT TO YOUR FRIENDS, BUT PLEASE KEEP THIS IDENTIFYING IMAGE AT THE TOP OF THE .PDF SO OTHERS CAN DOWNLOAD MORE!

UNCLASSIFIED

AD NUMBER
AD323598
CLASSIFICATION CHANGES
TO: **UNCLASSIFIED**
FROM: **CONFIDENTIAL**
LIMITATION CHANGES
TO: **Approved for public release; distribution is unlimited.**
FROM: **Distribution authorized to U.S. Gov't. agencies and their contractors; Administrative/Operational Use; 15 MAY 1961. Other requests shall be referred to Army Dugway Proving Ground, UT 84022.**
AUTHORITY
OSD/WHS ltr dtd 1 Aug 2013; OSD/WHS ltr dtd 1 Aug 2013

THIS PAGE IS UNCLASSIFIED

#12

Page determined to be Unclassified
Reviewed Chief, RDD, WHS
IAW EO 13526, Section 3.5
Date: JUL 19 2013

~~AD- 323898~~

SECURITY REMARKING REQUIREMENTS

DOD 5200.1-R~~A~~ DEC 78

REVIEW ON 28 MAY 81

Office of the Secretary of Defense 5U.S.C.§552
Chief, RDD, ESD, WHS
Date: 24 JUL Authority: EO 13526
Declassify: X Deny in Full: _____
Declassify in Part: _____
Reason: _____
MDR: 12-M-3155

R-1

12-M-3155

~~CONFIDENTIAL~~

AD 323 598

Reproduced
by the

ARMED SERVICES TECHNICAL INFORMATION AGENCY
ARLINGTON HALL STATION
ARLINGTON 12, VIRGINIA

DECLASSIFIED IN FULL
Authority: EO 13526
Chief, Records & Declass Div, WHS
Date: JUL 19 2013

~~CONFIDENTIAL~~

NOTICE: When government or other drawings, specifications or other data are used for any purpose other than in connection with a definitely related government procurement operation, the U. S. Government thereby incurs no responsibility, nor any obligation whatsoever; and the fact that the Government may have formulated, furnished, or in any way supplied the said drawings, specifications, or other data is not to be regarded by implication or otherwise as in any manner licensing the holder or any other person or corporation, or conveying any rights or permission to manufacture, use or sell any patented invention that may in any way be related thereto.

Page determined to be Unclassified
Reviewed Chief, RDD, WHS
IAW EO 13526, Section 3.5
Date: JUL 19 2013

CONFIDENTIAL

CATALOGED BY ASTIA
AS AD No. 323598

MECHANICAL DIVISION

General Mills

DECLASSIFIED IN FULL
Authority: EO 13526
Chief, Records & Declass Div, WHS
Date: JUL 19 2013

TO WIDER WORLDS — THROUGH MISSILE RESEARCH • CREATIVE ENGINEERING • PRECISION MANUFACTURING

CONFIDENTIAL

[redacted]

This document consists of 95 pages and is number 46 of 46 copies, series A, and the following — attachments.

Mechanical Division of
GENERAL MILLS, INC.
Research Department
2003 East Hennepin Avenue
Minneapolis 13, Minnesota

355900

THIRD QUARTERLY PROGRESS REPORT ON DISSEMINATION OF SOLID AND LIQUID BW AGENTS

(Unclassified Title)

XEROX

ASTIA
RECEIVED
JUN 13 1961
TIPDR A

For Period: 4 December, 1960 - 4 March, 1961

Contract No. DA-18-064-CML-2745

Prepared for

U. S. Army Biological Warfare Laboratories
Fort Detrick
Frederick, Maryland

[redacted]

Submitted by: GR Whitnah
G. R. Whitnah
Project Manager

Approved by: GR Whitnah for
S. P. Jones, Manager
Materials & Mechanics Research

Report No. 2200
Project No. 82408
Date: May 15, 1961

[redacted]

[redacted]

DECLASSIFIED IN FULL
Authority: EO 13526
Chief, Records & Declass Div, WHS
Date: JUL 10 2013

CONFIDENTIAL

ABSTRACT

This Third Quarterly Progress Report covers research on dissemination of solid and liquid BW agents. The objective toward which this research is directed is the development of weapon systems for line-source dissemination from high speed low-flying manned and unmanned aircraft.

Progress is reported on an experimental study of the effect of exposure to heated air streams on the viability of Sm aerosols.

Results from experiments on the characteristics of powders are presented. These include investigations of frictional forces between powders and channel walls and dynamic angle of repose of Sm powder.

Theoretical studies of load transmission in particulate materials are presented and several specific cases of force transmission are analyzed. Experimental investigations, conducted to explore our earlier theoretical results, are also covered.

The properties of slurries, as determined in our laboratory investigations, which include the thermal properties of egg slurry samples, are reported. Investigations of the properties of slurries of Sm in a fluorochemical liquid are presented.

Progress is reported on the wind tunnel investigations of the use of slip stream energy to deagglomerate finely divided solid materials. Experimental results on the performance of a high velocity sampling probe are also given.

The results of an analysis of the influence of the effective agent filling density on the aerodynamic drag of solid agent disseminating stores is presented.

DECLASSIFIED IN FULL
Authority: EO 13526
Chief, Records & Declass Div, WHS
Date: JUL 19 2013

CONFIDENTIAL

Systems analysis on BW dissemination systems is discussed, and the approach to be used in future studies is described.

The scope of two studies concerned with selection of a configuration for the liquid agent disseminating store is outlined.

DECLASSIFIED IN FULL
Authority: EO 13526
Chief, Records & Declass Div, WHS
Date: JUL 19 2013

FOREWORD

Members of Research and Engineering Staffs who have participated in directing and conducting the investigations and preparing the discussions presented in this report include Mr. S. P. Jones, Jr., Mr. C. Whitnah, Mr. A. Anderson, Dr. J. Baumstark, Dr. J. Park, Mr. W. L. Torgeson, Mr. J. Nash, Mr. J. Upton, Mr. C. Hagberg, Mr. P. Stroom, Mr. G. Morfitt, Mr. L. Graf, Mr. R. Griffith, Mr. I. Hall, Mr. J. Pilney, Mr. R. Dahlberg and Mr. J. Ungs.

Page determined to be Unclassified
Reviewed Chief, RDD, WHS
IAW EO 13526, Section 3.5
Date: JUL 19 2013

TABLE OF CONTENTS

Section		Page
Abstract		ii
Foreword		iv
1.	INTRODUCTION	1
2.	STUDY OF THE EFFECT OF EXPOSURE TO HEATED AIR STREAMS ON THE VIABILITY OF Sm AEROSOLS	2
3.	EXPERIMENTS ON THE CHARACTERISTICS OF POWDERS	5
3.1	Frictional Forces Between Powders and Channel Walls	5
3.1.1	Theory of Spencer, Gilmore and Wiley	5
3.1.2	Experimental Technique	7
3.1.3	Experimental Results	9
3.2	Dynamic Angle of Repose of Sm Powder	16
4.	THEORETICAL STUDIES OF LOAD TRANSMISSIONS IN PARTICULATE MATERIALS	22
4.1	Bulk Physical Properties of Powders Relating to Static Load Transmission and Yield Strength Characteristics	23
4.2	Theoretical Analysis of Load Transmission and Shear Failure in Particulate Beds	30
4.2.1	Analysis of the Load Distribution in a Powder Due to its Weight	30
4.2.2	Analysis of Critical Loads for Penetration of a Bed of Powder	31
5.	EXPERIMENTAL STUDIES OF LOAD TRANSMISSION IN SPECIFIC ARRAYS	39
6.	INVESTIGATIONS OF PROPERTIES OF SLURRIES	44
6.1	Properties of Egg Slurries	44
6.1.1	Specific Heat of Egg Slurries	44

DECLASSIFIED IN FULL
Authority: EO 13526
Chief, Records & Declass Div, WHS
Date: JUL 19 2013

TABLE OF CONTENTS (Continued)

Section		Page
6.1.2	Thermal Conductivity of Egg Slurries	56
6.2	Rheological Behavior of Sm Slurries	62
6.2.1	Apparatus and Experimental Behavior	62
6.2.2	Experimental Results	65
7.	DISSEMINATION AND DEAGGLOMERATION STUDIES	76
7.1	Experiments With the Isokinetic Sampling Probe	76
7.2	Modification of the Wind Tunnel Apparatus to Permit Dissemination Experiments With Sm Simulant	83
8.	STUDY OF THE INFLUENCE OF EFFECTIVE FILLING DENSITY ON THE AERODYNAMIC DRAG OF SOLID AGENT EXTERNAL STORES	85
9.	SYSTEM STUDY	88
10.	WORK ON LIQUID AGENT DISSEMINATING STORE	90
10.1	Work Statement - Study at North American Aviation, Inc.	90
10.2	Work Statement - Study at Fairchild Aircraft and Missiles Division	91
11.	SUMMARY AND CONCLUSIONS	93

DECLASSIFIED IN FULL
Authority: EO 13526
Chief, Records & Declass Div, WHS
Date: JUL 19 2013

LIST OF ILLUSTRATIONS

Figure		Page
2.1	Thermal Exposure System for Sm Aerosols	4
3.1.1	Piston-Cylinder Experimental Set-up	5
3.1.2	Apparatus for Measuring Frictional Force Between a Powder and Cylinder Wall	8
3.1.3	Piston-Cylinder Data on Talc Plotted as F_A/F_R Versus L_o/D	11
3.1.4	Piston-Cylinder Data on Talc Plotted as F_A/F_R Versus L/D	12
3.1.5	Column of Powder	13
3.2.1	Shape of Sm Powder Pile Obtained in Dynamic Angle of Repose Experiments	18
3.2.2	Dynamic Angle of Repose as a Function of Relative Humidity of Surrounding Air for Sm Powder	20
3.2.3	Dynamic Angle of Repose as a Function of Moisture Content of Sm Powder	21
4.1.1	Shear Strength Characteristics	25
4.1.2	Resolution of Stresses	25
4.1.3	Representation of Stresses by Means of Stress Circle	25
4.1.4	Triaxial Test Fixture	29
4.1.5	Determination of Shear Strength Characteristic from Triaxial Tests	29
4.2.1	Slip Line in Uniform Unstressed Particle Bed	32
4.2.2	Penetration of the Surface of a Particle Bed	33
4.2.3	Shear Surface and Load Distribution for Penetration of Surface of Particle Bed in Illustrative Example	35
5.1	Symmetric Hexagonal Arrangements of Disks in a Two-Dimensional Bed	40

DECLASSIFIED IN FULL
Authority: EO 13526
Chief, Records & Declass Div, WHS
Date: JUL 19 2013

LIST OF ILLUSTRATIONS (Continued)

Figure		Page
5.2	Two Illustrative Views of Shot Movement in a Two-Dimensional Bed	42.
6.1.1	Calorimeter for Specific Heat Determinations	46
6.1.2	Heating Circuit for Calorimeter	48
6.1.3	Temperature Response Curve During Specific Heat Determinations	50
6.1.4	Specific Heat Vs. Temperature for W.E.S. #1	52
6.1.5	Specific Heat Vs. Temperature for W.E.S. #2	53
6.1.6	Specific Heat Vs. Temperature for W.E.S. #3	54
6.1.7	Specific Heat Vs. Temperature for W.E.S. #4	55
6.1.8	Cross Section of Thermal Conductivity Cell	58
6.1.9	Calibration Curve for 6 Copper-Constantan Thermocouples	61
6.2.1	Schematic Diagram of the Rotating Coaxial Cylinder Viscometer	63
6.2.2	Consistency Curves for Sm Slurries	66
6.2.3	Applicability of Relationship $\dot{e} = \frac{(\tau - f)^n}{\eta^*}$ to Sm Slurries	71
6.2.4	Apparent Viscosity Versus Rate of Shear	73
6.2.5	Applicability of Relationship $\eta = k\dot{e}^{\frac{1}{n}}$ to Sm Slurries	74
7.1.1	Particle Size Frequency Distribution for Mistron #18 Talc Before Dissemination and After Sampling at Isokinetic Conditions.	78
7.1.2	Particle Size Frequency Distribution for Mistron #18 Talc Before Dissemination and After Sampling at Non-Isokinetic (50% Flow) Conditions	80
7.1.3	Particle Size Frequency Distribution for Mistron #25 Talc Before Dissemination and After Sampling at Isokinetic Conditions	81
7.1.4	Particle Size Frequency Distribution for Mistron #25 Talc Before Dissemination and After Sampling at Non-Isokinetic (50% Flow) Conditions	82
8.1	Aerodynamic Drag Versus Effective Filling Density for Solid Agent Stores	86

DECLASSIFIED IN FULL
Authority: EO 13526
Chief, Records & Declass Div, WHS
Date: JUL 19 2013

LIST OF TABLES

Table		Page
3.I	Piston-Cylinder Results with Talc Powder in a Glass Cylinder	10
3.II	Dynamic Angle of Repose for Sm Powder	19
6.I	Effect of Temperature and Solids Concentration on the Apparent Viscosity of Sm Slurries	68

DECLASSIFIED IN FULL
Authority: EO 13526
Chief, Records & Declass Div, WHS
Date: JUL 19 2013

1. INTRODUCTION

This is the Third Quarterly Progress Report on the program of research on dissemination of solid and liquid BW agents being conducted under Contract No. DA-18-064-CML-2745. This research is directed toward the development of disseminating stores to be carried externally on the delivery aircraft.

During this reporting period, Phase I of this program was completed and the Phase II work was initiated. The objective of Phase II, in the field of solid agent dissemination, is to advance the state of knowledge in the areas of characterization, delivery, metering, dissemination and deagglomeration of the finely divided solid materials to a point where design of a research prototype is feasible. In the field of liquid agent dissemination, the Phase II objectives include completion of the design requirements for an external store, design of the research prototype unit and manufacture of one unit in preparation for future field experiments. The beginning of Phase II is scheduled for 1 November 1961.

This report presents progress on several studies which are being conducted to reach these goals. Because of the nature of this program, research studies in many separate fields are required. The introductory statements in each section of the report relate the topics discussed to the overall project.

DECLASSIFIED IN FULL
Authority: EO 13526
Chief, Records & Declass Div, WHS
Date: JUL 19 2013

2. STUDY OF THE EFFECT OF EXPOSURE TO HEATED AIR STREAMS ON THE VIABILITY OF Sm AEROSOLS

In the process of dissemination of BW agents from jet aircraft, the possibility of the aerosol mixing to some degree with the hot gases from the engine has been recognized. Mixing with the plume is most likely if the external BW disseminating store is mounted close to an engine. In order to determine the importance of avoiding this mixing, data are required on the loss of viability produced.

It is known that both the temperature and the exposure time influence this process. However, previous research on the viability losses produced by exposure of aerosols to elevated temperatures has been in evaluating (1) the performance of incinerators and (2) the biological decay of an aerosol over time periods of minutes to hours at slightly elevated temperature. Neither of these cases are sufficiently close to the jet plume problem to provide useful data.

An experimental study was therefore initiated by General Mills, Inc. to evaluate viability losses produced by mixing Sm aerosols with heated air at temperatures from 75° to 200° C with exposure durations of one to two seconds. These conditions are believed to be of greatestinterest in connection with the jet plume problem.

A comparative approach was selected in which samples are collected in two All-Glass Impingers concurrently, one sample from the heated aerosol stream and the other from an unheated control stream.

DECLASSIFIED IN FULL
Authority: EO 13526
Chief, Records & Declass Div, WHS
Date: JUL 19 2019

In the initial experiments, a heated air stream was injected into one of the aerosol streams, while an equal quantity of room-temperature air was injected into the control stream. The first results showed very substantial effects. Approximately 80 percent of the aerosol was killed when the average temperature of the heated stream was 80° C, and the duration of the exposure was 1.2 seconds. In light of the short exposure time, this degree of loss was considered quite high. However, it was observed that this method of heating the aerosol (by injection of hot air) resulted in a local hot region in which the aerosol was exposed for a very small fraction of the total time to a temperature of approximately 175° C. For this reason the design of the apparatus was modified to provide uniform temperature along the exposure path before additional data were taken.

The final apparatus is shown in Figure 2.1. The aerosol is generated with a nebulizer and introduced into a glass carboy. The aerosol stream from this carboy is divided into two branches and injected into the heated and unheated air streams.

Several openings have been provided so that the effect of varying exposure time can be studied. The instrumentation includes provisions for controlling the electrical input to the heater and also measurement of the temperature of the mixed streams at several locations.

Experiments with the apparatus shown in Figure 2.1 will be conducted during the fourth quarterly reporting period. It is anticipated that data will be available for the next technical report, covering a range of temperatures up to 200° C.

Page determined to be Unclassified
Reviewed Chief, RDD, WHS
IAW EO 13526, Section 3.5
Date: JUL 19 2013

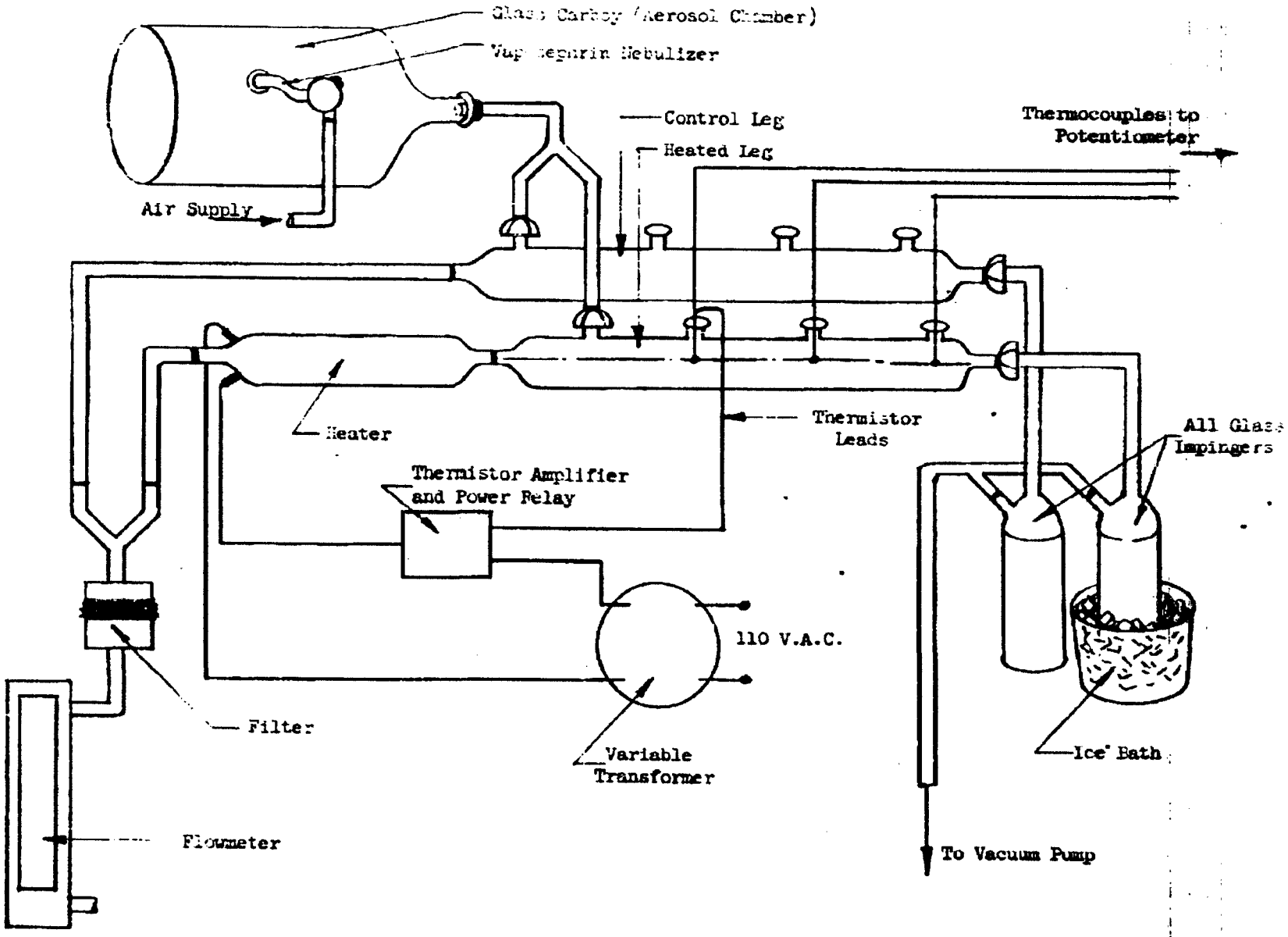

FIGURE 2.1 THERMAL EXPOSURE SYSTEM FOR Sm AEROSOLS (SHOWN WITH INSULATION REMOVED)

Page determined to be Unclassified
Reviewed Chief, RDD, WHS
IAW EO 13526, Section 3.5
Date: JUL 19 2013

3. EXPERIMENTS ON THE CHARACTERISTICS OF POWDERS

3.1 Frictional Forces Between Powders and Channel Walls

One of the main feeding techniques under consideration in this dissemination study is the piston feeder. A knowledge of frictional forces between powders and channel walls is vital to the evaluation of the feasibility of this approach.

Spencer, Gilmore and Wiley[3.1.1] devised a technique for studying forces between granular polymers and channel walls. This technique has been investigated during this reporting period using talc powder. The results indicate that a modification to this approach is required when studying very fine powders. An alternate approach has been developed.

3.1.1 Theory of Spencer, Gilmore and Wiley

Spencer, Gilmore and Wiley's theoretical derivation considers a plug of powder confined in a cylinder with a piston at each end as illustrated in Figure 3.1.1.

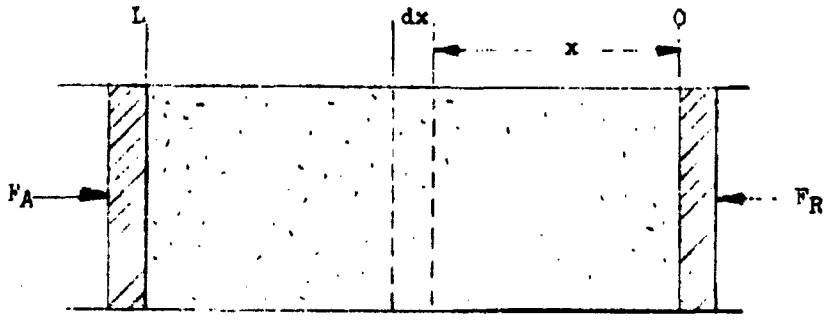

Figure 3.1.1. Piston-Cylinder Experimental Set-Up

3.1.1 Spencer, R. S., Gilmore, G. D., and Wiley, R. M., Behavior of Granulated Polymers under Pressure, J. Appl. Phys. 21, 527-531 (1950).

Page determined to be Unclassified
Reviewed Chief, RDD, WHS
IAW EO 13526, Section 3.5
Date: JUL 19 2013

F_A is the force necessary to initiate movement of the plug and F_R is the resistive force. The frictional force per particle at the wall is μf, where μ is the coefficient of friction between particle and wall and f is the contact force between particles (assumed to be the same in all directions at a point and normal to the walls and ends). The total frictional force acting on an element of powder of thickness dx is μf n $(2\pi R)$ dx, where n is the number of particles per unit area in contact with the wall at x. Let F be the total force normal to a cross section (in the direction of the cylinder axis) at x. Then the change in F in going from x to x + dx is $dF = (\pi R^2)\, n_o\, df$, where n_o is the number of particles per unit area in contact with a cross section and df is the incremental change in contact force per particle. If it is assumed that, in a given state of compaction, the only frictional forces arising are those due to particle-wall contacts, then for equilibrium conditions the two expressions can be equated:

$$(\pi R^2)\, n_o\, df = \mu f\, n(2\pi R)\, dx \qquad (3.1)$$

Rearranging and integrating between the proper limits, the following expression is obtained:

$$\int_{F_R}^{F_A} \frac{df}{f} = \frac{2\mu}{n_o R} \int_o^L n\, dx \qquad (3.2)$$

or

$$\ln F_A/F_R = \frac{2\mu}{n_o R} \int_o^L n\, dx \qquad (3.3)$$

Page determined to be Unclassified
Reviewed Chief, RDD, WHS
IAW EO 13526, Section 3.5
Date: JUL 19 2013

To evaluate the integral on the right hand side, it is assumed that the number of wall contacts is constant (independent of degree of compaction) and that $n = n_o$ prior to compaction. Equating the number of wall contacts prior to compaction to those after compaction, the following relation is obtained:

$$n_o(2\pi R)\, L_o = \int_o^L n(2\pi R)\, dx \tag{3.4}$$

or

$$n_o\, L_o = \int_o^L n\, dx \tag{3.5}$$

where: L_o is the length of the plug of powder prior to compaction;

L is the length of the plug at any given state of compaction. Substituting Equation (3.5) into Equation (3.3), the final expression is obtained:

$$\frac{F_A}{F_R} = \epsilon^{-\frac{2\mu L_o}{R}} \tag{3.6}$$

or

$$\frac{F_A}{F_R} = \epsilon^{-\frac{4\mu L_o}{D}} \tag{3.7}$$

3.1.2 Experimental Technique

The apparatus used to study frictional forces between powders and various cylinder materials is illustrated in Figure 3.1.2.

Page determined to be Unclassified
Reviewed Chief, RDD, WHS
IAW EO 13526, Section 3.5
Date: JUL 19 2013

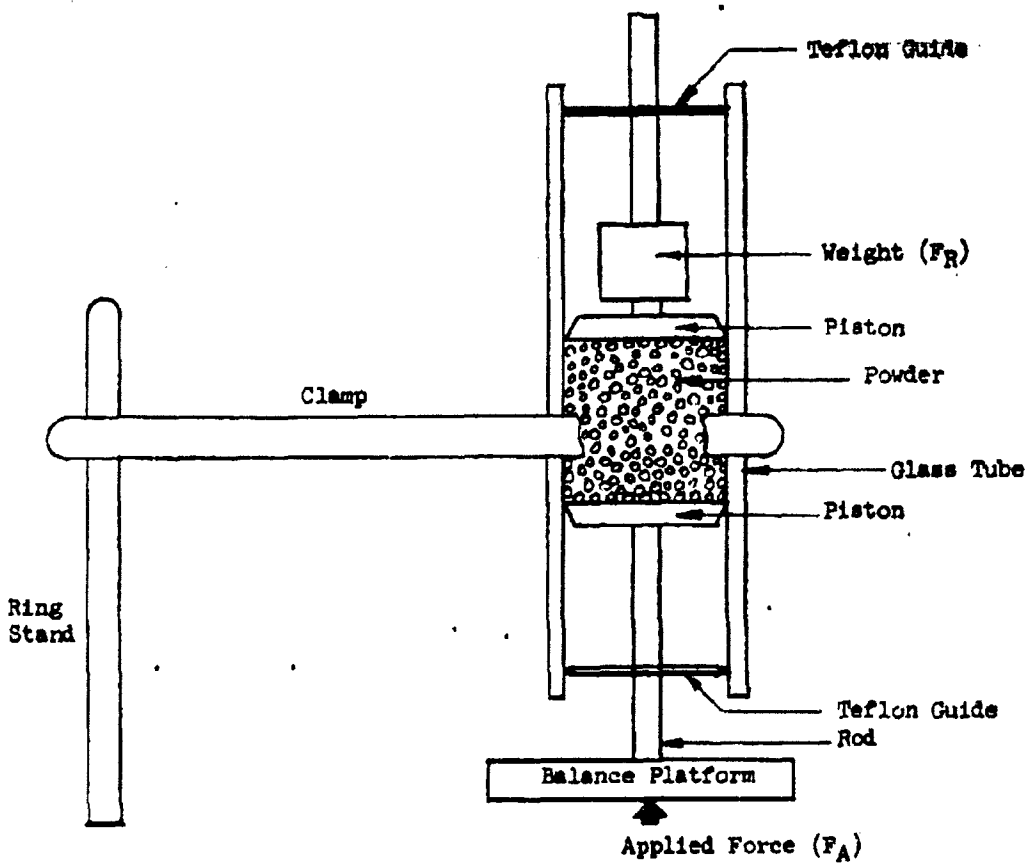

Figure 3.1.2 Apparatus for Measuring Frictional Force Between a Powder and Cylinder Wall

The procedure is to clamp the cylindrical tube (a precision bore glass tube with an I. D. of 1.185 inches was used in this study) in the upright position with the rod of the lower piston resting on the platform of a triple beam balance. The powder is then sifted through a screen and funnel into the tube. The powder is leveled off and the length of the powder column prior to compaction (L_o) is measured. The top piston and weight are carefully lowered into position. The weights on the triple beam balance are adjusted to the point where the plug of

Page determined to be Unclassified
Reviewed Chief, RDD, WHS
IAW EO 13526, Section 3.5
Date: JUL 19 2013

powder just begins to move, and this weight is recorded. This procedure is repeated using different amounts of powder and different resisting forces.

3.1.3 Experimental Results

The results of tests performed with talc powder in a glass cylinder of fixed diameter are presented in Table 3.I. The force necessary to initiate movement of the plug (F_A) was determined for a given uncompacted plug length (L_o) when subjected to four different resistive forces (F_R). The ratios L_o/D and F_A/F_R are tabulated. In addition, the length of the plug after compaction (L) and the ratio L/D also are included in the table.

If the theory of Spencer et al. is valid, according to Equation (3.7) it should be possible to plot the logarithm of the ratio F_A/F_R as a function of the ratio L_o/D and obtain a straight line. Such a plot has been made and is presented in Figure 3.1.3. It is apparent from this figure that log F_A/F_R versus L_o/D does yield a straight line for a given value of F_R. However, as F_R is varied, a different line with a different slope is obtained for each value of F_R. In general, the slope of the line becomes less as F_R is increased.

Upon finding this result, it was decided to plot log F_A/F_R versus L/D, where L is the length of the powder plug after compaction, to see if the data would present a more unified picture in this form. This plot is shown in Figure 3.1.4 where it is apparent that all of the experimental points fall very close to a single straight line even though F_R was varied by a factor of five.

Page determined to be Unclassified
Reviewed Chief, RDD, WHS
IAW EO 13526, Section 3.5
Date: JUL 19 2013

Table 3.I. Piston-Cylinder Results with Talc Powder in a Glass Cylinder

L_o (in)	$\frac{L_o}{D}$	L (in)	$\frac{L}{D}$	F_R (gm)	F_A (gm)	$\frac{F_A}{F_R}$
0.92	0.78	0.58	0.49	35.0	60	1.71
0.92	0.78	0.53	0.45	84.2	135	1.60
0.92	0.78	0.51	0.43	134.1	201	1.50
0.92	0.78	0.48	0.41	183.3	276	1.51
2.22	1.87	1.31	1.11	35.0	125	3.58
2.22	1.87	1.14	0.96	84.2	243	2.88
2.22	1.87	1.06	0.89	134.1	362	2.70
2.22	1.87	0.99	0.84	183.3	496	2.70
2.94	2.48	1.69	1.43	35.0	166	4.75
2.94	2.48	1.47	1.24	84.2	320	3.80
2.94	2.48	1.39	1.17	134.1	505	3.77
2.94	2.48	1.31	1.11	183.3	656	3.58
3.88	3.27	2.15	1.81	35.0	261	7.47
3.88	3.27	1.87	1.58	84.2	491	5.83
3.88	3.27	1.78	1.50	134.1	760	5.67
3.88	3.27	1.69	1.48	183.3	971	5.30

Page determined to be Unclassified
Reviewed Chief, RDD, WHS
IAW EO 13526, Section 3.5
Date: JUL 19 2013

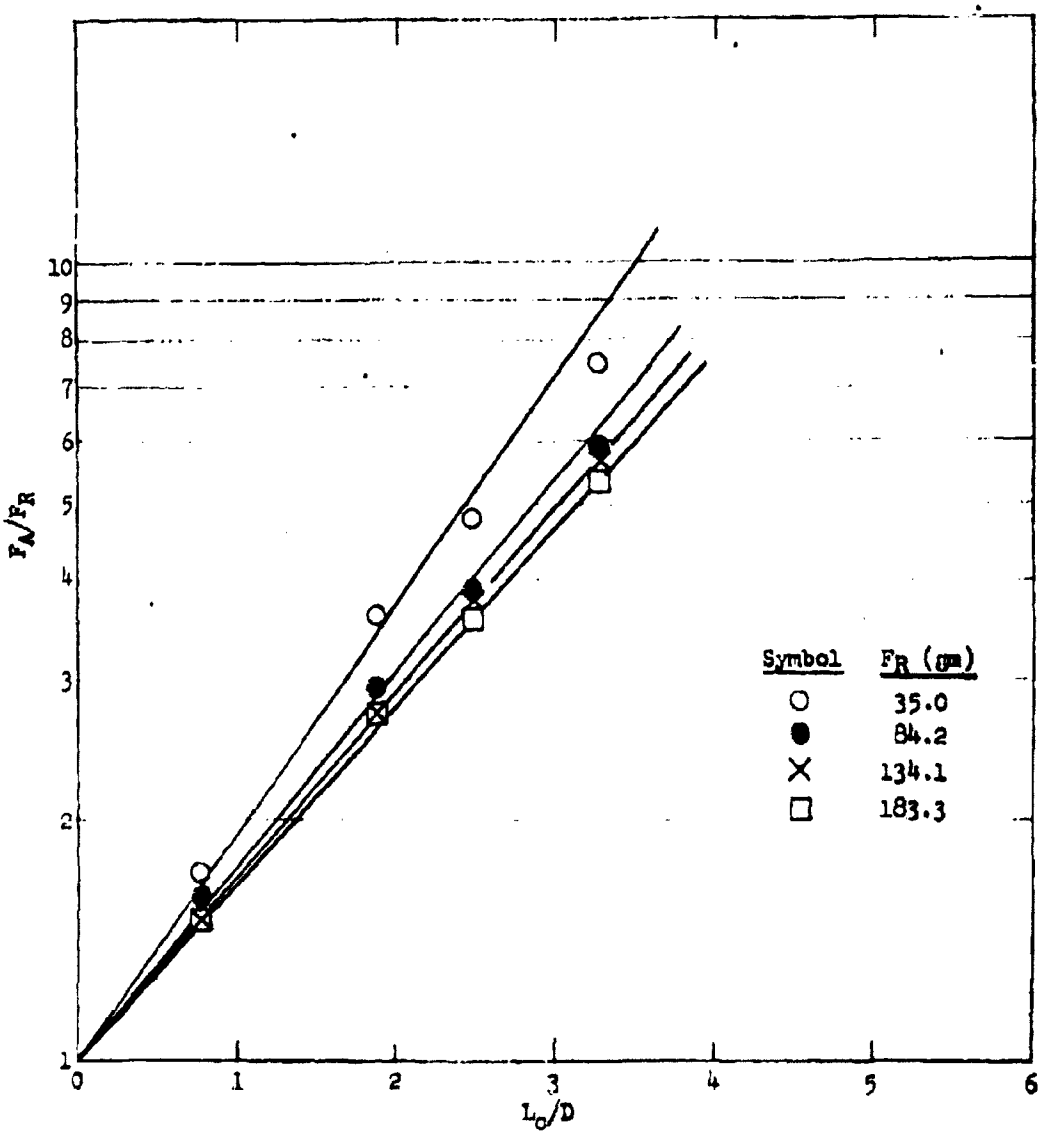

FIGURE 3.1.3 PISTON-CYLINDER DATA ON TALC PLOTTED AS F_A/F_R VERSUS L_o/D

Page determined to be Unclassified
Reviewed Chief, RDD, WHS
IAW EO 13526, Section 3.5
Date: JUL 19 2013

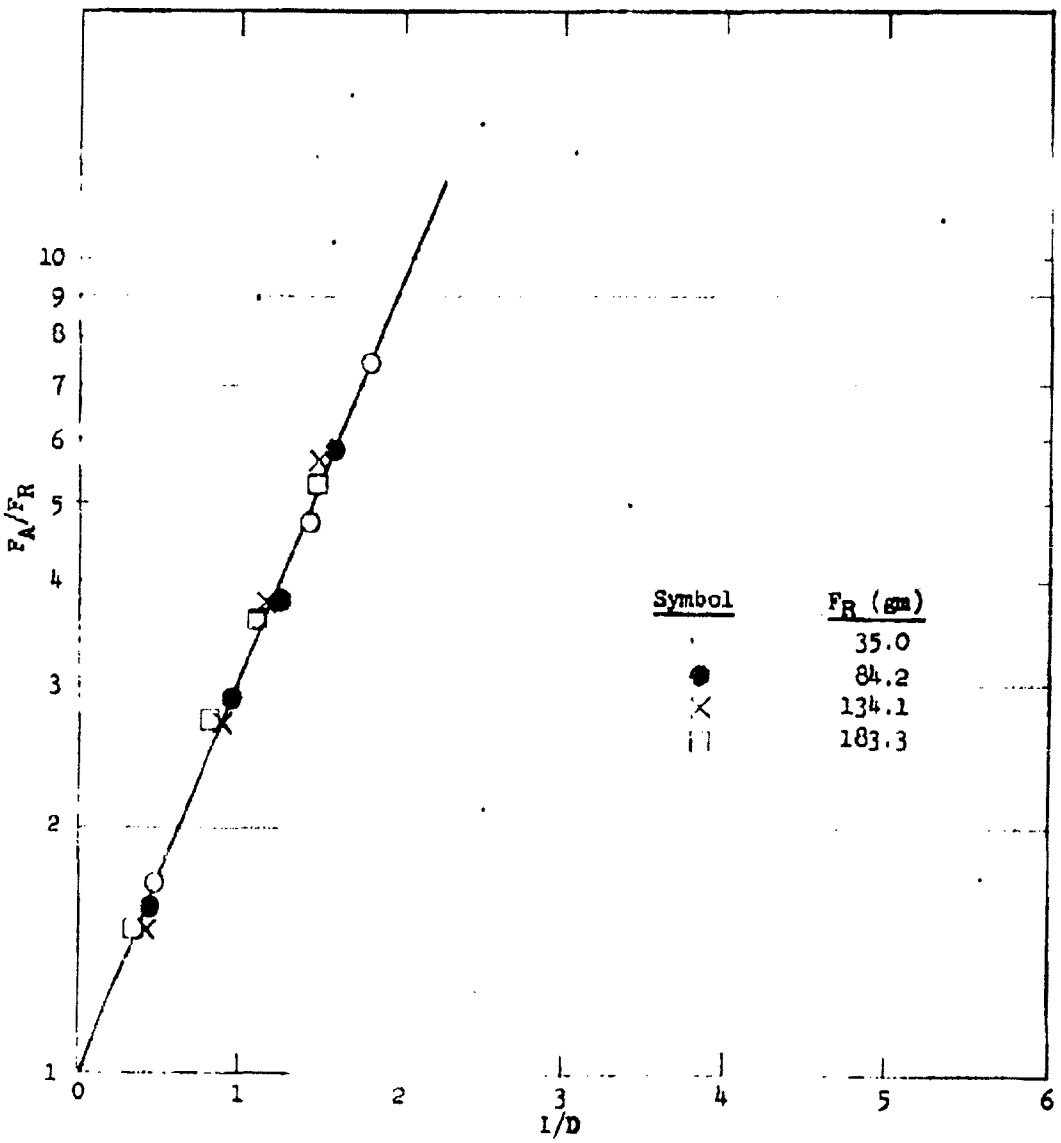

FIGURE 3.1.4 PISTON-CYLINDER DATA ON TALC PLOTTED AS F_A/F_R VERSUS L/D

Page determined to be Unclassified
Reviewed Chief, RDD, WHS
IAW EO 13526, Section 3.5
Date: JUL 19 2013

In view of this result, a new approach was sought in attempting to analyze this type of experiment. It was found that an analysis similar to the one applied to tensile strength measurements on compacted powders conducted under Contract DA-18-108-405-CML-824 for CRDL appeared to apply quite well to the present type of experiment. In the analysis, a column of powder confined in a cylinder is considered from a somewhat different approach than that taken by Spencer et al. as will be shown in the following discussion.

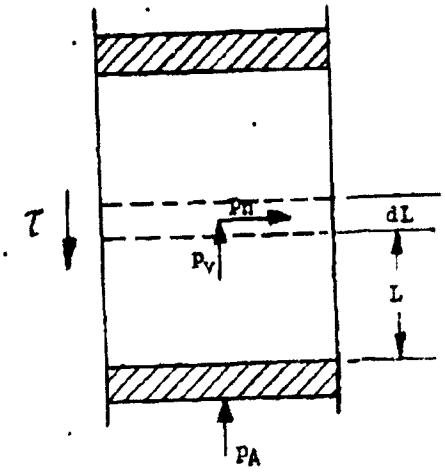

Figure 3.1.5. Column of Powder

Consider a cylinder full of powder with a piston at each end as depicted schematically in Figure 3.1.5. Pressure p_A is applied in the upward direction by the bottom piston. The top piston may be considered fixed in this analysis. An elemental layer of powder with thickness dL

Page determined to be Unclassified
Reviewed Chief, RDD, WHS
IAW EO 13526, Section 3.5
Date: JUL 19 2013

is located a distance L from the bottom piston. Assume that at a point the pressure acting in the horizontal direction, p_h, is proportional to the pressure acting in the vertical direction, p_v, and that the latter is uniform across a cross-section. Then:

$$p_h = C_1 p_v \tag{3.8}$$

where C_1 is a constant.

The frictional force per unit area acting on the cylinder wall is:

$$\tau = \mu p_h \tag{3.9}$$

where μ is the coefficient of friction between the powder and the cylinder wall. The equilibrium condition of the elemental layer of powder just prior to movement is.

$$-\pi R^2 \, dp_v = 2\pi R \tau \, dL \tag{3.10}$$

Substituting Equations (3.8) and (3.9) into Equation (3.10), we obtain:

$$-\pi R^2 \, dp_v = 2\pi R \mu C_1 p_v \, dL \tag{3.11}$$

Rearranging Equation (3.11), we obtain:

$$\frac{dp_v}{p_v} = -\frac{2\mu C_1}{R} dL \tag{3.12}$$

Equation (3.12) can then be integrated between the proper limits as follows:

$$\int_{p_A}^{p_R} \frac{dp_v}{p_v} = -\int_0^L \frac{2\mu C_1}{R} dL \tag{3.13}$$

Page determined to be Unclassified
Reviewed Chief, RDD, WHS
IAW EO 13526, Section 3.5
Date: JUL 19 2013

where p_R is the pressure exerted by the powder on the top cylinder. p_R may also be thought of as the resistive pressure exerted by the top cylinder on the powder.

The result of the integration is:

$$\ln p_A/p_R = \frac{2\mu C_1}{R} L \tag{3.14}$$

or

$$p_A/p_R = e^{\frac{2\mu C_1}{R} L} \tag{3.15}$$

The cross-sectional area A of both pistons is the same; therefore, the force applied to the bottom piston is $F_A = p_A A$ and that exerted by the powder on the top piston is $F_R = p_R A$. Equation (3 15) may then be written in the following manner:

$$F_A/F_R = e^{\frac{2\mu C_1}{R} L} \tag{3 16}$$

or

$$F_A/F_R = e^{\frac{4\mu C_1}{D} L} \tag{3.17}$$

Equation (3.17) is identical to Equation (3.7) with the exception that $C_1 L$ appears in the exponent in place of L_o.

On the basis of this analysis, it is possible to calculate the value of the term $C_1\mu$ from the slope of the straight line obtained in Figure 3 1.4 For talc, the value of the term $C_1\mu$ is 0.279. The exact value of the coefficient of friction, μ, cannot be calculated because C_1, the proportionality constant between the horizontal and vertical pressure in the powder column, is not known. If it is assumed that the horizontal and vertical pressures are approximately equal, then C_1 is near unity and the coefficient of friction is roughly 0.3.

Page determined to be Unclassified
Reviewed Chief, RDD, WHS
IAW EO 13526, Section 3.5
Date: JUL 19 2013

While only one powder (talc) has been tested thus far, the data indicate that Equation (3.17) is much more suitable for representing the behavior of finely divided powders than Equation (3.7). Future plans are to perform tests on other powders including Sm with cylinders of different materials in order to examine further the applicability of this new approach.

In addition, a technique is being developed to determine the coefficient of friction of a compressed powder plug against a plane surface using a tilting table. A knowledge of the friction coefficient, μ, will permit determination of the proportionality constant, C_1, between the horizontal and vertical pressure which exists in the powder column of the piston-cylinder test. With these tools, an investigation can be made of the effect of particle size and particle size distribution on force transmission in a powder bed.

3.2 Dynamic Angle of Repose of Sm Powder

The dynamic angle of repose of a powder is generally measured by allowing the powder to flow through a funnel onto a flat horizontal surface and then measuring the angle between the horizontal and the surface of the conical-shaped powder pile. Few investigators have been able to attach any real significance to the angle of repose other than a relative indication of how a powder flows. Wolf and von Hohenleiter[3.2.1], however, found a close correlation between the dynamic angle of repose and the angle at which a mass of powder slides off a tilting surface.

3.2.1 Wolf, E. F. and von Hohenleiter, H. L., Experimental Studies of the Flow of Coal in Chutes at Riverside Generating Station. Trans. A.S.M.E., pp 585-599 (1945)

Page determined to be Unclassified
Reviewed Chief, RDD, WHS
IAW EO 13526, Section 3.5
Date:
JUL 19 2013

Wolf and von Hohenleiter performed many tests on coal dust, measuring both dynamic angle or repose and slide angle as a function of moisture content of the powder. When they plotted either angle of repose or slide angle as a function of moisture content, they obtained curves of the same general shape, both of which indicated a maximum at about 12 percent moisture content. Upon examining the tilting surface after the powder had slid off, it was noted that a layer of powder still adhered to the surface. This observation suggests that the slide angle measurements were probably more of an indication of powder shear rather than sliding friction between the tilting surface and the powder.

A theoretical analysis of force distribution in a powder pile was presented in an earlier report on this contract[3.2.2]. The initial two-dimensional analysis assumed particles in the shape of uniform circular cylinders. From this analysis, it was concluded that the angle of repose is a direct measure of the coefficient of friction between cylinders. It was also stated that it is reasonable to assume that the angle of repose will be less than 60° for non-circular shapes.

The dynamic angle of repose of a sample of finely ground Sm was measured over a wide range of relative humidities (2.6% to 65%) at room temperature. The measurements were made inside a controlled humidity cabinet. Prior to each series of measurements at a given humidity, the powder was allowed to equilibrate at that humidity for a period of at least 16 hours. After each series of measurements at a given humidity, a sample of the powder was placed in a tared glass

---

3.2.2 Dissemination of Solid and Liquid BW Agents, General Mills, Inc. Res. Dept. Report No. 2125, First Quarterly Progress Report, Contract No. DA-18-064-CML-2745, p A-1, (Oct., 1960)

Page determined to be Unclassified
Reviewed Chief, RDD, WHS
IAW EO 13526, Section 3.5
Date: JUL 19 2013

weighing jar and removed from the cabinet for moisture content determination. Moisture content was determined by measuring the weight loss of the sample after being placed in a vacuum oven at a pressure of about 1 mm Hg and temperature of 50° C for a period of 24 hours.

When measuring the dynamic angle of repose of Sm powder, it was noted that the slope of the powder pile was not uniform but appeared as shown in Figure 3.2.1.

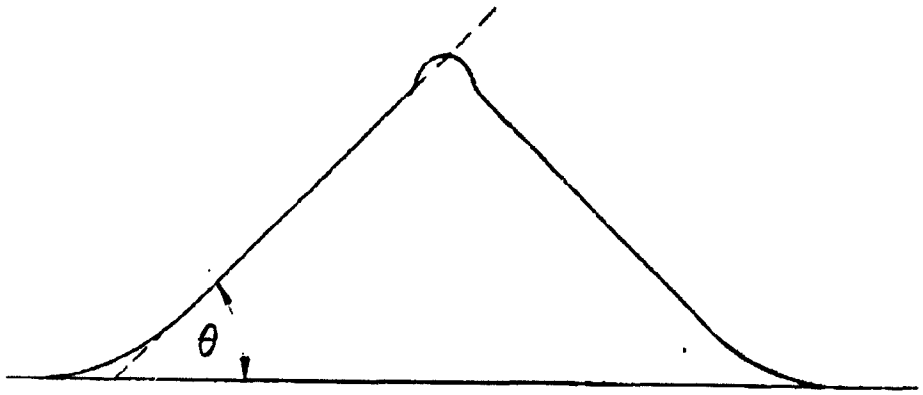

Figure 3.2.1. Shape of Sm Powder Pile Obtained in Dynamic Angle of Repose Experiments

The changing slope of the powder pile may be attributed to electrostatic charges on the particles. As the powder is sifted through the funnel, the large clumps have enough mass to overcome the electrostatic forces and fall straight downward onto the center of the pile, whereas smaller individual particles tend to be deflected outward and deposit around the periphery of the pile. This causes the slope of the powder

Page determined to be Unclassified
Reviewed Chief, RDD, WHS
IAW EO 13526, Section 3.5
Date: JUL 19 2013

pile to gradually approach zero at the base. It was noted, however, that there was generally a portion (approximately in the middle of the pile) where the slope was uniform. In the present tests, the angle of repose θ was measured along this middle portion. The results of the measurements on Sm are given in Table 3.II.

Table 3.II. Dynamic Angle of Repose for Sm Powder

Rel Humidity (%)	Moisture Content (% by weight)	Angle of Repose	Deviation
2.6	2.9	46.9°	1.6°
12	3.9	45.5°	1.5°
24	4.7	49.0°	2.0°
42	7.2	53.9°	1.4°
65	16.9	50.7°	2.7°

The data in Table 3.II are presented graphically in Figures 3.2.2 and 3.2.3. Figure 3.2.2 shows the relationship between the dynamic angle of repose and the percent relative humidity of the air inside the cabinet. Figure 3.2.3 shows the relationship between the dynamic angle of repose and the moisturecontent of the powder sample. It is seen that the angle of repose is maximum for a relative humidity of about 42% and for a moisture content between 7.2% and 16.9%.

It is planned to perform additional tests on Sm powder including the piston-cylinder tilting table and disc-lifting experiments. These investigations will be conducted at various relative humidities in an environmental chamber. An attempt will be made to correlate the present data on angle of repose with these measurements in order to determine the significant properties of Sm powder which affect the angle of repose measurements.

Page determined to be Unclassified
Reviewed Chief, RDD, WHS
IAW EO 13526, Section 3.5
Date: JUL 19 2013

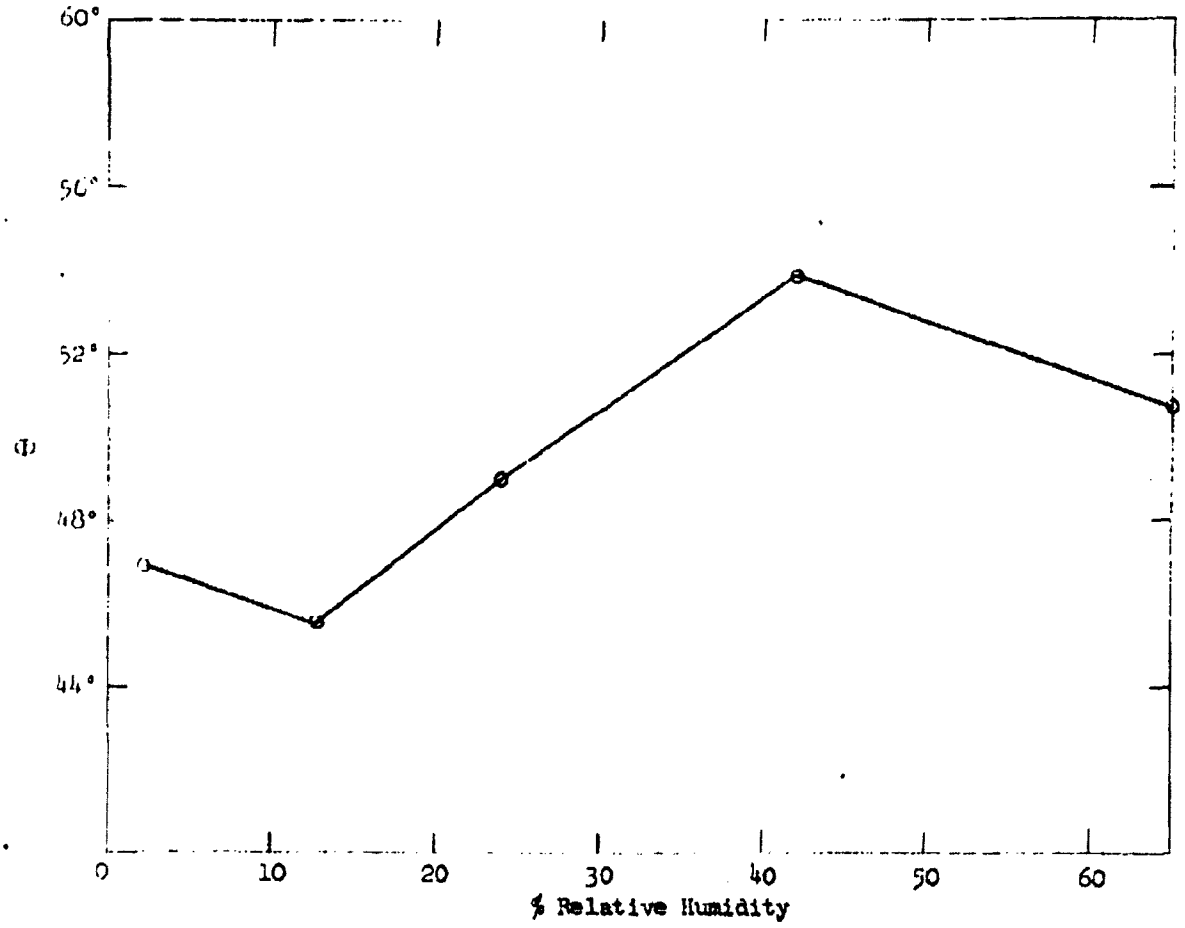

FIGURE 3.2.2 DYNAMIC ANGLE OF REPOSE (θ) AS A FUNCTION OF RELATIVE HUMIDITY OF SURROUNDING AIR FOR SM POWDER

Page determined to be Unclassified
Reviewed Chief, RDD, WHS
IAW EO 13526, Section 3.5
Date: JUL 19 2013

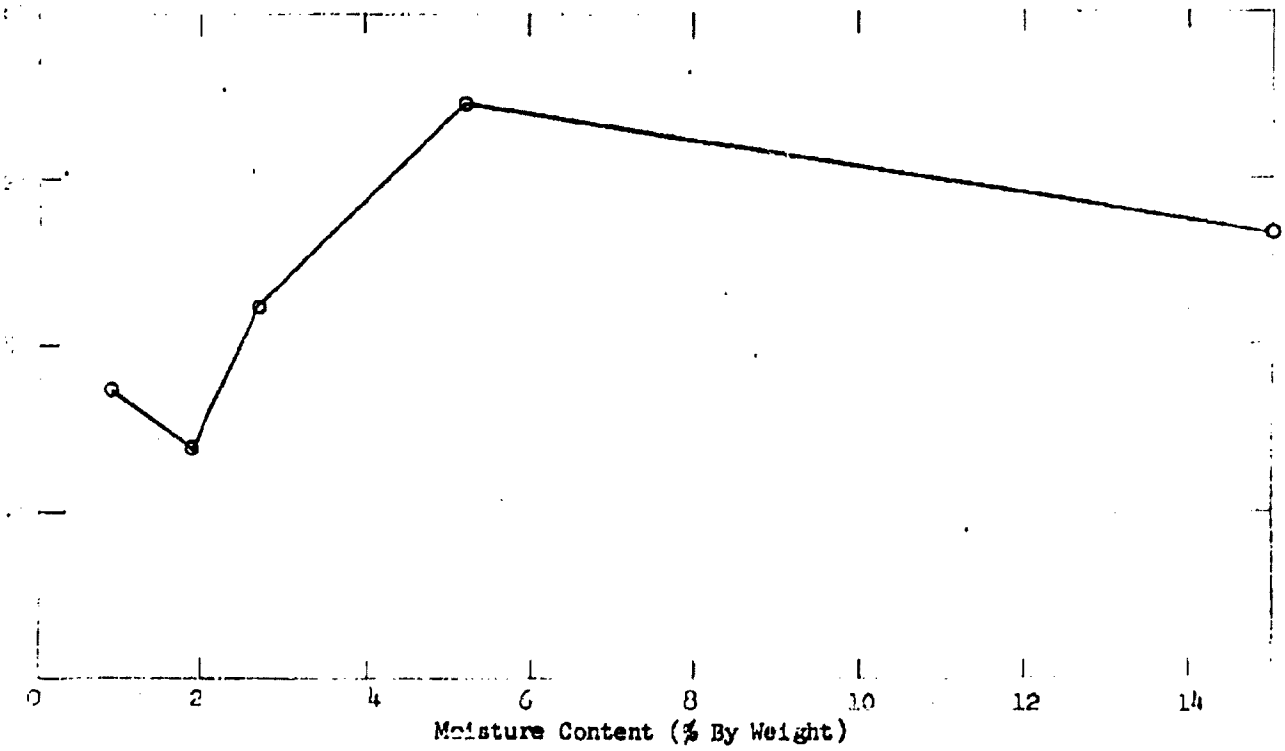

FIGURE 3.2.3 DYNAMIC ANGLE OF REPOSE (θ) AS A FUNCTION OF MOISTURE CONTENT OF SM POWDER

Page determined to be Unclassified
Reviewed Chief, RDD, WHS
IAW EO 13526, Section 3.5
Date: JUL 19 2013

4. THEORETICAL STUDIES OF LOAD TRANSMISSIONS IN PARTICULATE MATERIALS

One aspect of the current study of dry agent dissemination systems is the examination of feeding and handling characteristics of dry particulate materials. These characteristics may reasonably be expected to depend on certain bulk properties of the material such as density, compactibility and shear strength. In turn, these bulk properties are dependent upon interparticle forces and interactions among individual particles and groups of particles.

One of the goals of the present study is to determine the bulk physical properties of a particulate material which are responsible for its behavior under applied loads. On the basis of information available at the present time, it appears likely that the compactibility and shear strength characteristics of a particulate material are of primary importance in defining the static load-carrying and yield characteristics of the material.

The physical properties which govern the behavior of particulate materials may be different for different types of materials. For example, an immediate distinction can be made between materials exhibiting dilatant characteristics and compactible materials. Materials in the former category (e.g., dry sand or steel shot) appear to have well-defined shear yield characteristics over a wide range of stresses.[4.1] On the other hand, compactible materials are subject to secondary effects of compaction on shear strength which modifies and complicates their behavior.

4.1 Terzaghi, C., Theoretical Soil Mechanics, John Wiley and Sons, N. Y., (1943)

Page determined to be Unclassified
Reviewed Chief, RDD, WHS
IAW EO 13526, Section 3.5
Date: JUL 19 2013

A further classification of dilatant materials can be made on the basis of particle size. For large particles, interparticle forces will generally be small compared with the mass of individual particles. As the particle size decreases, it is clear that interparticle forces will assume relatively greater importance. As a consequence, finely divided dry materials can be expected to exhibit increased shear strength when compared to materials of the same type which are composed of large particles. Furthermore, the finely divided material will retain some shear resistance at zero compressive load, whereas the shear strength of dry particulate materials made up of large particles must vanish at zero load.

From this brief discussion it is apparent that dry powders can be separated into several categories with respect to the bulk physical properties which determine the behavior of these materials under load. Classification of materials in this way depends upon experimental studies of the various types of powders conducted under carefully controlled conditions. A promising experimental technique for measuring the shear strength and compactibility characteristics of particulate materials is discussed in the following pages.

4.1 Bulk Physical Properties of Powders Relating to Static Load Transmission and Yield Strength Characteristics

The most important bulk properties of a particulate material insofar as static behavior is concerned appear to be density, compactibility and shear strength. These properties are of course interrelated; i.e., the shear strength characteristics will in general depend on the degree of com-

Page determined to be Unclassified
Reviewed Chief, RDD, WHS
IAW EO 13526, Section 3.5
Date: JUL 19 2013

paction of the powder, as will the density. In the present context, factors which influence the behavior of a powder such as humidity, presence of additives, etc., are considered to be implicit in the bulk properties of the material.

Experiments have shown that the shear strength characteristics of many granular and particulate materials are of the type illustrated by Figures 4.1.1-a and 4.1.1-b. For dilatant materials such as dry sand, glass beads, etc., which are composed of particles whose weight is large compared to inter-particulate attractive forces, the shear strength τ_c can be represented by the following equation:

$$\tau_c = \sigma \tan \phi \qquad (4.1)$$

where σ is the compressive stress. The angle ϕ, called the "shear angle," is a constant for a given material of this type. Departures from this equation may be expected at very high compressive stresses due to fracture of particles.

In the case of compressible materials, the critical shearing stress may be represented by an equation of the form:

$$\tau_c = (\sigma + \sigma_o) \tan \phi \qquad (4.2)$$

The constant σ_o in this expression defines the shearing strength of the material at zero load. The shear strength characteristic expressed by Equation (4.2) has not been adequately verified experimentally for compressible

Page determined to be Unclassified
Reviewed Chief, RDD, WHS
IAW EO 13526, Section 3.5
Date: JUL 19 2013

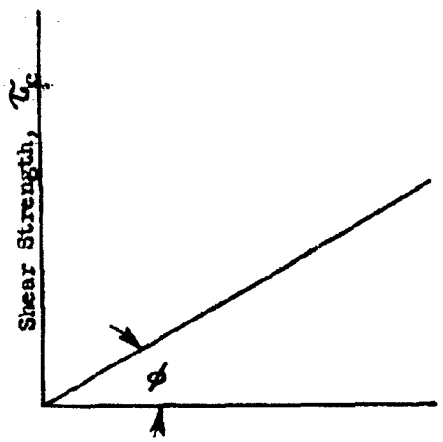

a) Dry Dilatant Materials

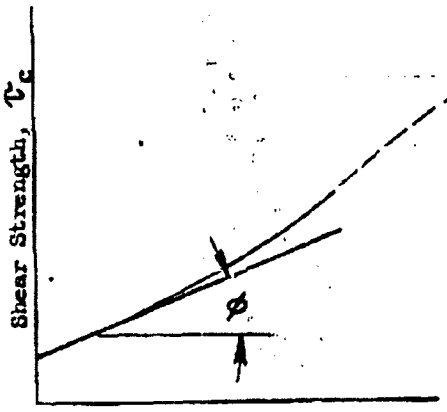

b) Compactible Materials

Figure 4.1.1 SHEAR STRENGTH CHARACTERISTICS

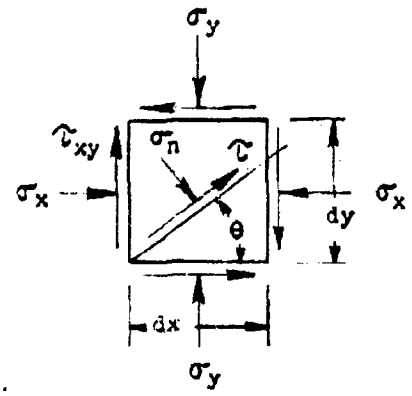

FIGURE 4.1.2 RESOLUTION OF STRESSES

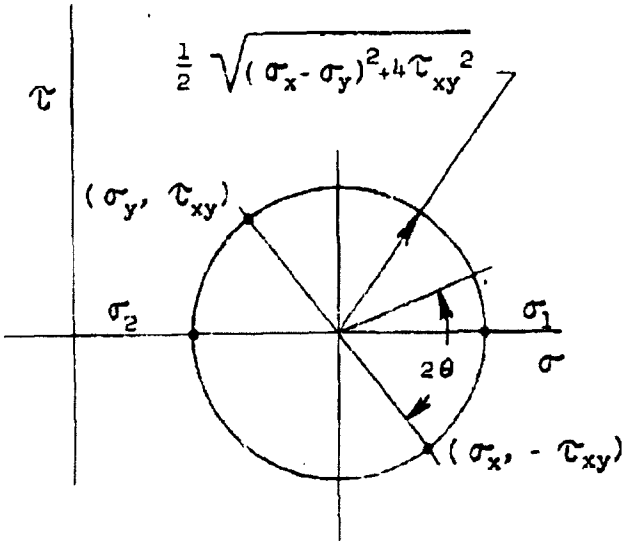

FIGURE 4.1.3 REPRESENTATION OF STRESSES BY MEANS OF STRESS CIRCLE

Page determined to be Unclassified
Reviewed Chief, RDD, WHS
IAW EO 13526, Section 3.5
Date: JUL 19 2013

organic materials. However, available information[4.1,4.2] indicates that the following behavior may be expected:

(a) σ_o will increase with increasing density (i.e., compaction) for a given material,

(b) Equation (4.2) will apply as a good approximation to shear strength characteristics over a restricted range of compressive stresses,

(c) the curve of τ_c vs σ will be concave upward with increasing compressive stress as indicated in Figure 4.1.1-b. This characteristic would correspond to test conditions in which τ_c is determined for a sequence of increasing compressive stresses. If the materials is compressed sufficiently to cause compaction prior to shear testing at reduced compressive stresses, σ_o will be increased. However, if shear failure occurs at reduced load, it may be expected that the shear strength will drop considerably after failure. This surmise, which will be checked experimentally, may account for the type of shear failure observed in disc-lifting experiments with organic powders.[4.3]

At sufficiently high stresses, particulate materials may exhibit plastic characteristics as indicated by the dashed line in Figure 4.1.1-b

The yield-stress conditions for a powder under load can be formulated in terms of the applied stresses by means of the following analysis. Consider a small volume element in a bed of powder as shown in Figure 4.1.2.

4.2 Taylor, D. W., Fundamentals of Soil Mechanics, John Wiley and Sons, N. Y., (1948).

4.3 General Mills, Inc. Report No. 2125, Dissemination of Solid and Liquid BW Agents (Unclassified Title) p. 46 (October 13, 1960) (SECRET).

Page determined to be Unclassified
Reviewed Chief, RDD, WHS
IAW EO 13526, Section 3.5
Date: JUL 19 2013

It is assumed that the stress distribution is two-dimensional so that the state of stress is fully described by the normal stress components (σ_x, σ_y) and the shearing stress τ_{xy}. If the normal and shearing stresses on a plane at an angle θ to the x-axis are determined (see Figure 4.1.2), it is found that the state of stress can be expressed by the equations:

$$\sigma_n = \frac{1}{2}(\sigma_x + \sigma_y) + \frac{1}{2}(\sigma_y - \sigma_x)\cos 2\theta - \tau_{xy}\sin 2\theta \qquad (4.3)$$

$$\tau = \frac{1}{2}(\sigma_y - \sigma_x)\sin 2\theta + \tau_{xy}\cos 2\theta \qquad (4.4)$$

These equations can be interpreted in terms of a "circle of stress" in the stress plane, as illustrated by Figure 4.1.3. If a circle is drawn through the points $(\sigma_x, -\tau_{xy})$, $(\sigma_y, +\tau_{xy})$ in the stress plane, the stresses σ_n and τ corresponding to the angle θ will lie on this circle at an angle 2θ from the point $(\sigma_x, -\tau_{xy})$. The yield condition expressed by Equation 4.1) corresponds to the case for which the stress circle is tangent to the line $\tau = \sigma \tan\phi$. In Figure 4.1.3 the maximum and minimum compressive stresses, corresponding to $\tau = 0$, are denoted by σ_1 and σ_2 respectively. From the figure it is easily seen that the condition for shear failure is:

$$\sin\phi = \frac{\sigma_1 - \sigma_2}{\sigma_1 + \sigma_2} \qquad (4.5)$$

In terms of the x,y coordinate system and the corresponding stresses σ_x, σ_y and τ_{xy}, the condition for shear failure is:

$$\sin\phi = \frac{\sqrt{(\sigma_x - \sigma_y)^2 + 4\tau_{xy}^2}}{\sigma_x + \sigma_y} \qquad (4.6)$$

Page determined to be Unclassified
Reviewed Chief, RDD, WHS
IAW EO 13526, Section 3.5
Date: JUL 19 2013

Equation (4.5) is the basis for the so-called "triaxial shear test" for determining the critical shear strength of a particulate material.[4.2] Triaxial shear tests are carried out with the apparatus shown schematically in Figure 4.1.4. A cylindrical sample of the material to be tested is sealed within a thin rubber membrane. The sample is then placed in the cylindrical barrel of the test apparatus as shown in the figure. Provision is made for pressuring the chamber to a pressure p_2. The volume change during pressurization can be measured if desired. An axial load, F, is then applied by means of a piston as indicated in the figure. If p_2 is maintained constant while F is increased until the sample fails, a stress circle corresponding to shear failure at the mean stress $\frac{p_1 + p_2}{2}$ is obtained, where $F = (p_1 - p_2)A$. By conducting these tests over a range of values of p_2, the shear strength characteristic may be established as the envelope of a series of stress circles as shown in Figure 4.1.5. With suitable instrumentation, the linear and volume compression (or dilatation) of the sample may also be determined. Triaxial tests are commonly used for evaluating soil samples. It is possible that such tests could also be employed to advantage in defining the physical characteristics of organic particulate materials. Because of the considerable information available from these tests and the possibility of closely controlling the test conditions, triaxial tests might be useful as consistency tests for dry agent materials.

4.2 Taylor, D. W., Fundamentals of Soil Mechanics, John Wiley and Sons, N.Y. (1948).

Page determined to be Unclassified
Reviewed Chief, RDD, WHS
IAW EO 13526, Section 3.5
Date: JUL 19 2013

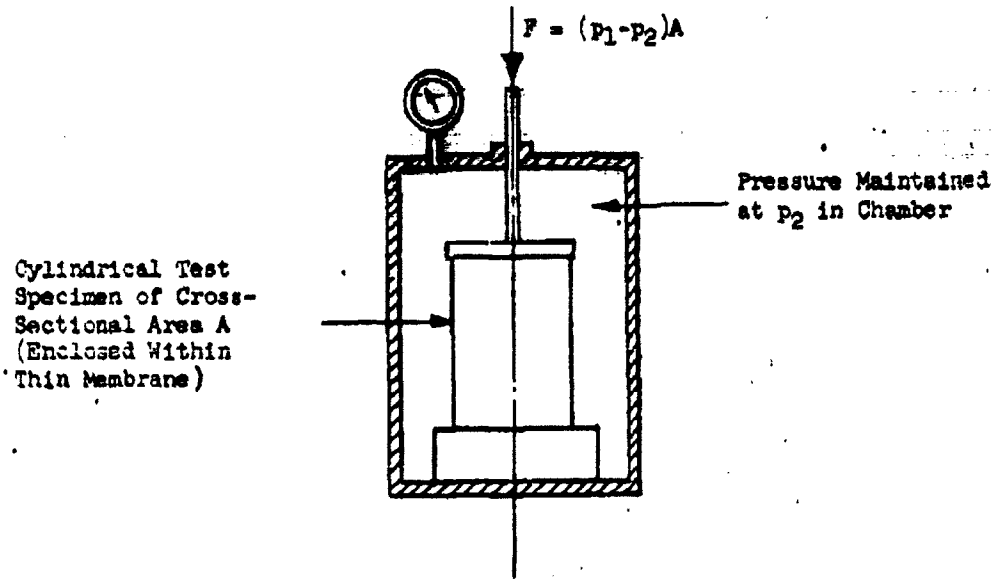

FIGURE 4.1.4 TRIAXIAL TEST FIXTURE

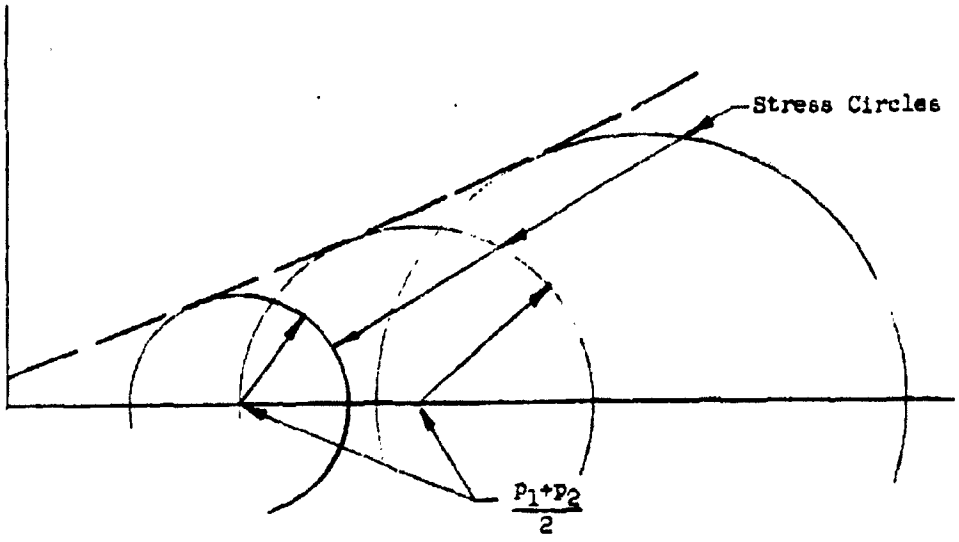

FIGURE 4.1.5 DETERMINATION OF SHEAR STRENGTH CHARACTERISTIC FROM TRIAXIAL TESTS

Page determined to be Unclassified
Reviewed Chief, RDD, WHS
IAW EO 13526, Section 3.5
Date: JUL 19 2013

4.2 Theoretical Analysis of Load Transmission and Shear Failure in Particulate Beds

A survey of the literature pertaining to load transmission in gramular or particulate materials has failed to disclose a general theory for analyzing the stress distribution and yield conditions in such materials. Most of the available theoretical, empirical and experimental investigations reported in the literature are concerned with soils and soil mechanics (an extensive bibliography is given in Reference 4.2). The theory and methods of soil mechanics are for the most part too specialized for direct application in the present study. However, considerable benefit has been derived from a study of this literature, which has helped to define the existing "state of the art" with regard to the mechanics of particulate materials.

The principal difficulty in analyzing the behavior of particulate beds under static loads lies in the analysis of stress conditions within the material which lead to rupture. In special cases where the principal stresses are known, Equation (4.5) can be applied directly to determine the shear lines in a particulate bed. An example of this type is given below. Generally, the stress distribution at rupture cannot be readily found, even if it is assumed that the material behaves elastically up to the point of shear failure. Two examples based on the assumption of elastic behavior are presented and discussed in the following pages.

4.2.1 Analysis of the Load Distribution in a Powder Due to its Weight

Consider a powder of density γ in equilibrium under its own weight in a large container. The average vertical stress at a depth y is $\sigma_y = \gamma y$.

Page determined to be Unclassified
Reviewed Chief, RDD, WHS
IAW EO 13526, Section 3.5
Date: JUL 19 2013

The permissible range of lateral stresses σ_x can be determined from Equation (4.5) since σ_x and σ_y are principal stresses. Solving Equation (4.5) for the ratio σ_1/σ_2 we obtain:

$$\frac{\sigma_1}{\sigma_2} = \frac{1 + \sin\phi}{1 - \sin\phi} = \tan^2\left(\frac{\pi}{4} + \frac{\phi}{2}\right) \qquad (4.7)$$

where $\sigma_1 = \gamma_y$ in the present case. Since the roles of σ_1 and σ_2 may be interchanged, we find that the ratio $\frac{\sigma_x}{\sigma_y}$ must lie in the range:

$$\tan^2\left(\frac{\pi}{4} - \frac{\phi}{2}\right) \leqq \frac{\sigma_x}{\sigma_y} \leqq \tan^2\left(\frac{\pi}{4} + \frac{\phi}{2}\right) \qquad (4.8)$$

The limits in this inequality correspond to the onset of slippage of the material in the bed. The corresponding slip planes are indicated by the diagonal lines in Figure 4.2.1. When concentrated loads are applied to a particulate material the slip surfaces are difficult to define, as can be seen by the following example.

4.2.2 Analysis of Critical Loads for Penetration of a Bed of Powder

In an effort to gain insight into the behavior of a particle bed when subjected to concentrated loads, the following special case was examined in some detail. Consider a homogeneous bed of powder subjected to a downward load applied at the surface of the bed by means of a rod of rectangular cross-section as shown in Figure 4.2.2-a. The rod is of width 2a and so long that the stress distribution within the particle bed can be considered two-dimensional in vertical planes normal to the axis of the rod. The load per unit length required for penetration of the bed is to be found, assuming a shear strength characteristic expressed by Equation (4.2).

Page determined to be Unclassified
Reviewed Chief, RDD, WHS
IAW EO 13526, Section 3.5
Date: JUL 19 2013

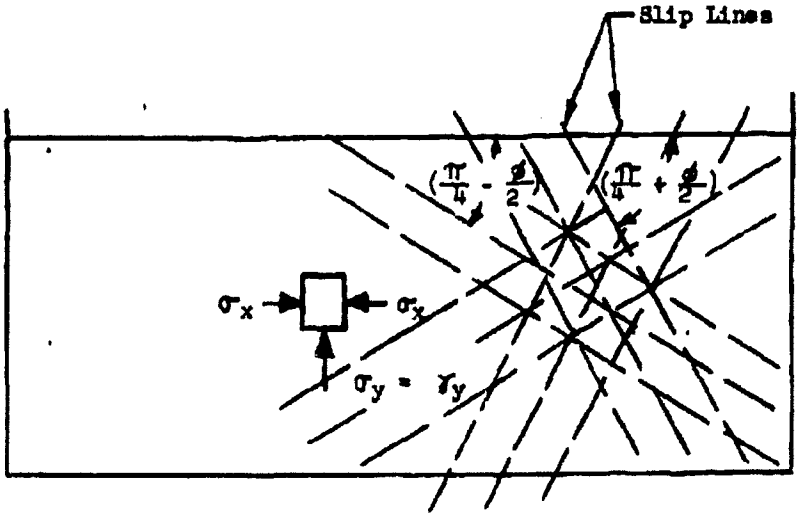

FIGURE 4.2.1 SLIP LINES IN UNIFORM UNSTRESSED PARTICLE BED

Page determined to be Unclassified
Reviewed Chief, RDD, WHS
IAW EO 13526, Section 3.5
Date: JUL 19 2013

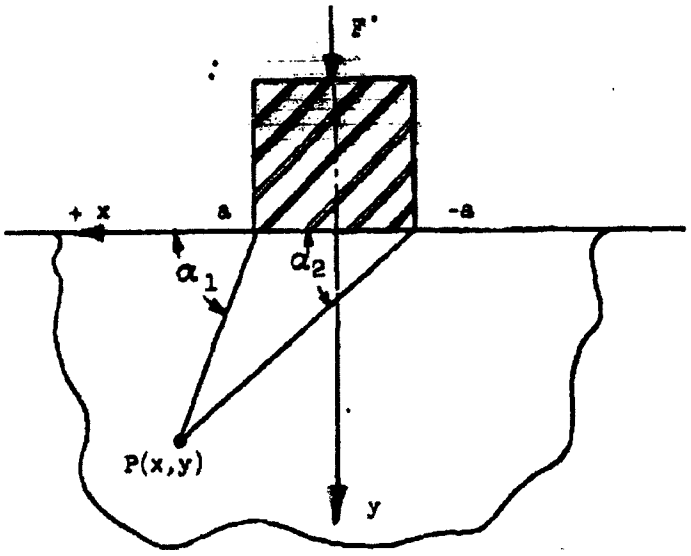

a) Loading of Bed by Means of Long Rectangular Rod

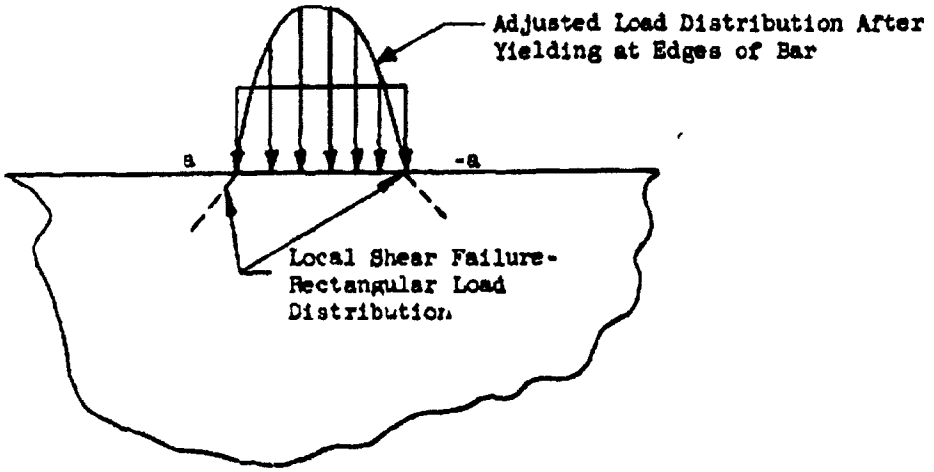

b) Load Readjustment Due to Local Shear Failure

FIGURE 4.2.2 PENETRATION OF THE SURFACE OF A PARTICLE BED

Page determined to be Unclassified
Reviewed Chief, RDD, WHS
IAW EO 13526, Section 3.5
Date: JUL 19 2013

In carrying out this analysis, it may be assumed that the stress distribution would correspond to elastic behavior of the particulate material up to the point of shear failure. If the applied load results in local shear failure, a readjustment of the loading must occur. This is illustrated by Figure 4.2.2-b. The rectangular loading indicated in Figure 4.2.2-b results in local shear failure at the edge of the rod, thus requiring a redistribution of loading with a greater concentration in the center of the rod. The maximum load which can be carried corresponds to a load distribution which would result in simultaneous shear failure along a continuous surface within the bed as shown in Figure 4.2.3.

The stress distribution in a semi-infinite solid subjected to a uniform surface pressure p between x = -a and x = a (see Figure 4.2.2-a) is expressed by the equations:[4.4]

$$\sigma_x = \frac{p}{\pi}\left\{\alpha_1 - \alpha_2 + \frac{1}{2}(\sin 2\alpha_1 - \sin 2\alpha_2)\right\}$$

$$\sigma_y = \frac{p}{\pi}\left\{\alpha_1 - \alpha_2 - \frac{1}{2}(\sin 2\alpha_1 - \sin 2\alpha_2)\right\} \qquad (4.9)$$

$$\tau_{xy} = \frac{p}{2\pi}\left\{\cos 2\alpha_2 - \cos 2\alpha_1\right\}$$

By using these equations the stresses due to a generalized pressure p(x) in $-a \leq x \leq a$ can be expressed in the following form:

4.4 Jürgenson, L., The Application of Theories of Elasticity and Plasticity to Foundation Problems, J. Boston Soc. C.E. (July 1934)

Page determined to be Unclassified
Reviewed Chief, RDD, WHS
IAW EO 13526, Section 3.5
Date: JUL 19 2013

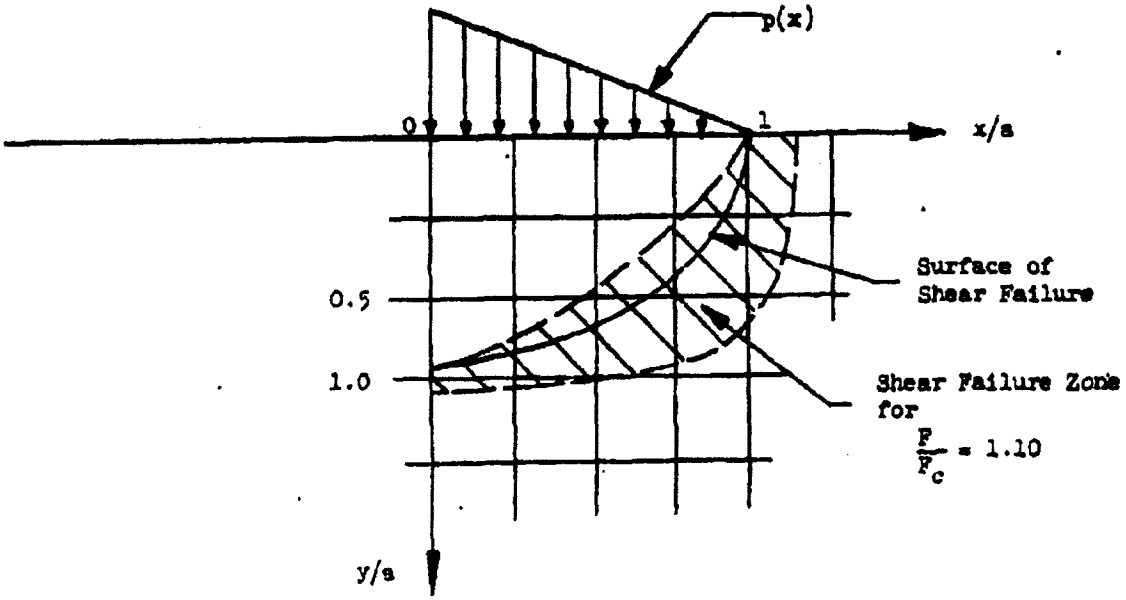

FIGURE 4.2.3 SHEAR SURFACE AND LOAD DISTRIBUTION FOR PENETRATION OF SURFACE OF PARTICLE BED IN ILLUSTRATIVE EXAMPLE

Page determined to be Unclassified
Reviewed Chief, RDD, WHS
IAW EO 13526, Section 3.5
Date: JUL 19 2013

$$\sigma_x(\bar{x},\bar{y}) = \frac{2\bar{y}}{\pi}\int_{-a}^{a}\frac{p(x)\,(\bar{x}-x)^2}{\left[(\bar{x}-x)^2+\bar{y}^2\right]^2}\,dx$$

$$\sigma_y(\bar{x},\bar{y}) = \frac{2\bar{y}^3}{\pi}\int_{-a}^{a}\frac{p(x)}{\left[(\bar{x}-x)^2+\bar{y}^2\right]}\,dx \qquad (4.10)$$

$$\tau_{xy}(\bar{x},\bar{y}) = \frac{2\bar{y}^2}{\pi}\int_{-a}^{a}\frac{p(x)\,(\bar{x}-x)}{\left[(\bar{x}-x)^2+\bar{y}^2\right]^2}\,dx$$

From Equation (4.2) the shear yield condition can be expressed in the form:

$$\sin\phi = \frac{\sqrt{(\sigma_{x'}-\sigma_{y'})^2+4\tau'^2}}{\sigma_{x'}+\sigma_{y'}+\frac{2\sigma_o}{p_o}+\frac{2\gamma a}{p_o}\left(\frac{\bar{y}}{a}\right)} \qquad (4.11)$$

where $\sigma_{x'} = \frac{\sigma_x}{p_o}$, $\sigma_{y'} = \frac{\sigma_y}{p_o}$, $\tau' = \frac{\tau_{xy}}{p_o}$, γ is the density of the material and $p_o = p(o)$. The maximum load supported by the particle bed before shear failure occurs can be determined from Equations (4.10) and (4.11). For given values of ϕ, σ_o and γa, it is necessary to determine the pressure distribution $p(x)$ which yields the maximum load F, where:

$$F = \int_{-a}^{a} p(x)\,dx \qquad (4.12)$$

The maximum load is very difficult to determine in general because of the nature of the shear failure condition given by Equation (4.11). A specific

Page determined to be Unclassified
Reviewed Chief, RDD, WHS
IAW EO 13526, Section 3.5
Date: JUL 19 2013

example has been worked out for the conditions: $\phi = 25.8°$, $\sigma_o = 0.1\ p_o$, $\gamma_b = 0.15\ p_o$. By choosing σ_o and γ_b in this manner, (i.e., so that these factors are proportioned to p_o) it was found possible to use a triangular loading. The resulting force for penetrating the surface of the bed is $F_c = 6.67\ \gamma_b^2$. The shear failure surface corresponding to this load is depicted in Figure 4.2.3. If the load is increased by 10 percent, the shear failure region prior to collapse is shown as the shaded area in Figure 4.2.3.

The shape of the failure zone suggests that shear failure would be accompanied by heaving up of the material close to the rod. This type of failure has been observed qualitatively, although no measurements have been made to determine critical loads.

This example indicates the computational difficulties which are encountered in analyzing the loads which can be sustained by beds of powder. A much simpler case of the resistance offered by a bed of powder to penetration from above has also been analyzed. From Equation (4.9), it can be shown that, in the limit as "a" tends to zero while $P = 2\pi a^2 \gamma$ is held constant, the stress distribution becomes radial and is expressed by the equations:

$$\sigma_r = \frac{2P}{\pi} \frac{\gamma}{r^2}\ ;\ \sigma_\theta = 0;\ \tau = 0 \qquad (4.13)$$

In a bed of powder for which the pressure distribution due to the weight of the powder is hydrostatic, the principal stresses will be radial and tangential with magnitudes:

$$\sigma_1 = \frac{2P}{\pi} \frac{\gamma}{r^2} + \gamma y$$
$$\sigma_2 = \gamma y$$

Page determined to be Unclassified
Reviewed Chief, RDD, WHS
IAW EO 13526, Section 3.5
Date: JUL 19 2013

Thus, from Equation (4.5):

$$\sin \phi = (1 + \frac{\pi \gamma}{p} r^2)^{-1}$$

Surfaces of shear failure are thus cylindrical with the axis lying at the powder surface. From this it follows that if a smooth rod of radius R is embedded in the powder to a depth R, the force P, per unit length, required to force the rod into the bed is:

$$P = \gamma \pi R^2 \frac{\sin \phi}{1 - \sin \phi}$$

The above theoretical results rest upon several important assumptions: (1) the particulate material behaves elastically and isotropically up to the point of shear failure, (2) the stresses are sufficiently low to avoid compaction under the applied loads (which might modify the shear strength characteristics or destroy the isotropy of the material, (3) the dimensions of the container are large compared to the width of the loaded area of the bed surface.

These theoretical conclusions are subject to experimental verification for various types of granular or particulate materials. Such experiments are planned in future work relative to the physical behavior of particle aggregations.

Page determined to be Unclassified
Reviewed Chief, RDD, WHS
IAW EO 13526, Section 3.5
Date: JUL 19 2013

5. EXPERIMENTAL STUDIES OF LOAD TRANSMISSION IN SPECIFIC ARRAYS

In a previous report,[5.1] results were presented from a theoretical study of load transmission in regular arrays of disks and cylinders. In order to verify these conclusions experimentally, tests with regular arrays were carried out using the test fixture shown in Figure 5.1-a. This device consists of an aluminum frame, 18 cm high by 39 cm wide, designed to support the plexiglass side walls with a spacing of 0.38 cm. Teflon cylinders with a diameter of 0.95 cm and a thickness of 0.25 cm were used in the tests. An upward force could be applied to one of the cylinders in the bottom row by a small platform at the floor of the test fixture.

The first configuration considered was the hexagonal arrangement shown in Figure 5.1-b. According to the theoretical analysis, the force required to lift the platform is $\frac{n}{2}(n+1)W$ where n is the number of tiers and W is the weight of one disk.

When an upward force was applied to the platform, the cylinders experiencing movement were found to be contained within a wedge whose sides form an isoceles triangle, as predicted by the theory (see Figure 5.1-a).

Tests were performed with the aid of a Jolly Balance to determine the force necessary to displace the wedge at various depths of the cylinders. The results are as follows:

5.1. General Mills, Inc. Report No. 2161, Second Quarterly Progress Report on Dissemination of Solid and Liquid BW Agents (Unclassified Title) Feb. 13, 1961, pp. 40-55 (Confidential).

Page determined to be Unclassified
Reviewed Chief, RDD, WHS
IAW EO 13526, Section 3.5
Date: JUL 19 2013

Page determined to be Unclassified
Reviewed Chief, RDD, WHS
IAW EO 13526, Section 3.5
Date: JUL 19 2013

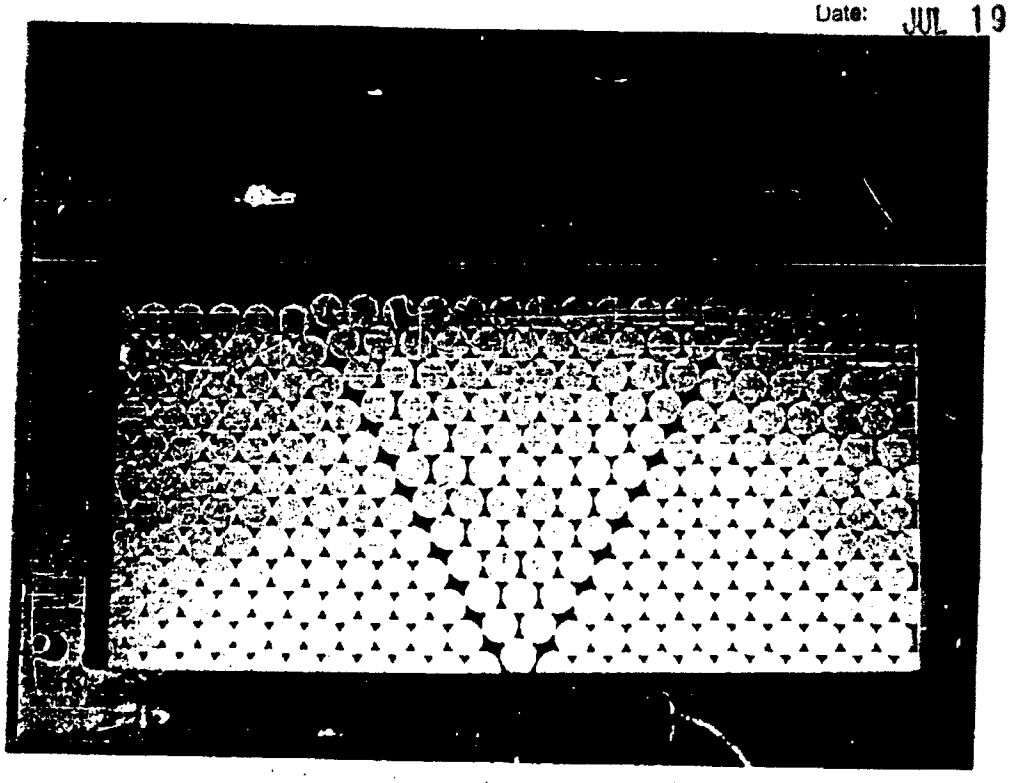

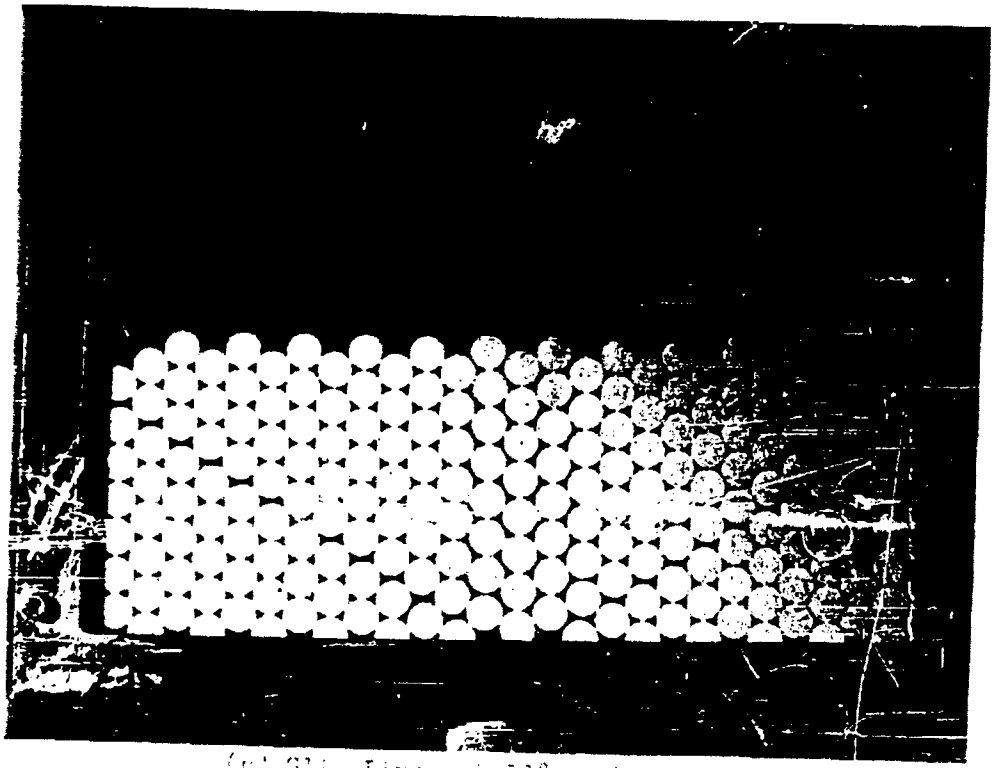

(c) S21 Lines at 30° + Horizontal

Height (No. of Tiers)	Theoretical Force	Force to Displace Wedge
6	8.15 grams	11.32 grams
9	17.47	22.90
12	30.26	39.00

The discrepancy between the force required to displace the wedge and the weight of the wedge may be attributed to friction in various parts of the system, i.e., friction between the pin used to raise the platform and the base of the model, between the cylinders and the walls, and between the cylinders. It is interesting to note that the difference between the measured and predicted force is very nearly proportional to the measured force, which indicates that the discrepancy is due to frictional effects.

The second configuration considered was the hexagonal arrangement shown in Figure 5.1-b. For this arrangement the predicted load for raising the platform is $(n + 1)(n - 1) W$. The force required to displace the wedge in this case was also found to exceed the force predicted by the theory. Again the percentage increase above the yield force predicted theoretically was found to be proportional to the applied force, the constant of proportionality being very nearly the same as in the previous case.

Figure 5.1-b indicates how the cylinders are displaced when an upward force is applied to the platform. The vertical row of cylinders directly above the platform move the same distance that the platform moves. These cylinders in turn displace the cylinders in the triangular regions at each side of the central row at an angle of 30° to the horizontal in accordance with the theory.

Page determined to be Unclassified
Reviewed Chief, RDD, WHS
IAW EO 13526, Section 3.5
Date: JUL 19 2013

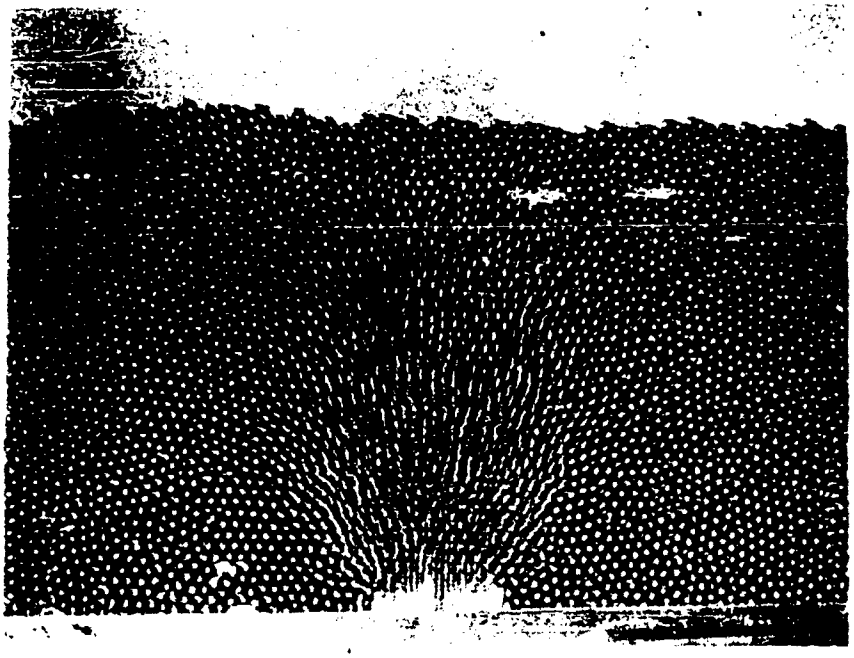

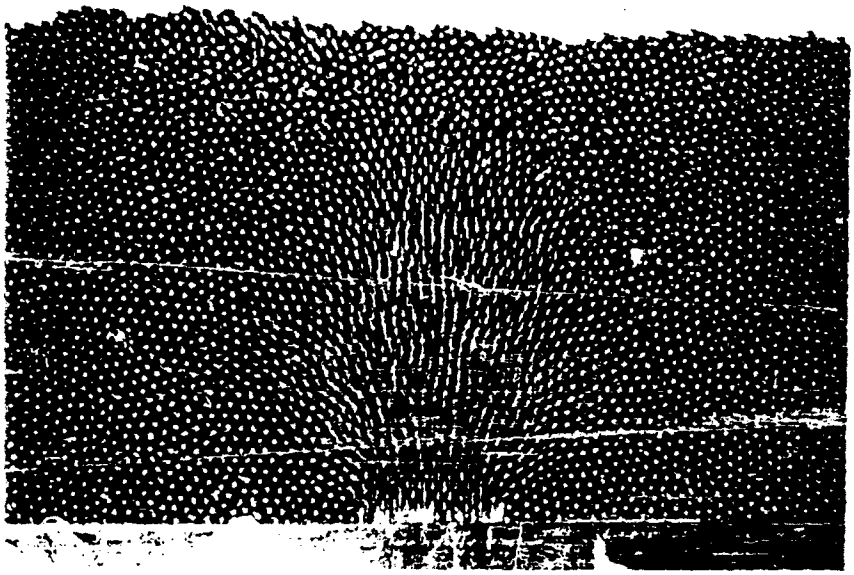

Page determined to be Unclassified
Reviewed Chief, RDD, WHS
IAW EO 13526, Section 3.5
Date: JUL 19 2013

Experiments have also been performed with the teflon cylinders replaced by a mixture of different sizes of lead shot. The sizes ranged from 0.228 cm to 0.320 cm diameter. A random distribution was obtained.

Time exposure pictures were taken as an upward force was applied to a one-inch long platform on the floor of the model (Figure 5.2). Movement of particles is indicated by the appearance of blurred spots.

Observations indicated that particles at the base of the bed could experience considerable movement before particles at the top of the bed would move. The particles directly above the platform experience the most movement at any given level in the bed. Near the base of the bed particles which are at a considerable distance to the right or to the left of the platform experience movement while at the top of the bed the particles which are not directly over the platform experience little movement. These observations indicate that configurations which are not in a minimum-volume state are able to accommodate considerable local displacement without large-scale displacement of material. This is evidenced by the rapid decay of displacement with increasing distance from the point of load application.

Page determined to be Unclassified
Reviewed Chief, RDD, WHS
IAW EO 13526, Section 3.5
Date: JUL 19 2013

6. INVESTIGATIONS OF PROPERTIES OF SLURRIES

During this reporting period, experimental work on egg slurries was continued to provide data necessary for the proper design of dissemination systems for agents involving this type of liquid carrier.

Accumulation of rheological data on suspensions of Sm in a liquid fluorochemical was continued to provide information needed for evaluating the feasibility of disseminating normally dry, powdered agents through use of concentrated slurries.

6.1 Properties of Egg Slurries

At the present time, certain agents must be prepared in an egg slurry carrier medium. Disseminators for such liquid agents must provide facilities to prevent solidification of the slurry in the store when the ambient temperature falls below the freezing point. Among the factors determining the nature of these facilities are the specific heat and thermal conductivity of the slurry.

Apparatuses for determining these two thermal properties of slurries were designed and constructed. The heat capacities of the four frozen egg slurry samples received from Fort Detrick (W.E.S. #1, #2, #3, and #4) were determined as a function of temperature. The thermal conductivity apparatus is being calibrated at the present time, and measurements on these egg slurry samples will be completed in the near future.

6.1.1 Specific Heat of Egg Slurries

The specific heats of the four egg slurry samples designated W.E.S. #1, #2, #3, and #4 were determined by the heating-curve method at intervals of about 1.3°C in the temperature range from 0 to 34°C. A measured quantity of

DECLASSIFIED IN FULL
Authority: EO 13526
Chief, Records & Declass Div, WHS
Date: JUL 19 2013

electrical energy was supplied to a heating coil immersed in the liquid contents of a calorimeter and the temperature response was recorded before, during, and after energy input.

6.1.1.1. Theory

When a constant current, I, under a constant emf, $\mathcal{E}$, is maintained through a heating coil for a period of time, t, the equivalent heat supplied to the calorimeter may be calculated from:

$$Q = \frac{\mathcal{E} I t}{J} \qquad (6.1)$$

where: J = 4.184 joules/cal (the mechanical equivalent of heat).

This quantity of heat causes a rise in temperature of the calorimeter and its contents such that:

$$Q = Wc_p \Delta T + C_p \Delta T \qquad (6.2)$$

where: W = weight of liquid in calorimeter (gm)

c_p = specific heat of liquid (cal/gm °C)

ΔT = temperature rise

C_p = average heat capacity of the calorimeter including container, thermometer, stirrer, etc. (cal/°C)

6.1.1.2 Apparatus and Technique

The specific heat of the egg slurry samples was determined using the apparatus shown in Figure 6.1.1. The Dewar flask, insulated with two inches of Styrofoam, is equipped with a glass stirrer, Beckmann differential thermometer, and immersion heater.

Page determined to be Unclassified
Reviewed Chief, RDD, WHS
IAW EO 13526, Section 3.5
Date: JUL 19 2013

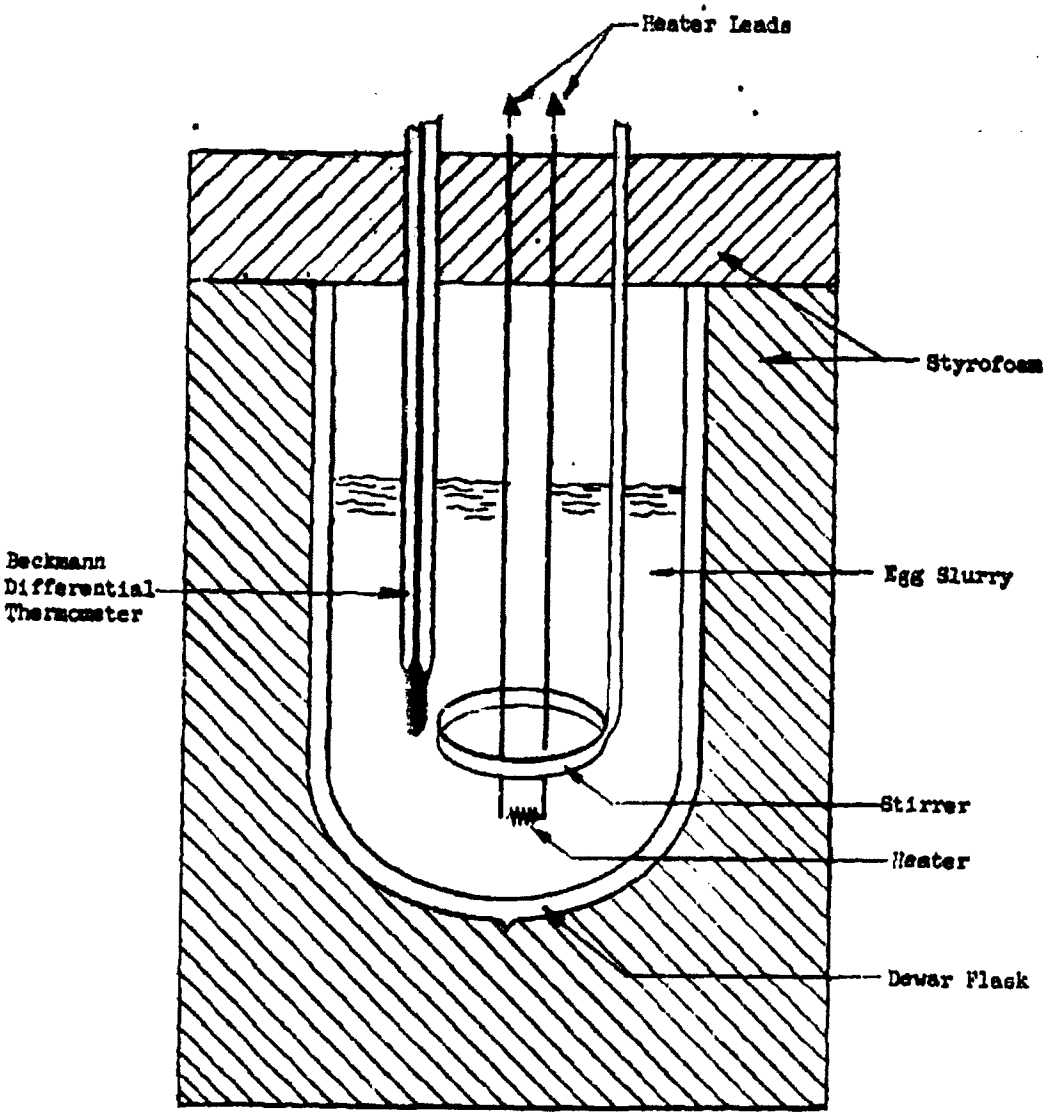

FIGURE 6.1.1 CALORIMETER FOR SPECIFIC HEAT DETERMINATIONS

Page determined to be Unclassified
Reviewed Chief, RDD, WHS
IAW EO 13526, Section 3.5
Date: JUL 19 2013

Proper stirring conditions were determined experimentally in order to insure adequate mixing of the Dewar contents, prevent coagulation of the egg protein on the surface of the heater, and prevent foaming of the slurry.

The Beckman differential thermometer used to measure temperature rise has a 6°C range and is readable to the nearest 0.002°C. The absolute temperature of the slurry was determined at the beginning of an experiment with a National Bureau of Standards calibrated thermometer.

The heating element is a small resistor of approximately 150 ohms resistance. The resistor and its copper leads are coated with epoxy resin to prevent deterioration. The heating circuit consists of a d.c. power supply operated off a constant voltage transformer, a differential voltmeter and a milliammeter as shown schematically in Figure 6.1.2. The voltmeter can be read to the nearest 0.01 volt and the ammeter to the nearest 0.001 ampere. In use, 40.00 volts were impressed across the resistor resulting in a current of 0.268 amperes. The duration of the heating cycle, three minutes in all experiments, was measured to the nearest 0.05 second. The heat produced resulted in a temperature rise of about 1.3°C.

The average heat capacity of the calorimeter, C_p in Equation (6.2), was determined from experiments conducted with double distilled water. The specific heat of water as a function of temperature is well known, and the value at the mean temperature of each experiment was used in the calculations. By delivering a known amount of electrical energy to the calorimeter filled with an accurately weighed quantity of water, the heat capacity of the calorimeter could be determined from the temperature rise. An average value of

Page determined to be Unclassified
Reviewed Chief, RDD, WHS
IAW EO 13526, Section 3.5
Date: JUL 19 2013

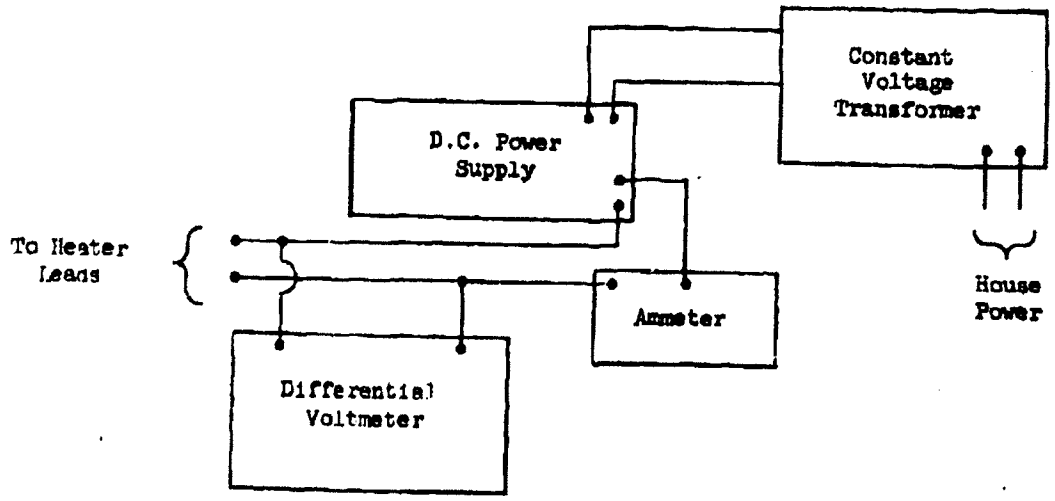

FIGURE 6.1.2 HEATING CIRCUIT FOR CALORIMETER

Page determined to be Unclassified
Reviewed Chief, RDD, WHS
IAW EO 13526, Section 3.5
Date: JUL 19 2013

20.29 ± 0.10 cal/°C was determined from six measurements made at temperatures in the range from 0 to 34°C.

From experiments conducted below room temperature, a plot of the temperature of the calorimeter (Figure 6.1.3-a) will show a gradual rise with time both before and after input of electrical energy. This rise is due to heat input from the surroundings and from stirring. Plots from experiments conducted above room temperature will show a gradual fall in temperature with time (Figure 6.1.3-b). The time rate of change of temperature during the fore and after periods was found to be small and constant for a particular temperature interval. Under conditions of greatest extraneous heat input (calorimeter temperature near 0°C), the rate of change was found to be 0.003°C/minute when monitored over a period of 15 hours. With this small a drift, the observed temperature rise of the calorimeter during the heating cycle can be corrected for extraneous heat gain or loss as follows (see Figure 6.1.3 for notations):

$$\Delta T = T_2 - T_1 - \frac{1}{2}\left(\frac{T_1 - T_o}{t_1 - t_o} + \frac{T_3 - T_2}{t_3 - t_2}\right)(t_2 - t_1)$$

where: $t_2 - t_1$ = length of heating cycle in seconds. To obtain the data necessary for this calculation, the temperature response was recorded for a period of five minutes before and after each run. Temperature readings were taken at thirty-second intervals during the fore and after periods as well as during the heating cycle.

The specific heats of the egg slurry samples were determined at temperature intervals of about 1.3° C in the range from 0 to 34° C. The upper limit

Page determined to be Unclassified
Reviewed Chief, RDD, WHS
IAW EO 13526, Section 3.5
Date: JUL 19 2013

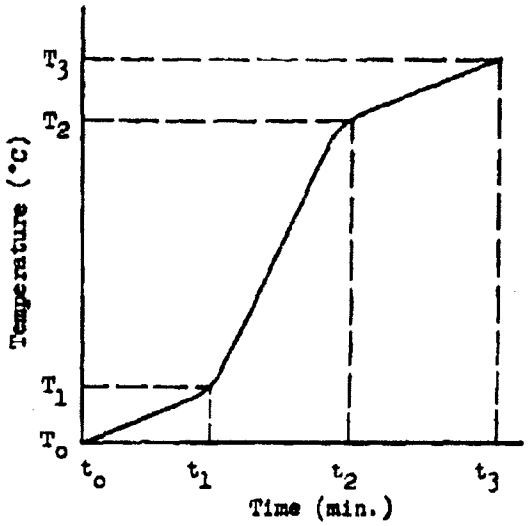

a) Calorimeter Below Room Temperature

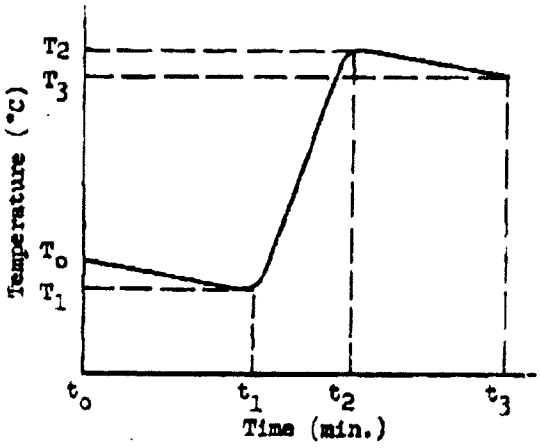

a) Calorimeter Above Room Temperature

FIGURE 6.1.3 TEMPERATURE RESPONSE CURVE DURING SPECIFIC HEAT DETERMINATIONS

Page determined to be Unclassified
Reviewed Chief, RDD, WHS
IAW EO 13526, Section 3.5
Date: JUL 19 2013

of 34° C is set by the coagulation temperature of egg protein, and the lower limit by the freezing point of the slurry. Duplicate determinations at random temperatures were made periodically to check for the existence of a systematic error, but agreement was good in all cases.

Approximately twenty determinations were made with each particular egg slurry sample in this temperature range.

Slurry samples of 300 - 500 gm were used in order to reduce error due to evaporation. Weight loss was determined by weighing the calorimeter with slurry before and after a set of runs and was found to be negligible (less than 0.2 percent). The slurry samples were kept frozen until the time of testing.

6.1.1.3 Experimental Results

Values for the specific heats of the four egg slurry samples designated W.E.S. #1, #2, #3, and #4 are plotted as function of temperature in Figures 6.1.4, 6.1.5, 6.1.6, and 6.1.7 respectively. The straight lines through the points were calculated by the method of least squares and appear to be an adequate representation of the data. The largest deviation from the straight line was about 1.5 percent.

The specific heats of W.E.S. #1 and #2 were found to be essentially constant over the temperature range from 0 to 34° C, the values being 0.86 and 0.91 cal/gm-°C, respectively. Sample W.E.S. #3 exhibited an increase in specific heat with increasing temperature (0.98 at 0° C to 1.00 at 34° C). The specific heat of W.E.S. #4, on the other hand, decreased with increasing temperature (1.00 at 0° C to 0.96 at 34° C).

Page determined to be Unclassified
Reviewed Chief, RDD, WHS
IAW EO 13526, Section 3.5
Date: JUL 19 2013

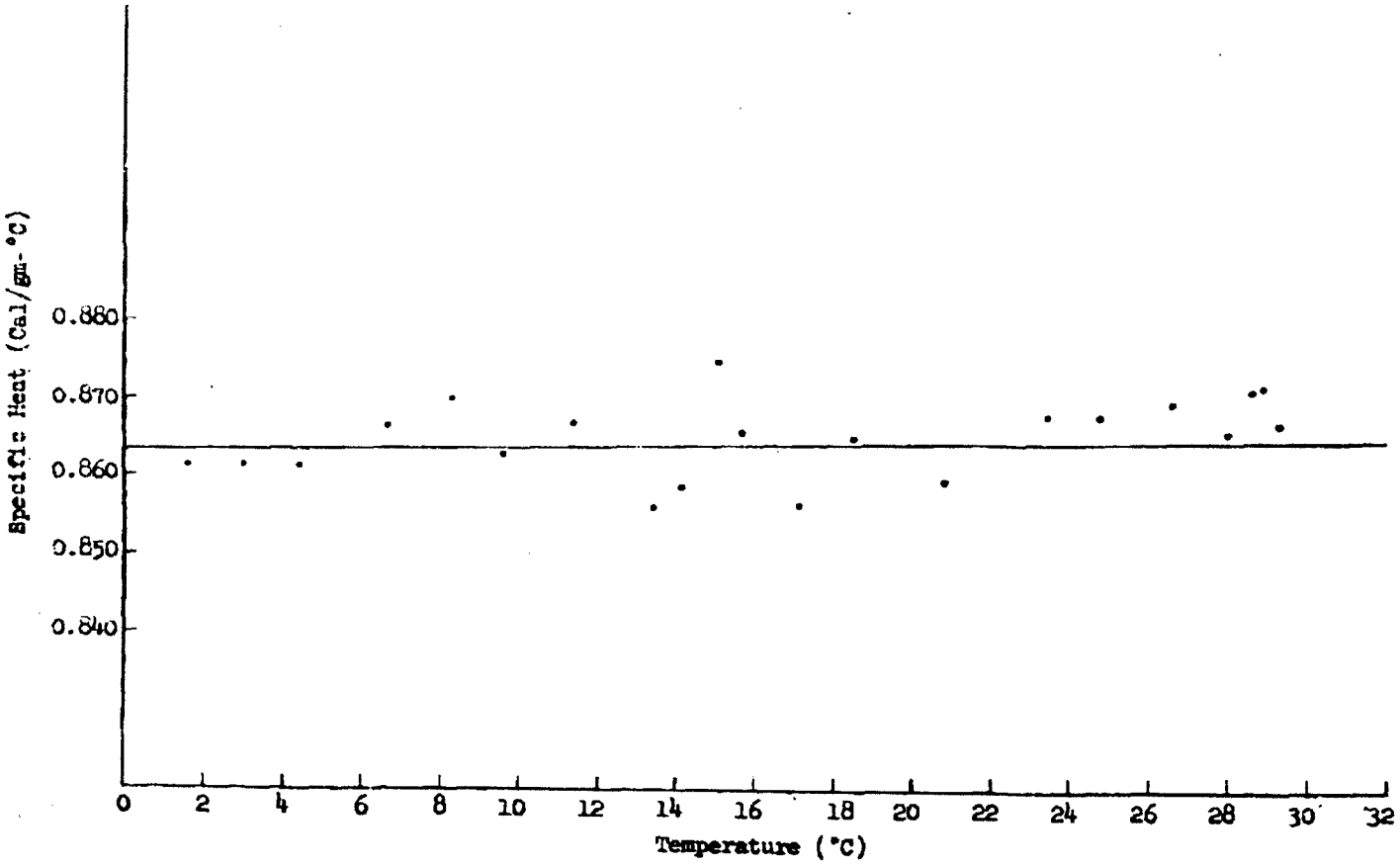

FIGURE 6.1.4 SPECIFIC HEAT VS TEMPERATURE FOR W.E.S. #1

Page determined to be Unclassified
Reviewed Chief, RDD, WHS
IAW EO 13526, Section 3.5
Date: JUL 19 2019

Page determined to be Unclassified
Reviewed Chief, RDD, WHS
IAW EO 13526, Section 3.5
Date: JUL 19 2013

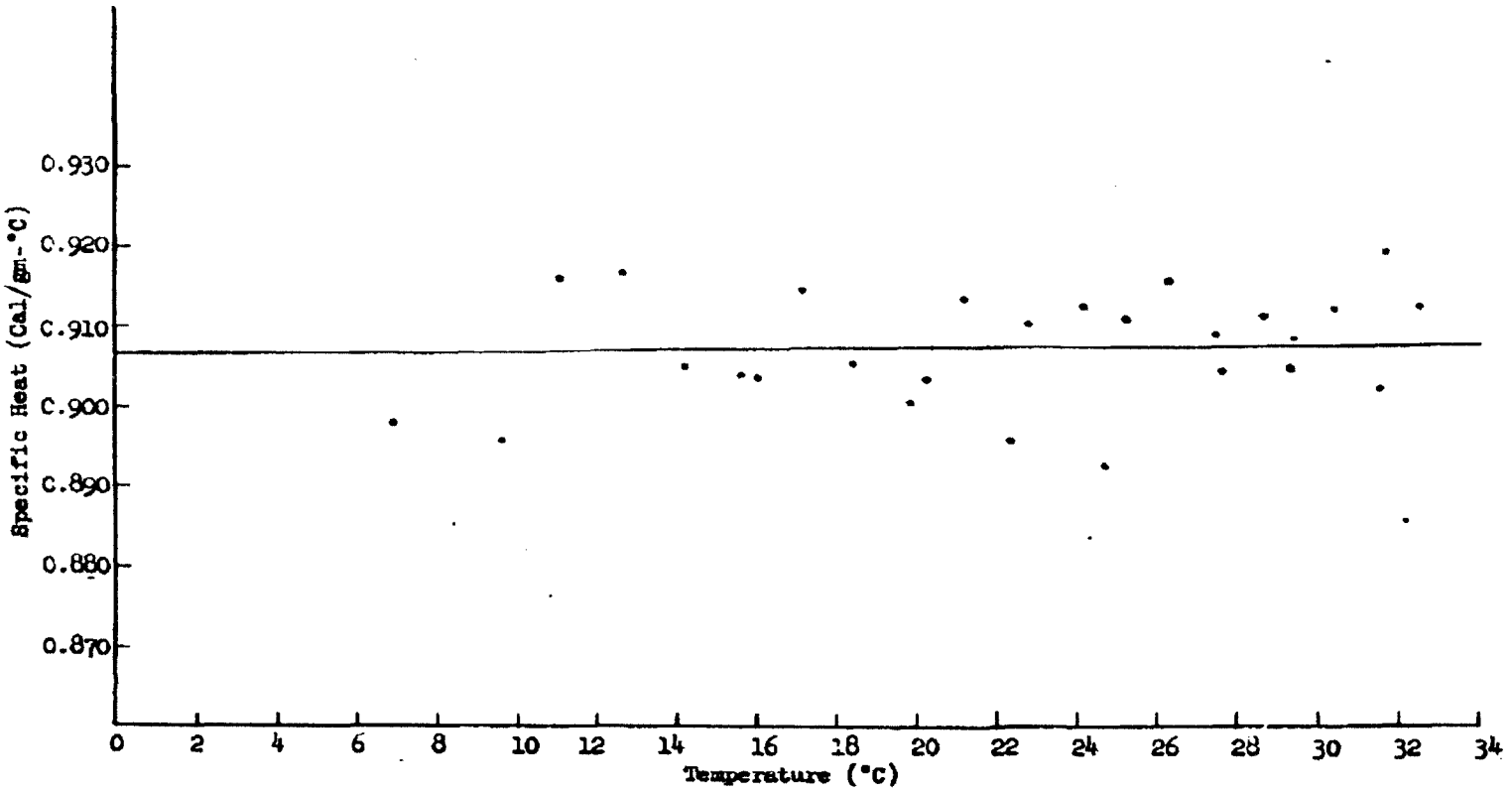

FIGURE 6.1.5 SPECIFIC HEAT VS TEMPERATURE FOR W.E.S. #2

Page determined to be Unclassified
Reviewed Chief, RDD, WHS
IAW EO 13526, Section 3.5
Date: JUL 19 2013

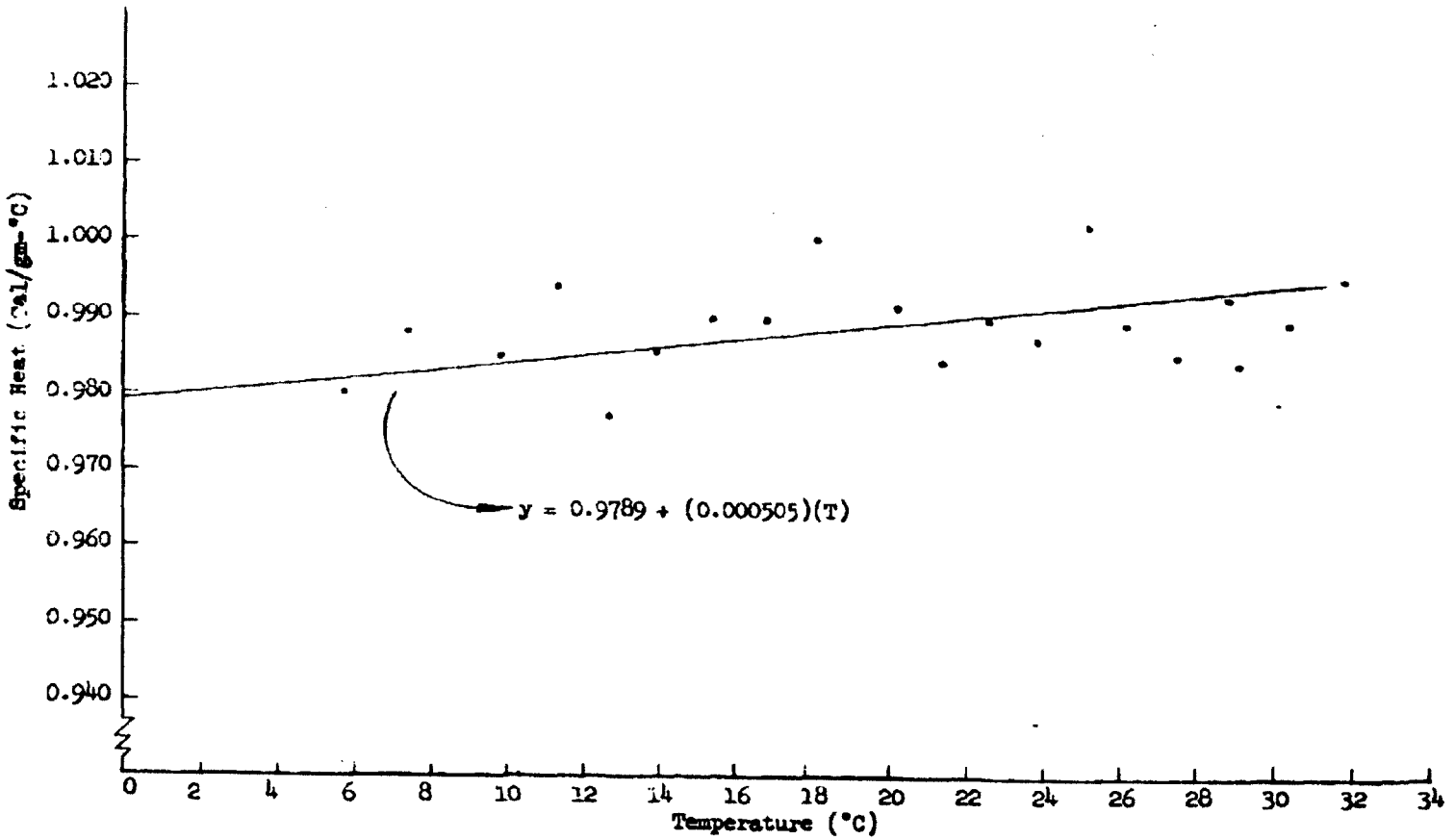

FIGURE 6.1.6 SPECIFIC HEAT VS TEMPERATURE FOR W.E.S. #3

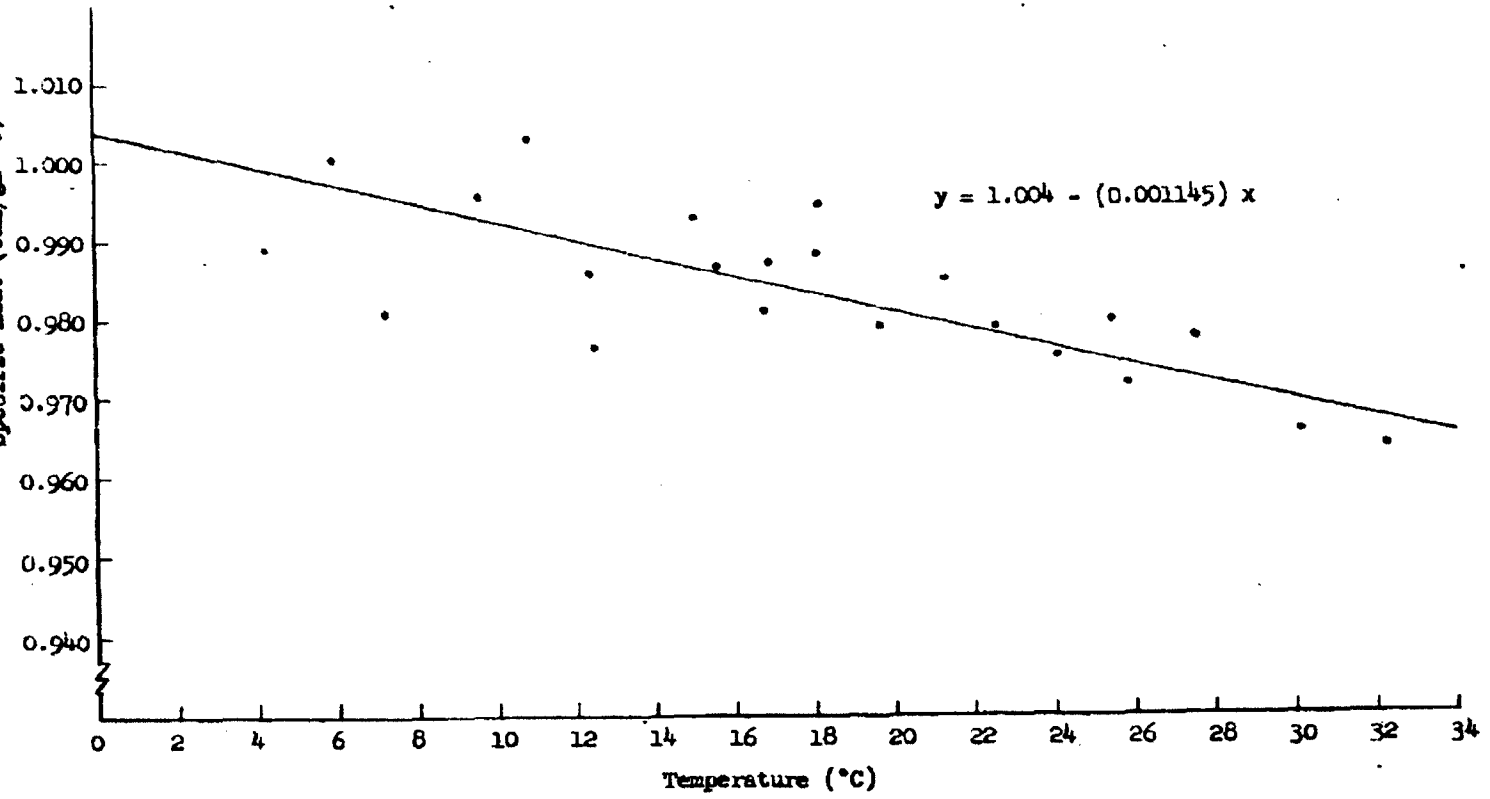

FIGURE 6.1.7 SPECIFIC HEAT VS TEMPERATURE FOR W.E.S. #4

Page determined to be Unclassified
Reviewed Chief, RDD, WHS
IAW EO 13526, Section 3.5
Date: JUL 19 2010

6.1.2 Thermal Conductivity of Egg Slurries

A method for measuring the thermal conductivity of egg slurries has been selected. An apparatus has been built and currently is being calibrated. The preliminary design considerations and details of construction of the thermal conductivity cell are presented in this report.

6.1.2.1 Theory

The Fourier heat conduction equation for one-dimensional steady flow in a homogeneous medium can be written as:

$$q = - KdA \left(\frac{dT}{dx}\right) \tag{6.3}$$

This equation states that the steady rate of heat conduction, q, is proportional to the product of the cross-sectional area, dA, normal to the flow, and the temperature gradient, $\left(\frac{dT}{dx}\right)$, along the conduction path. The thermal conductivity coefficient, K, is the true thermal conductivity of the medium and is defined as the heat flow per unit time, per unit temperature gradient, through unit thickness and across unit cross-sectional area. In metric units, K will have the dimensions:

$$cal - cm/sec\ cm^2\ ^\circ C.$$

The mean thermal conductivity of a material is given by:

$$K_m = q\ (X_1 - X_2)/A\ (T_1 - T_2) \tag{6.4}$$

Both the mean and the true thermal conductivity of a given material vary with temperature. The relation between the true and mean thermal conductivity is

$$K_m\ (T_1 - T_2) = - \int_{T_1}^{T_2} KdT \tag{6.5}$$

Page determined to be Unclassified
Reviewed Chief, RDD, WHS
IAW EO 13526, Section 3.5
Date: JUL 19 2013

For small path lengths, ΔX, K may be considered to vary linearly with temperature. K_m may be measured at the arithemetic mean of T_1 and T_2 to give $K = K_m$.

A literature search of methods for measuring thermal conductivity of liquids revealed that the method chosen must provide one-dimensional heat flow with negligible natural convection in the liquid. From this survey, it appeared that natural convection could be eliminated most readily by enclosing the liquid slurry in a thin horizontal canister and supplying heat to the canister from the top. Either adequate insulation of the vertical edges of the canister or the use of guard heaters can reduce conduction in the horizontal direction to a negligible value.

6.1.2.2 Experimental Apparatus and Technique

Figure 6.1.8 shows schematically the completed thermal conductivity cell. Two thin canisters are formed by the three copper discs which are enclosed in a large diameter Lucite tube insulated with Styrofoam. The upper canister is filled with ion-free water, the thermal conductivity of which is known to within 0.6 percent, while the lower canister is filled with the egg slurry under test. The cell is heated from the top with a disc-type heater and after passing through the two liquid layers, the heat is removed by the heat sink. Constant-temperature water supplied from a large, constant-temperature reservoir, which is thoroughly insulated with Styrofoam, is circulated through the heat sink.

With this arrangement of the cell, thermal conductivity of the slurry sample can be determined from the temperature differences across each liquid (slurry and water) and the thermal conductivity of the water at its mean

Page determined to be Unclassified
Reviewed Chief, RDD, WHS
IAW EO 13526, Section 3.5
Date: JUL 19 2013

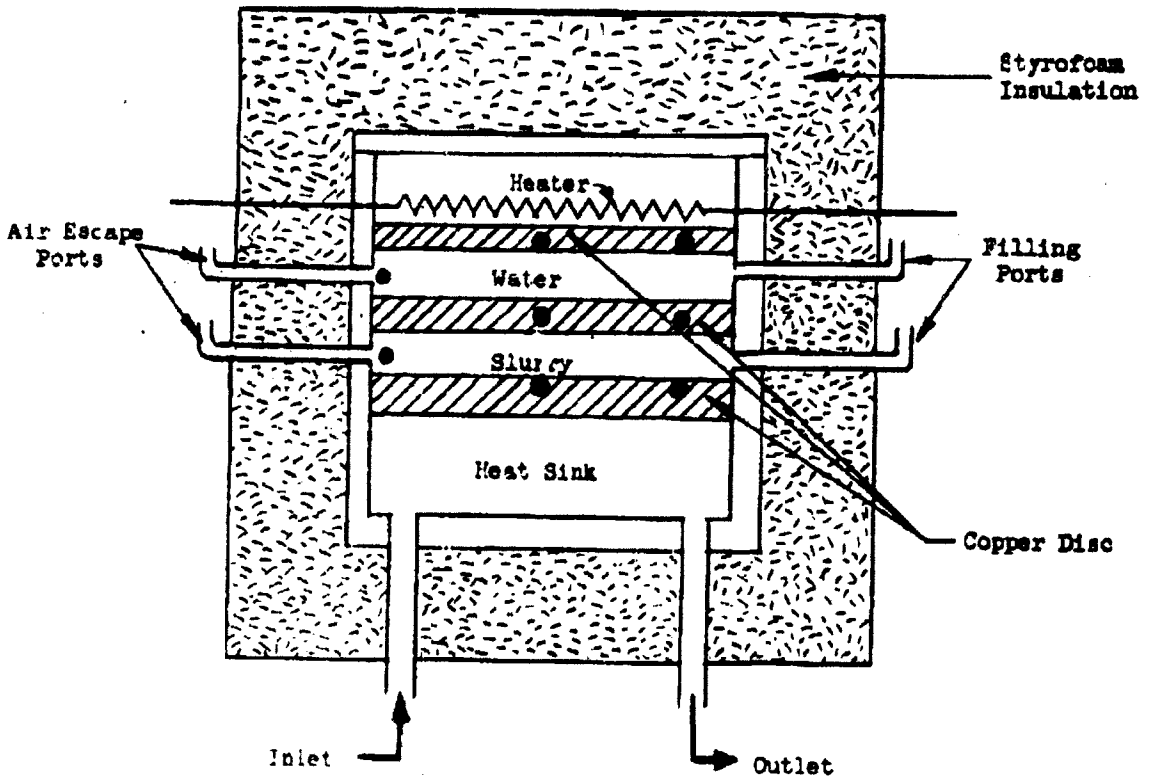

FIGURE 6.1.3 CROSS SECTION OF THERMAL CONDUCTIVITY CELL

Page determined to be Unclassified
Reviewed Chief, RDD, WHS
IAW EO 13526, Section 3.5
Date: JUL 19 2018

temperature. This relationship is derived as follows for one-dimensional heat flow (i.e., negligible heat losses through the walls):

$$q = K_w A \frac{\Delta T_w}{\Delta X} = K_s A \frac{\Delta T_s}{\Delta X} \tag{6.6}$$

where q = heat flux through the cell

K_w = thermal conductivity of water

K_s = thermal conductivity of slurry

ΔT_w = temperature drop across the water layer

ΔT_s = temperature drop across the slurry layer

A = area through which heat flows (equal for both liquids)

ΔX = distance between the discs (equal for both liquids).

Thus:

$$K_w \Delta T_w = K_s \Delta T_s \tag{6.7}$$

and:

$$K_s = K_w \frac{\Delta T_w}{\Delta T_s} \tag{6.8}$$

The temperature drop across each liquid will be measured by copper-constantan thermocouples buried in the surface of the copper discs. The thickness of the liquid layers between the copper discs is 0.254 ± 0.001 cm. With a heat flux of about 7 cal/sec supplied by the heater, a temperature difference of approximately 8° C will be created across each layer. These temperature differentials can be measured with an accuracy of $\pm 2.5\%$ if the maximum error in individual thermocouple readings does not exceed ± 0.1° C.

The accuracy of the thermal conductivity measurements, therefore, will depend largely upon the ability to measure accurately these small temperature differences. To insure maximum accuracy, each of the thermocouples in the

Page determined to be Unclassified
Reviewed Chief, RDD, WHS
IAW EO 13526, Section 3.5
Date: JUL 19 2013

discs has been calibrated by comparison with a high precision, glass-mercury thermometer. The calibration curve obtained is given in Figure 6.1.9. The data points for all six thermocouples used in the discs are plotted in this figure. The maximum deviation from a straight line through these points is less than 0.005 mv, corresponding to a maximum temperature error of less than 0.13° C. Therefore, the desired accuracy in thermal conductivity values should be obtained.

The thermocouples were calibrated over the temperature range of 0 to 34° C. This is the contemplated range over which thermal conductivity measurements will be made.

Each of the copper discs has been lapped and plated with nickel to prevent corrosion. The two thermocouples in each disc are placed one at the center and one near the edge to permit measurement of the radial heat flow in the discs. In addition, a thermocouple is placed at the surface of the Lucite wall halfway between the two discs to permit evaluation of the radial heat losses from the liquid layers. Theoretical calculations show that these radial losses will be negligible; however, experimental verification of this theoretical conclusion will be obtained through the use of the additional thermocouples.

Determination of the thermal conductivity of the four egg slurry samples designated W.E.S. #1, #2, #3, and #4 should be completed in the very near future.

Page determined to be Unclassified
Reviewed Chief, RDD, WHS
IAW EO 13526, Section 3.5
Date: JUL 19 2013

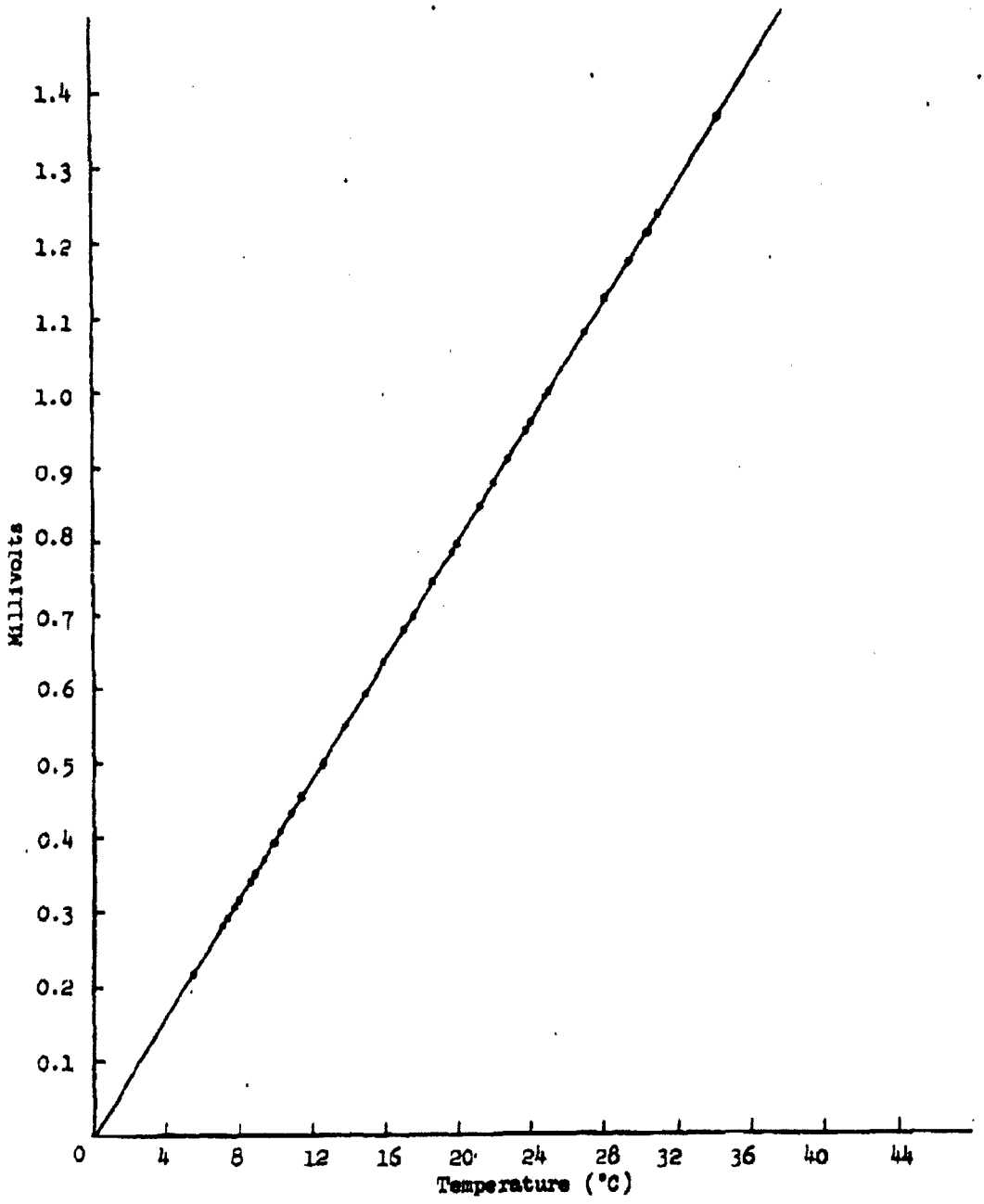

FIGURE 6.1.9 CALIBRATION CURVE FOR 6 COPPER CONSTANTAN THERMOCOUPLES

Page determined to be Unclassified
Reviewed Chief, RDD, WHS
IAW EO 13526, Section 3.5
Date: JUL 19 2013

6.2 Rheological Behavior of Sm Slurries

Agents available as finely divided powders conceivably can be disseminated from a store of the dry material or from thick slurries of the powder in a compatible carrier liquid. The feasibility of either system depends on factors such as number of viable organisms per unit volume in the store, maintenance of viability, energy required to transport material in the store to exit port, flow rates obtainable through exit port, and extent to which the agent breaks up into the finely divided state after dissemination.

To determine the feasibility of using suspensions of dry agents in a fluid, an investigation has been made of the rheological properties of a simulant agent in a compatible liquid. Flow characteristics have been determined as a function of solids concentration, temperature, and shear rate. Rheological equations developed from this data will enable prediction of flow rates through pipes and orifii for given driving pressures.

To date, the flow characteristics as a function of solids concentration has been determined for slurries of Sm in FC-75, a fluorochemical liquid manufactured by Minnesota Mining and Manufacturing Co. Data have been obtained in the temperature range from 20 to -20°C and at shear rates of 3 to 350 sec^{-1}.

6.2.1 Apparatus and Experimental Technique

The apparatus used in determining the rheological properties of Sm slurries is the rotating coaxial cylinder viscometer shown in Figure 6.2.1. The apparatus consists of a rotating inner solid cylinder called the bob and a stationary outer cylinder called the cup. The bob is driven by means of a dead weight operating through a pulley, drum and gear train. The slurry

DECLASSIFIED IN FULL
Authority: EO 13526
Chief, Records & Declass Div, WHS
Date: JUL 19 2013

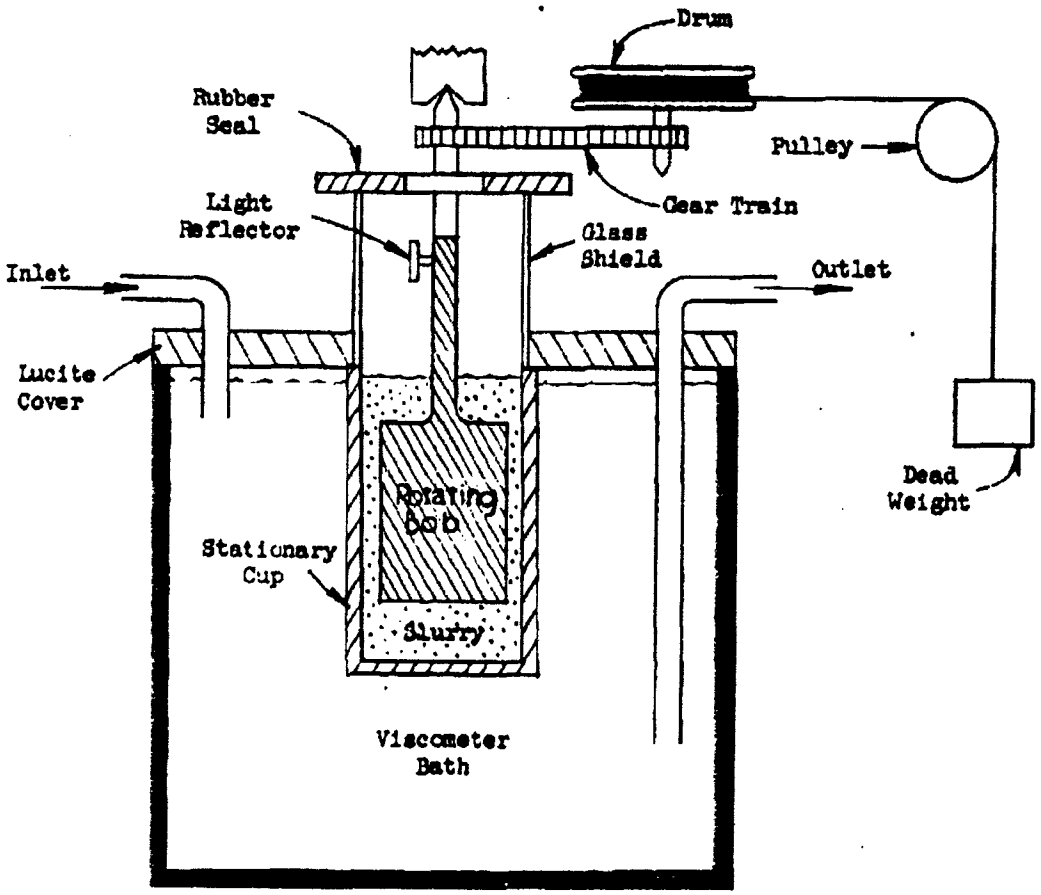

FIGURE 6.2.1 SCHEMATIC DIAGRAM OF THE ROTATING COAXIAL CYLINDER VISCOMETER

Page determined to be Unclassified
Reviewed Chief, RDD, WHS
IAW EO 13526, Section 3.5
Date: JUL 19 2013

is placed in the small annular space between the cup and bob where it is sheared under a constant torque applied to the bob. Because thick slurries can exhibit the property of thixotropy (reversible gel-sol-gel transformation) it is desirable to measure bob revolutions (proportional to shear rate) on a time base. To accomplish this, a reflective coating has been placed on the set screw which holds the bob in position on the drive shaft. The reflector, rotating with the same angular velocity as the bob, reflects light from a pencil source to a photo-electric cell. The electrical pulse, generated once each revolution, is amplified and recorded on a time base using a Brush amplifier-recorder system. In this manner, it is possible to determine change in viscosity with time of shearing.

The viscometer cup is submerged in a small temperature regulated bath. Control of temperature is accomplished in a larger temperature bath equipped with a sealed platinum wire to a mercury-type thermoregulator which controls the operation of a submersible heating element. Liquid from the large constant temperature bath is circulated through the small viscometer bath by means of two small centrifugal pumps to maintain the desired temperature in the small bath within $\pm$ 0.02°C.

Investigations to date have covered a temperature range of 20 to -20°C. Temperature below ambient are achieved by circulating alcohol from a dry ice-alcohol bath through copper coils in the large temperature bath. All components of the system are well insulated to prevent excessive heat loss. Flow of the cooling liquid in the large temperature bath is regulated to provide a temperature slightly lower than that desired and the thermoregulator and heater provide the final control.

Page determined to be Unclassified
Reviewed Chief, RDD, WHS
IAW EO 13526, Section 3.5
Date: JUL 19 2013

The two component parts of the slurry are FC-75 ($C_8F_{16}O$) and Sm, the biological agent simulant. These materials are weighed on an analytical balance to provide the desired solid to liquid weight ratio. The liquid-solid mixture is then blended with a specially designed power stirrer. The stirrer is equipped with a round, perforated disc. Using this technique it has been possible to mix the slurry thoroughly without causing air entrainment. The weighing and mixing of the slurry components is conducted in the viscometer cup to eliminate the need for transferring the sample. Thirty minutes is allowed for the slurry specimen to reach temperature equilibrium with the viscometer bath before testing is begun. Sm weight concentrations which have been investigated to date cover a range from 16.7 to 25 percent.

6.2.2 Experimental Results

The mechanical response of the slurry to a shearing stress is most easily depicted by means of a consistency curve which is a plot of rate of shear ($\dot{\epsilon}$) as a function of shearing stress (τ). The results of the present investigation are presented in this form in Figure 6.2.2. It is apparent from the shape of the consistency curves that the response of these Sm slurries to a shearing stress is complex.

Not apparent from Figure 6.2.2 is the fact that Sm in FC-75 is a gel system exhibiting a yield point. In other words, the consistency curves intersect the shear stress axis at a finite, positive value. The yield points for the various concentrations and temperatures have not been plotted in Figure 6.2.2 because of the extremely variable results which have been obtained thus far. In a typical experiment it was found that the bob would not begin rotating until sufficient torque was placed on it.

Page determined to be Unclassified
Reviewed Chief, RDD, WHS
IAW EO 13526, Section 3.5
Date: JUL 19 2013

FIGURE 6.2.2 CONSISTENCY CURVES FOR Sm SLURRIES

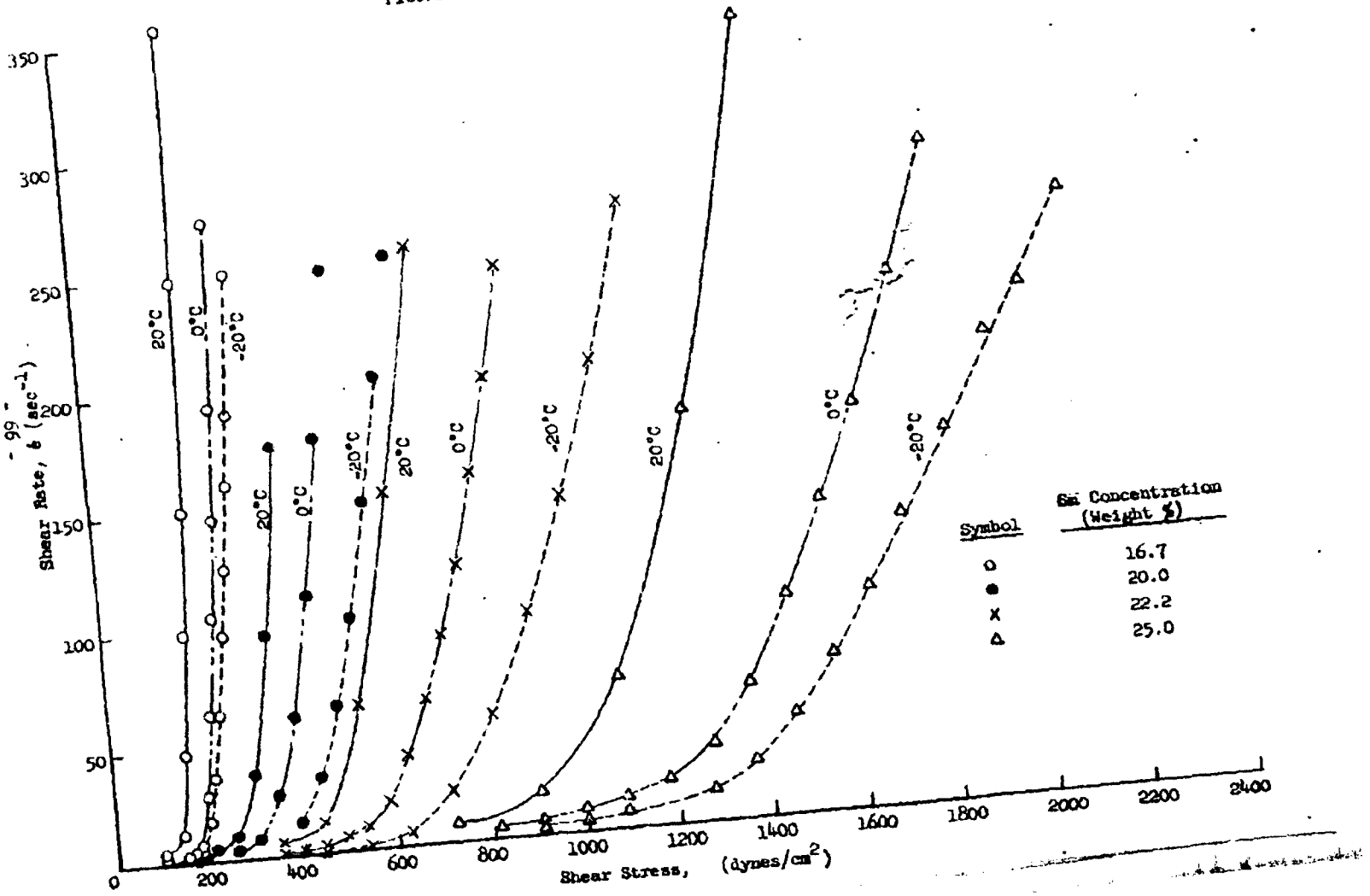

Page determined to be Unclassified
Reviewed Chief, RDD, WHS
IAW EO 13526, Section 3.5
Date: JUL 19 2019

When the critical torque was exceeded, rotation would begin slowly, then cease. Additional torque was required to initiate rotation again, but movement would soon stop. By gradually increasing the torque applied, a value finally was reached which produced a slow but constant rate of rotation. The corresponding shearing stress and rate of shear for this condition are the initial points of the consistency curves in Figure 6.2.2. Future work will be directed at providing a realistic value for the yield stress of the slurries.

The yield value observed in many slurry systems is believed to be a measure of the force of flocculation per unit area which exists between suspended particles[6.2.1]. When the yeild value is exceeded, the flocculated particles begin to separate. Upon increasing the rate of shear, the solvent which had been trapped within the voids of the flocculated material is released and the resistance to flow decreases. This phenomenon gives rise to a consistency curve which is convex toward the shear stress axis (Figure 6.2.2). This type of flow behavior cannot be represented by a single viscosity parameter as is the case with Newtonian materials for which a plot of shearing stress versus rate of shear yields a straight line passing through the origin. For Newtonian materials, the viscosity is single valued, i.e.,

$$\mu = \frac{\tau}{\dot{e}} = \text{constant}$$

where: μ = coefficient of viscosity

τ = shear stress

$\dot{e}$ = rate of shear.

6.2.1 Eirich, F. R., Rheology, 3, Academic Press, New York, p. 198 (1960).

Page determined to be Unclassified
Reviewed Chief, RDD, WHS
IAW EO 13526, Section 3.5
Date:
JUL 19 2013

The consistency curve obtained with Sm slurries has been termed "quasi-plastic"[6.2.2] and represents one of several different types of "non-Newtonian" flow behavior.

The term apparent viscosity, η, is frequently used in the investigation of non-Newtonian materials. Apparent viscosity is defined as the ratio of shearing stress to rate of shear:

$$\eta = \frac{\tau}{\dot{\theta}} \tag{6.9}$$

It is apparent from the shape of the curves presented in Figure 6.2.2 that η decreases with increasing rate of shear. Therefore, the apparent viscosity has little significance unless it is specified for a definite condition of shearing stress and shear rate.

A qualitative statement can be made in terms of apparent viscosity about the consistency curves presented in Figure 6.2.2. The apparent viscosity at a given rate of shear increases with decreasing temperature and with increasing Sm concentration. Calculated apparent viscosities at a rate of shear of 200 sec^{-1} are presented in Table C.I.

TABLE 6.I

Effect of Temperature and Solids Concentration on the Apparent Viscosity of Sm Slurries

(Shear Rate = 200 sec^{-1})

Solids Conc. (% by weight of Sm)	Apparent Viscosity (η) (poise)		
	20° C	0° C	- 20° C
16.7	1.0	1.4	1.6
20.0	2.1	2.6	3.2
22.2	3.4	4.3	5.4
25.0	6.5	8.4	9.8

6.2.2 Houwink, R., Elasticity, Plasticity ans Structure of Matter, Harren Press, Washington D. C., p. 10 (1953).

Page determined to be Unclassified
Reviewed Chief, RDD, WHS
IAW EO 13526, Section 3.5
Date: JUL 19 2013

Many formulae can be found in the literature[6.2.3] to describe the type of curves obtained with Sm slurries. The Herschel and Bulkley formula[6.2.4] is:

$$\dot{\epsilon} = \frac{1}{\eta^*} (\tau - f)^n \qquad (6.10)$$

where: f = yield stress

η^* and n = constants for a given curve.

η^* is not the same as the apparent viscosity η since $n \neq 1$. The dimensions of η^* are different from those of η, so that the value of η^* cannot be expressed in poises.

One of the objectives of the rheological investigation of Sm slurries is to obtain such formula describing the shear stress-rate of shear relationships as a function of temperature and solids concentration. With these formulae it will be possible to calculate flow rates through pipes and orifi as a function of driving pressure.

A second objective of this study is to provide rheological data for use in theoretical and experimental studies on the aerodynamic breakup of these slurries. Equations have been developed and experimentally verified[6.2.5-6.2.7] for predicting the drop size and size distribution resulting from dissemination of Newtonian fluids. However, with non-Newtonian materials the property of viscoelasticity will retard the breakup of fluid drops. Thus, new theories will have to be developed and experimentally verified for these materials.

6.2.3 Reiner, J., J. Rheology 1: 11 (1929).

6.2.4 Herschel, W. and Bulkley, R., Koll Z. 39: 291 (1926).

6.2.5 Turner, G. M. and Moulton, R. W., Chem. Eng. Prog., 49: 4, 185 (1953).

6.2.6 Nukiyama, S. and Tanasawa, Y., Trans. Soc. Mech. Engrs. (Japan) 4: nos. 14, 15; 5: no. 18; 6: nos. 22, 23 (1938-40).

6.2.7 Bitron, M. O., Ind. & Eng. Chem. 47: 23 (1955).

Page determined to be Unclassified
Reviewed Chief, RDD, WHS
IAW EO 13526, Section 3.5
Date: JUL 19 2013

Another objective of the rheological investigation is to interpret the consistency curves in terms of particle shape, particle-particle interactions, and particle-liquid interactions. A knowledge of the basic factors which determine the shear stress-rate of shear response is necessary in order to alter the components of the slurry system or to incorporate additives which will create more desirable flow characteristics.

Efforts to date have been concentrated on obtaining the consistency curves shown in Figure 6.2.2 and in attempting to represent these curves by a generalized formula. The latter work is not yet complete. The preliminary analysis which has been done will be presented at this time.

The Herschel and Bulkley formula, Equation (6.10), has been applied to the Sm slurry consistency curves with some degree of success. Equation (6.10) can be rewritten as follows:

$$\log \dot{e} = n \log (\tau - f) - \log \eta^* \qquad (6.11)$$

It follows that a log-log plot of $\dot{e}$ versus $(\tau - f)$ will yield a straight line of slope n and intercept - log η^*. Several such plots of data from Figure 6.2.2 are presented in Figure 6.2.3. Equation (6.11) appears to represent adequately the consistency curves for shear rates in excess of 10 sec^{-1} for all but the thickest slurry (25% Sm by weight). The theoretically determined yield stresses used in obtaining the straight lines of Figure 6.2.3, however, are larger than the experimentally observed yield stresses by a factor of at least two in every case. Therefore, the theoretical curves will diverge from the experimental curves at a point in the vicinity of 10 sec^{-1} shear rate and will approach the shear stress axis more rapidly. As was discussed previously, future experimental work will be directed at obtaining higher concentrations of Sm in FC-75.

Page determined to be Unclassified
Reviewed Chief, RDD, WHS
IAW EO 13526, Section 3.5
Date: JUL 19 2013

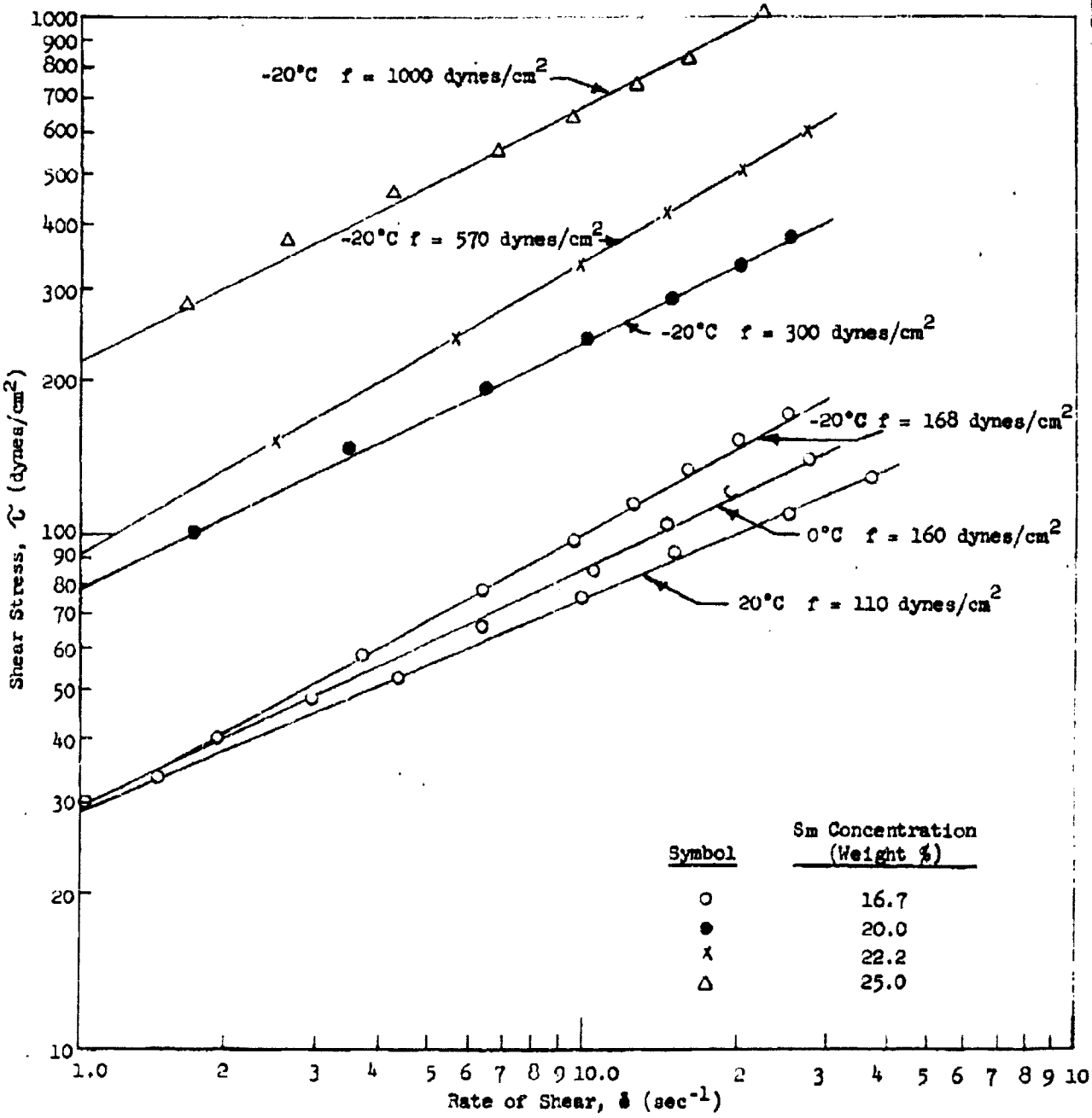

FIGURE 6.2.3 APPLICABILITY OF RELATIONSHIP $\dot{e} = \frac{(\tau - f)^n}{\eta^*}$ to SM SLURRIES

Page determined to be Unclassified
Reviewed Chief, RDD, WHS
IAW EO 13526, Section 3.5
Date:
JUL 19 2019

Upon obtaining this data, further attempts will be made to represent the consistency curves in mathematical form. Determination of the constants n and η^* Equation (6.11) from the curves shown in Figure 6.2.3 has not been completed at this time.

A second approach toward representing the Sm slurry consistency curves has been investigated. Again, this approach is limited to data obtained at shear rates in excess of 10 sec^{-1}. This approach is based on the concept of apparent viscosity η. When the apparent viscosities are calculated for various points on a single consistency curve and these values of η are plotted against the corresponding rates of shear, curves of the type shown in Figure 6.2.4 are obtained. From a preliminary analysis of these curves, it appears that an equation of the form:

$$\eta = k \dot{e}^{-\frac{1}{n}} \qquad (6.12)$$

where: k and n are constants,

represents the data adequately at all temperatures and Sm concentrations. Furthermore, it appears that n does not vary with solids concentration or temperature as evidenced by the equal slope of the lines plotted in Figure 6.2.5. An analysis of the dependence of k on Sm concentration and temperature has not been completed at this time. This approach appears to offer considerable promise for attaining a generalized formula representing flow behavior at shear rates in excess of 10 sec^{-1}, but does not take into account the existence of a yield point. Further analysis will be needed before adequate mathematical representation of the rheological behavior of these slurries at very low shear rates is achieved.

Page determined to be Unclassified
Reviewed Chief, RDD, WHS
IAW EO 13526, Section 3.5
Date: JUL 19 2019

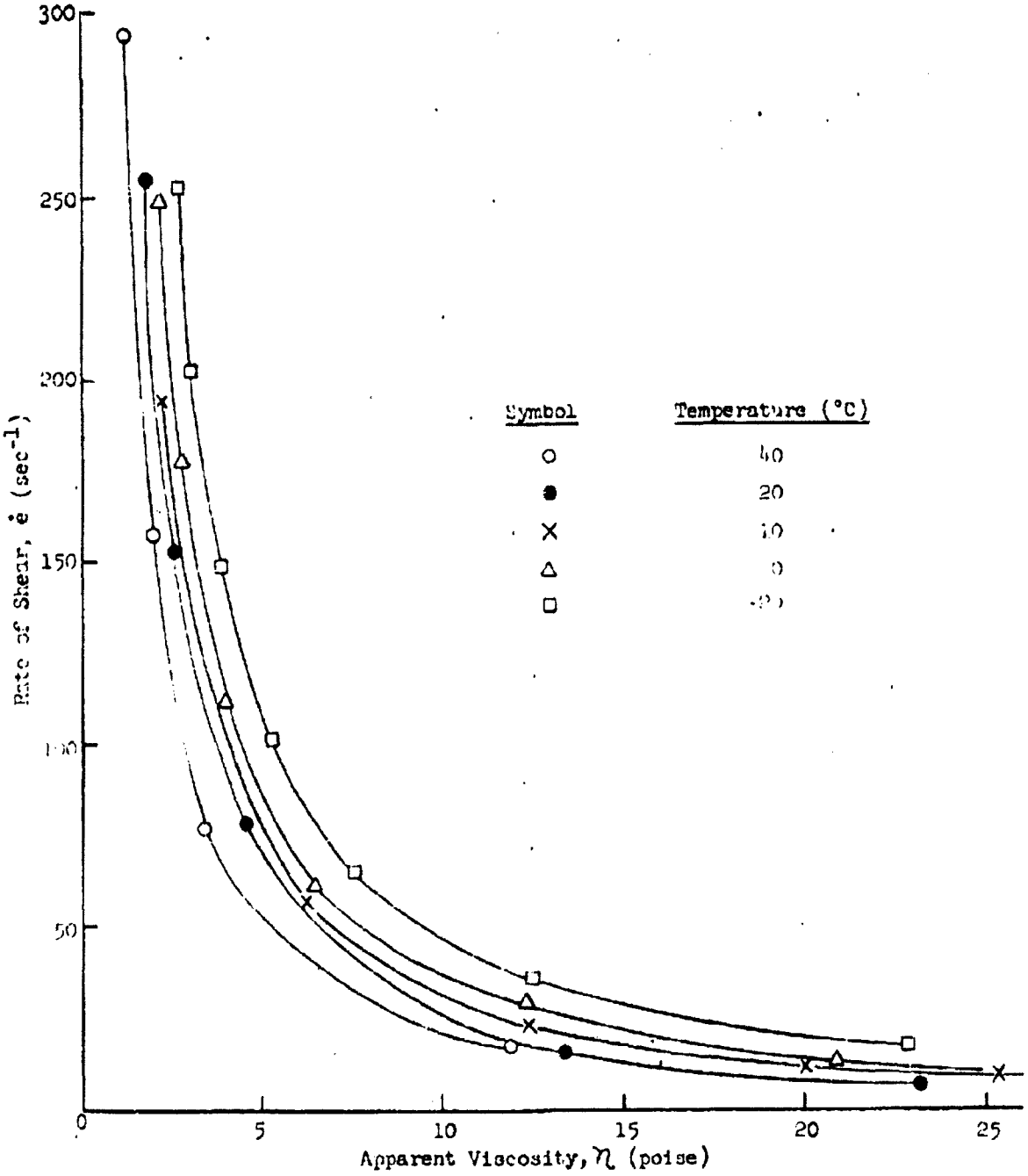

FIGURE 6.2.4 APPARENT VISCOSITY VERSUS RATE OF SHEAR (20.0% Sn BY WEIGHT)

Page determined to be Unclassified
Reviewed Chief, RDD, WHS
IAW EO 13526, Section 3.5
Date: JUL 19 2013

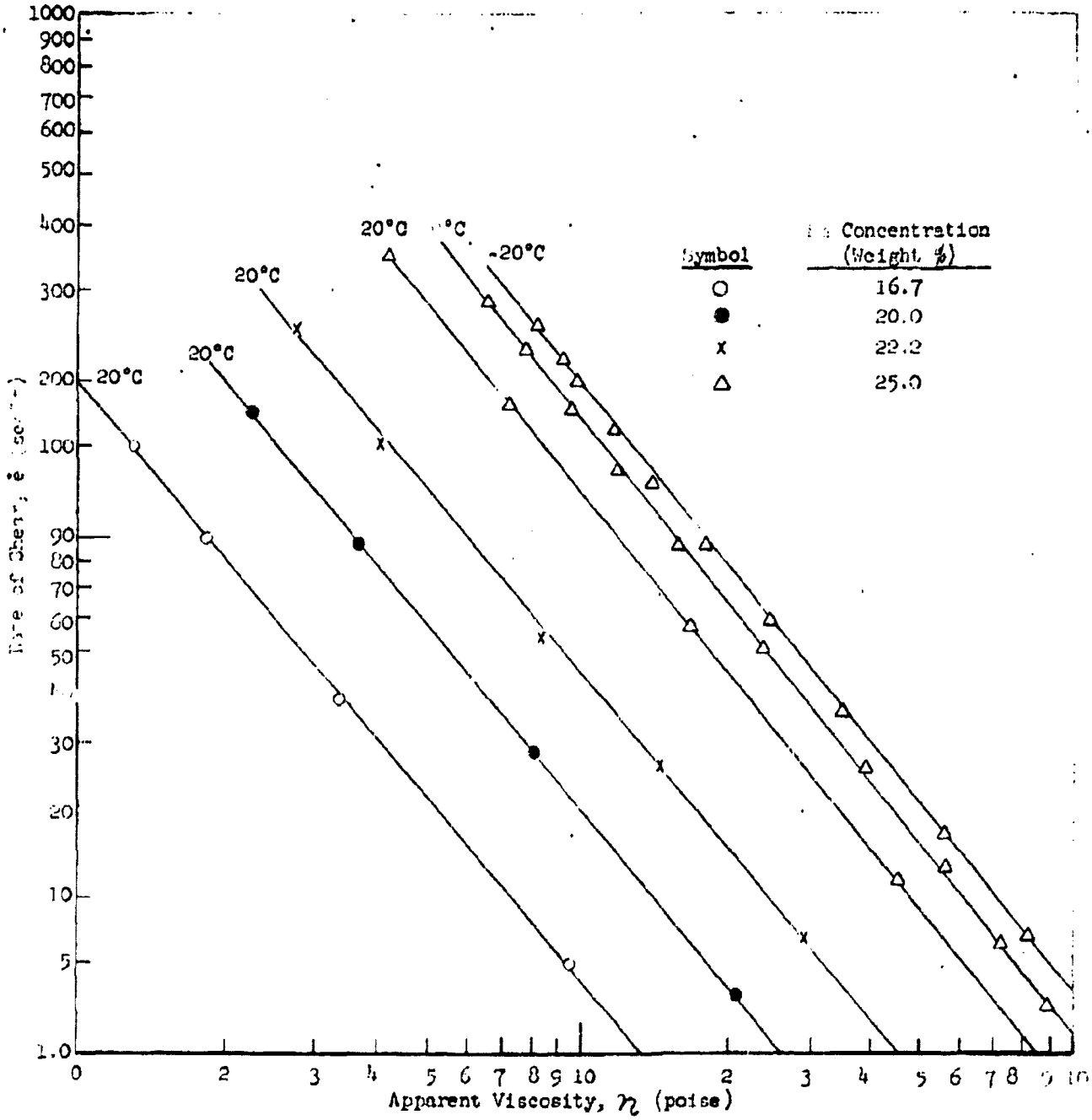

FIGURE 6.2.5 . APPLICABILITY OF RELATIONSHIP

$\eta = k \dot{\epsilon}^{\frac{1}{n}}$ TO Sm SLURRIES

Page determined to be Unclassified
Reviewed Chief, RDD, WHS
IAW EO 13526, Section 3.5
Date: JUL 19 2013

This investigation of the flow behavior of Sm slurries has been simplified by the fact that no evidence of thixotropy has been encountered in obtaining the consistency curves. Measurements are performed by obtaining shear rates at increasing and then decreasing shear stresses. The up and down curves agree very well. In addition, the 16.7% Sm slurry was sheared continuously under a 200 dyne/cm^2 shear stress for 3000 revolutions of the bob with no appreciable change in apparent viscosity. Thicker slurries will be tested in the same manner to verify the present opinion that thixotropic behavior is absent in this slurry system.

In addition to the future work which has been mentioned in this discussion, it is planned to extend this rheological investigation to higher shear rates. A rate of 350 sec^{-1} is about the upper limit for the coaxial-cylinder rotational viscometer being used. At higher rates turbulence and centrifugal effects distort the results obtained. In order to examine flow behavior at higher rates of shear, capillary viscometry will be employed using compressed nitrogen as the driving force.

Page determined to be Unclassified
Reviewed Chief, RDD, WHS
IAW EO 13526, Section 3.5
Date: JUL 19 2018

7. DISSEMINATION AND DEAGGLOMERATION STUDIES

During this reporting period, we have continued work with the high-subsonic wind tunnel in connection with our study of the use of slipstream energy for deagglomeration of finely divided solid materials. This work has included experiments to evaluate the high velocity sampling system and also modifications of the apparatus to permit dissemination experiments with S. simulant, as discussed in sections 7.1 and 7.2 below.

7.1 Experiments With the Isokinetic Sampling Probe

Experiments to determine the particle sampling characteristics of the high velocity sampling probe have been made, utilizing the wind tunnel and piston-type disseminator discussed in our previous technical report.[7.1]

In these studies, two types of talc.- Mistron 18 and 25 - were injected into the wind tunnel where the air velocity was maintained at Mach number 0.50 The resulting aerosol was then sampled at a distance of 67 cm downstream of the injector (10 cm upstream of the end of the wind tunnel) with the probe. Since the aerosol concentration varies from top to bottom in the tunnel, particle size data were obtained at two vertical locations, 0.4 cm and 1.5 cm from the top tunnel wall. A calibrated vacuum pump located downstream of the sampling probe was regulated so that the appropriate flow rate for isokinetic flow at the probe inlet was obtained. Off-design conditions, 50% flow rate and angle of attack, were also investigated.

7.1 General Mills Report No. 2161, Second Quarterly Progress Report on Dissemination of Solid and Liquid BW Agents (Unclassified Title) Feb. 13, 1961, p. 35 (Confidential).

Page determined to be Unclassified
Reviewed Chief, RDD, WHS
IAW EO 13526, Section 3.5
Date: JUL 19 2013

The samples were collected on 76 mm, type AA, Millipore filters which have an 0.8 micron pore size. In order to minimize the effect of particles settling in the sampling system, the filter was located at the probe exit.

In the particle size analysis, the filters were dissolved in acetone and the resulting solution was extracted from the sample after a preparatory centrifuge step. The size distribution was then determined by using the well known Whitby Centrifuge technique.

The advantage of using talc in these studies is that it does not form strong agglomerants. This is important, since the degree of agglomeration may be affected by both the dissemination and size analysis processes. Microscopic observations of the talc indicated that the particles consisted of platelets and acicular both before and after dissemination.

Control data on the particle size distribution of the two types of talc were also obtained by the Whitby Centrifuge technique. Two analyses were made for each type which showed good reproducibility. They were averaged together for comparison with samples taken in the wind tunnel.

Figure 7.1.1 shows the particle size frequency distribution by mass of talc, Mistron 18, before and after dissemination at the isokinetic flow rate. The data are presented as percent in the size range shown on the abscissa and are plotted at the midpoint of the range. The data show the bi-modal distribution resulting from the two particle shapes observed under the microscope.

Statistical data on the particles in each sample, the mass median diameter (MMD), geometric standard deviation (GSD), and percent by mass smaller than 5 microns are also given in the figure.

Page determined to be Unclassified
Reviewed Chief, RDD, WHS
IAW EO 13526, Section 3.5
Date: JUL 19 2013

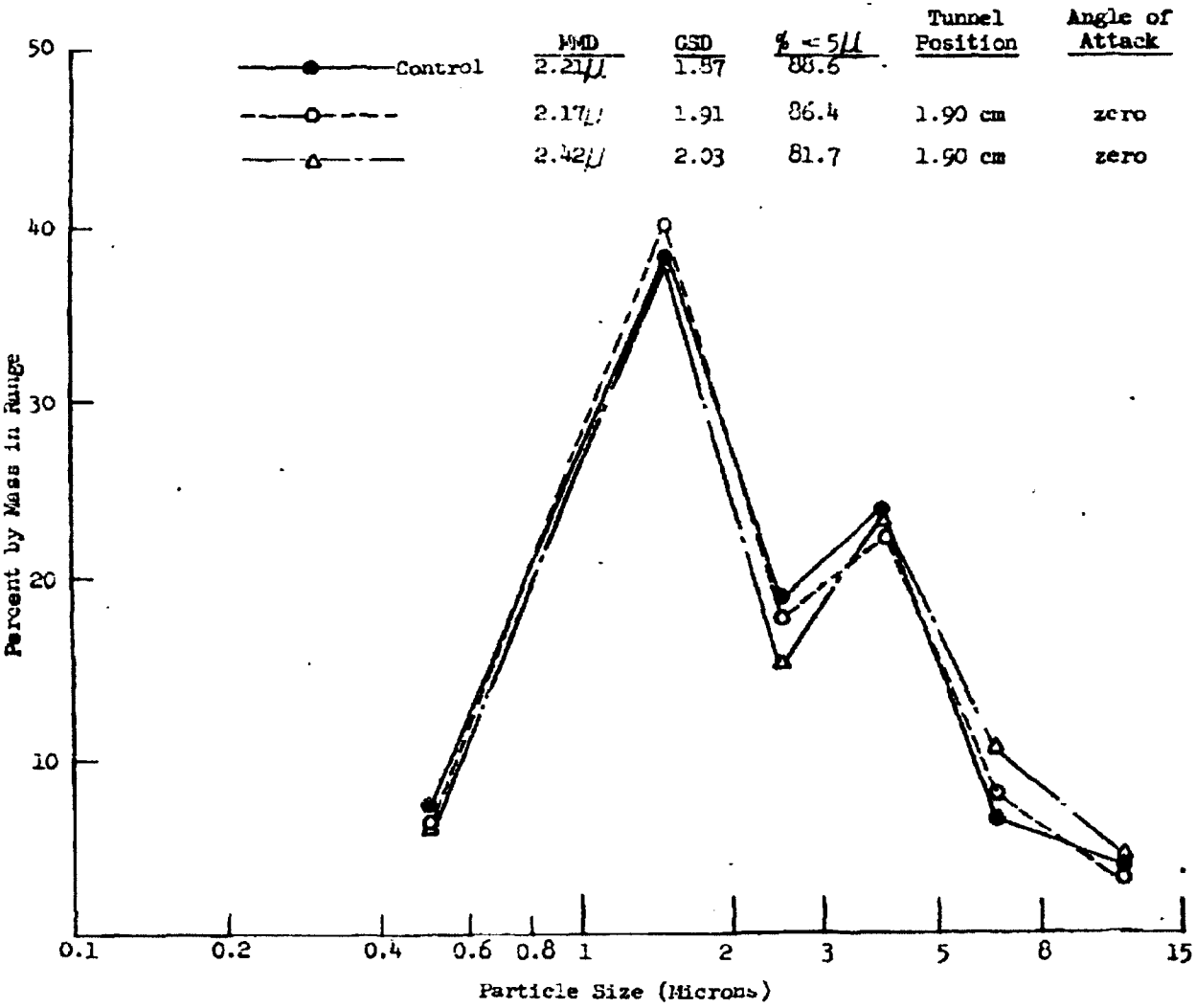

FIGURE 7.1.1 PARTICLE SIZE FREQUENCY DISTRIBUTION FOR MISTRON #18 TALC BEFORE DISSEMINATION AND AFTER SAMPLING AT ISO-KINETIC CONDITIONS TUNNEL MACH NUMBER 0.5

Page determined to be Unclassified
Reviewed Chief, RDD, WHS
IAW EO 13526, Section 3.5
Date: JUL 19 2013

It is felt that the data indicate that the sampling technique employed in this work is satisfactory. The small scatter is believed to be largely due to random error in the sampling and size analysis processes.

A shift in particle size distribution due to systematic errors resulting from non-isokinetic flow conditions is shown in Figure 7.1.2. The flow rate in both cases was 50 percent of the proper flow rate, while the angle of attack in each case was zero and 5 degrees. At zero degrees angle of attack the sample was biased toward the larger particles, indicating that the smaller ones followed the diverging streamlines more readily than the large ones at the probe inlet. At 5 degrees angle of attack there is bias towards small particles; a very interesting result. It is felt that the interaction between the flow streamlines and particle paths at the probe inlet are quite complicated under this condition and we will not attempt to explain it in this discussion, since it will not be pertinent in future tests (i.e., the probe will be mounted at zero angle of attack in all dissemination studies).

Figures 7.1.3 and 7.1.4 show the particle size frequency distribution for talc, Mistron 25. In this case there is very close agreement between the isokinetic samples and the control. The relatively better correlation obtained with this material is felt to be due to the smaller particle size range. The off-design data show again the tendency for bias towards larger particles when 50 percent of the isokinetic flow rate is drawn through the sampler at zero angle of attack.

It should be noted that the Mistron 18 data were obtained with the probe at 1.90 cm from the tunnel top wall, while that of Mistron 25 were obtained at

Page determined to be Unclassified
Reviewed Chief, RDD, WHS
IAW EO 13526, Section 3.5
Date: JUL 19 2018

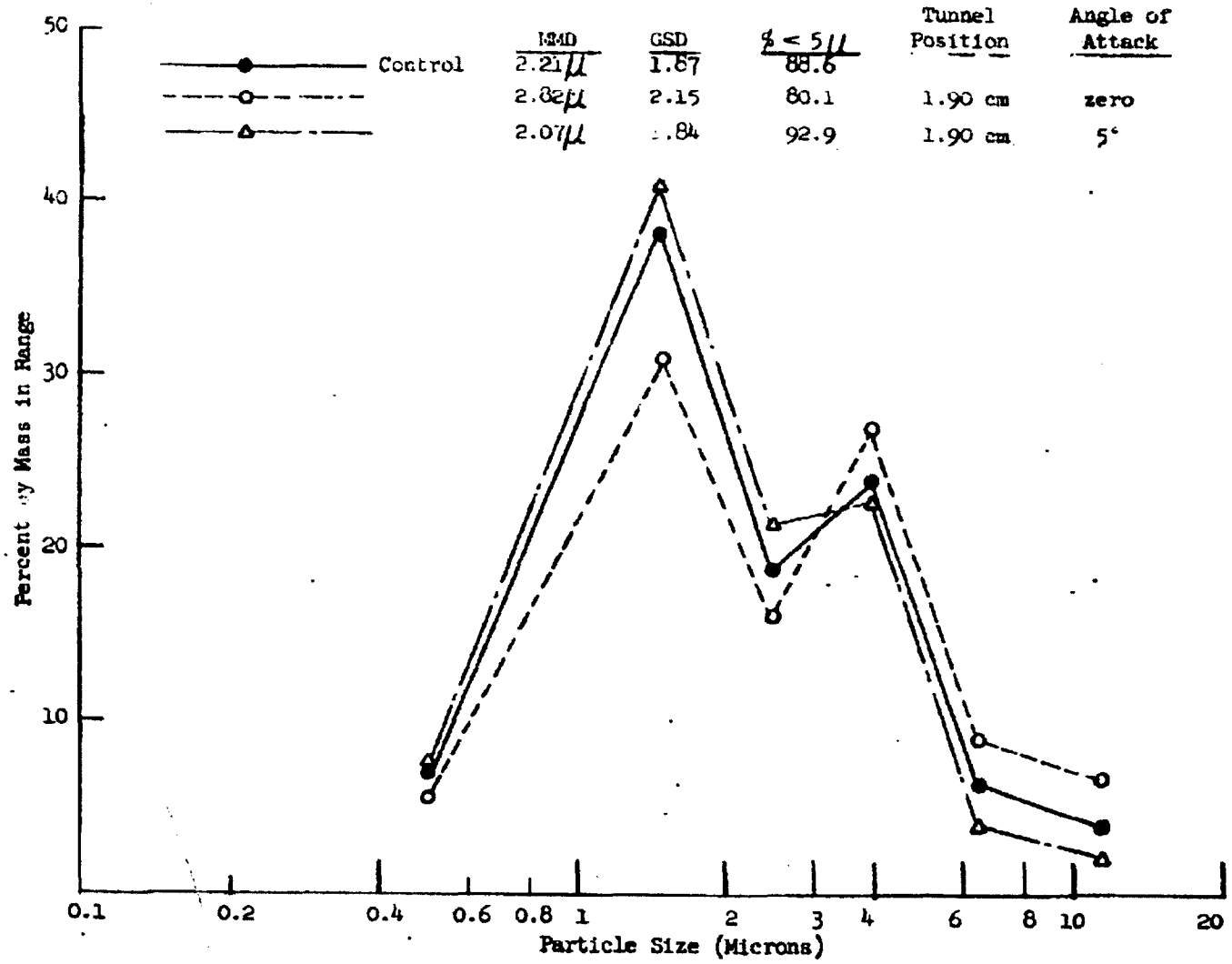

FIGURE 7.1.2 PARTICLE SIZE FREQUENCY DISTRIBUTION FOR MISTRON #18 TALC BEFORE DISSEMINATION AND AFTER SAMPLING AT NON-ISOKINETIC (50% FLOW) CONDITIONS. TUNNEL MACH NUMBER 0.5

Page determined to be Unclassified
Reviewed Chief, RDD, WHS
IAW EO 13526, Section 3.5
Date: JUL 19 2018

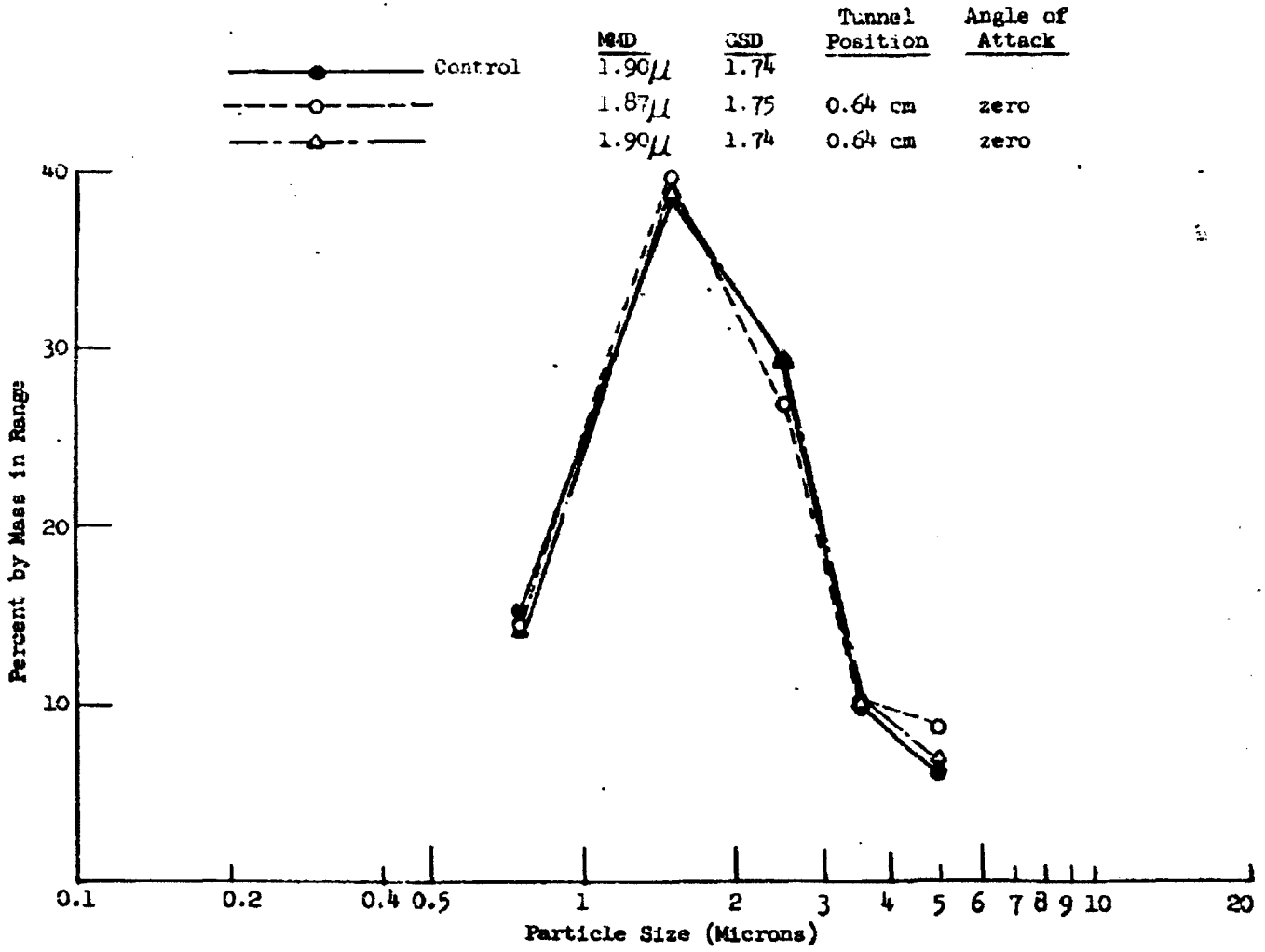

FIGURE 7.1.3 PARTICLE SIZE FREQUENCY DISTRIBUTION FOR MISTRON #25 TALC BEFORE DISSEMINATION AND AFTER SAMPLING AT ISOKINETIC CONDITIONS. TUNNEL MACH NUMBER 0.5.

Page determined to be Unclassified
Reviewed Chief, RDD, WHS
IAW EO 13526, Section 3.5
Date: JUL 19 2013

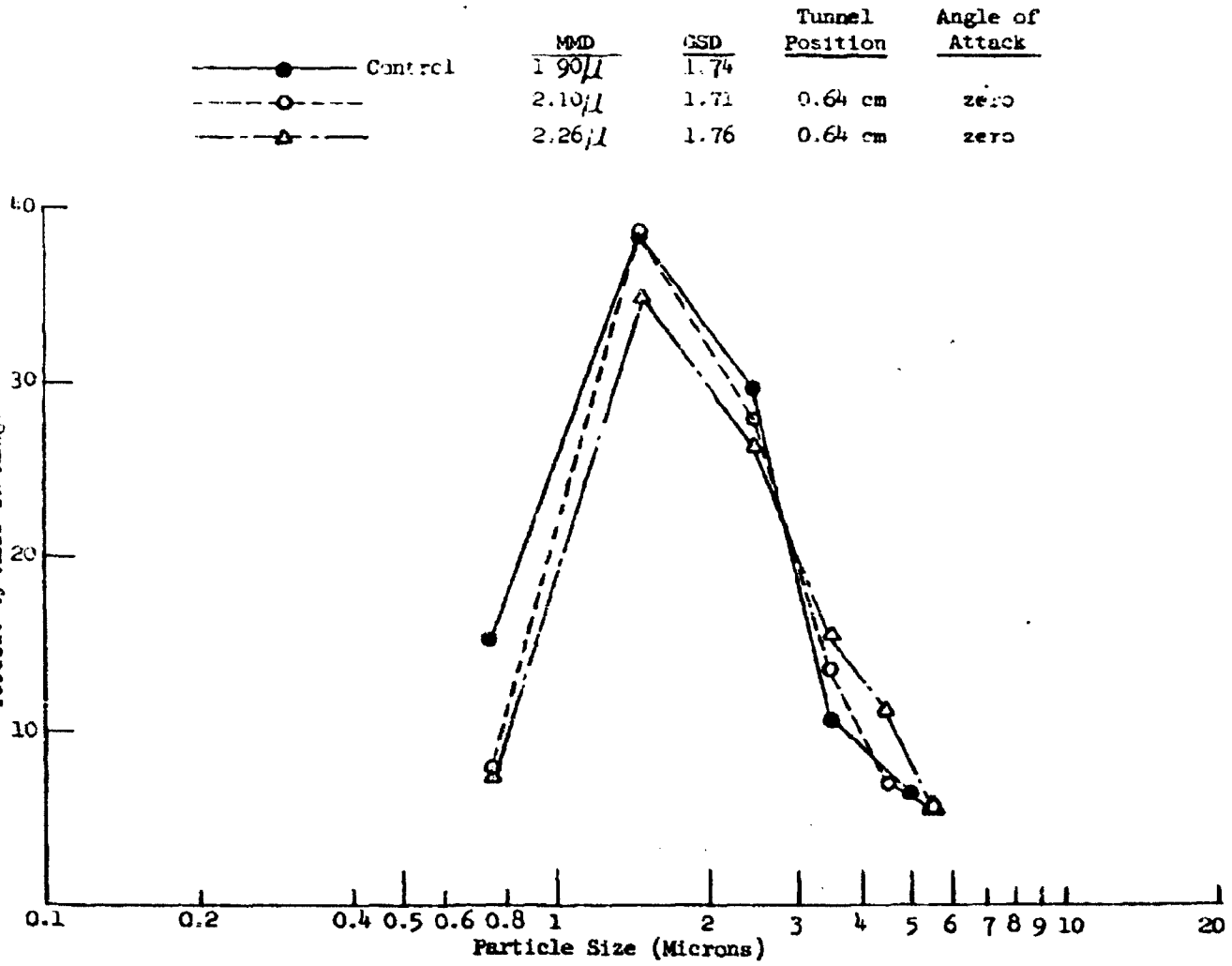

FIGURE 7.1.4 PARTICLE SIZE FREQUENCY DISTRIBUTION FOR MISTRON #25 TALC BEFORE DISSEMINATION AND AFTER SAMPLING AT NON-ISOKINETIC (50% FLOW) CONDITIONS. TUNNEL MACH NUMBER 0.5

Page determined to be Unclassified
Reviewed Chief, RDD, WHS
IAW EO 13526, Section 3.5
Date: JUL 19 2013

0.64 cm. In studying the isokinetic samples in each case, it seems that the particle size distribution is quite uniform at both these levels in the tunnel.

Additional experiments, similar to those discussed here, will be conducted with talc at tunnel Mach numbers 0.5 and 0.8. The results should make possible a statistical analysis of the random errors associated with high velocity sampling and thereby establish the accuracy of the sampling probe for dissemination studies.

7.2 Modification of the Wind Tunnel Apparatus to Permit Dissemination Experiments with Sm Simulant

During this reporting period we have designed apparatus modifications to permit the dissemination of Sm simulant in the high-subsonic wind tunnel. The principal change includes a closed filter chamber, approximately one cubic meter in size, which receives the discharge from the wind tunnel. The chamber is of welded aluminum construction, and is designed for a pressure differential of approximately 0.15 Atmosphere, so that high efficiency filtering of the discharge air can be accomplished. The filter opening has an area of approximately 1/3 meter^2. Two layers of I.P.C. filter paper will be used at this point in the system. The filter chamber includes a sealed door for access to the isokinetic sampling probe and related equipment. This chamber will provide protection against discharging Sm aerosols into the occupied areas of our laboratories.

Another apparatus modification is the addition of instrumentation to record the displacement versus time for the piston-type powder disseminator

Page determined to be Unclassified
Reviewed Chief, RDD, WHS
IAW EO 13526, Section 3.5
Date: JUL 19 2013

on the wind tunnel. Since this process takes place in about 1/100 of a second, a high speed system is required. A Minneapolis Honeywell Visicorder is employed which records the signal from a slide-wire resistor which is directly connected to the feeding piston.

The record is obtained on a light sensitive paper which receives a light beam from a galvanometer in the recorder. Knowledge of the piston displacement versus time and the bulk density of the sample of powder permits calculation of the instantaneous feeding rate

During the next reporting period, several experiments on the dissemination of dust simulant are planned, including investigation of the effects of powder mass flow rate, bulk density, moisture content, and air velocity.

Page determined to be Unclassified
Reviewed Chief, RDD, WHS
IAW EO 13526, Section 3.5
Date: JUL 19 2013

8. STUDY OF THE INFLUENCE OF EFFECTIVE FILLING DENSITY ON THE AERODYNAMIC DRAG OF SOLID AGENT EXTERNAL STORES

A brief analysis has been made to explore the importance of the effective filling density, ρ_f, on the aerodynamic drag of solid agent external stores. The term ρ_f is arbitrarily defined as the product of the mean bulk density of the finely divided solid agent and the fraction of the total volume enclosed by the skin of the aircraft store which is occupied by the agent.

The aerodynamic study presented in our Second Quarterly Progress Report[8.1] was used as a basis for this analysis. Calculations were based on data given in Figure 5.1.2 of Reference 8.1, on the drag of a NACA-65A Series store of fineness ratio 8.0. Figure 8.1 summarizes results for sea level flight at 0.7 Mach number, for illustrative cases in which the agent payloads are 100, 200, 300 and 400 pounds.

The influence of the effective filling density, ρ_f, was found to be quite pronounced. Figure 8.1 shows the rapid increase in drag penalty when ρ_f decreases to values in the range of 0.2 to 0.05 gm/cm^3. As an example, 400 pounds of a finely divided solid agent in a low density state (assume a bulk density of 0.2) contained in a store in which it occupies 50 percent of the total volume ($\rho_f = 0.1$) would result in a drag of approximately 600 pounds. The same mass of agent carried in a compacted form (for example, a bulk density of 0.5) in a store in which 70% of the

---

8.1 General Mills, Inc. Report No. 2161, Second Quarterly Progress Report on Dissemination of Solid and Liquid BW Agents. (Unclassified Title) February 13, 1961, pp. 69-80 (Confidential)

DECLASSIFIED IN FULL
Authority: EO 13526
Chief, Records & Declass Div, WHS
Date: JUL 19 2013

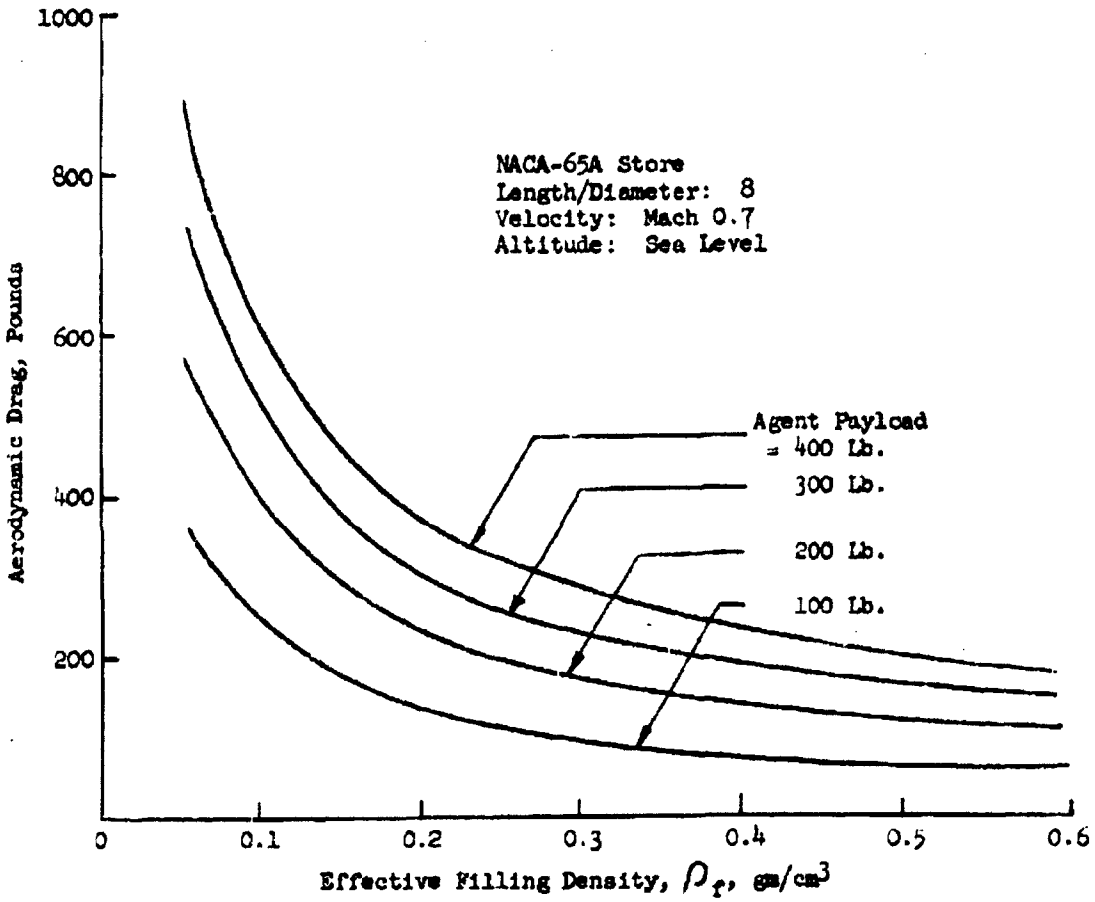

FIGURE 8.1 AERODYNAMIC DRAG VERSUS EFFECTIVE FILLING DENSITY FOR SOLID AGENT STORES

DECLASSIFIED IN FULL
Authority: EO 13526
Chief, Records & Declass Div, WHS
Date: JUL 19 2013

volume is filled (ρ_f = 0.35), would result in a drag force of approximately 240 pounds, or 40% of the first case. The illustration points out that there is a substantial incentive to avoid store designs which result in very low values of ρ_f. On the other hand, the technical problems incurred in reaching very high values of ρ_f (above 0.4) may outweigh the advantages.

The results of the analyses will be considered in future work on disseminating store concept selection and experimentation on feeding techniques.

DECLASSIFIED IN FULL
Authority: EO 13526
Chief, Records & Declass Div, WHS
Date: JUL 19 2013

9. SYSTEM STUDY

A systems study on the dissemination of solid BW agents has been initiated by the Systems Analysis Group at General Mills, Inc.

The initial work has included a review of the recent literature on mathematical models for diffusion of the aerosol clouds, discussions with members of the Ft Detrick technical staff and a study to establish an approach for the first detailed calculations.

To arrive at an evaluation of the effectiveness of a BW mission, a large number of factors must be taken into account, including delivery vehicle capabilities, vehicle attrition, agent dosage requirements, disseminator storage capacity and flow rate, flight speed and height of release, dissemination efficiency, aerosol diffusion and meteorological influences, aerosol physical and biological decay, lung retention, and other factors associated with the end effect such as incubation period, duration of incapicitation and mortality rate.

The work in the near future will be restricted mainly to investigation of target area coverage as influenced by the agent dosage requirements, agent capacity, flow rate, flight speed, height of release, dissemination efficiency, aerosol diffusion and decay.

The above effects will be investigated through an appropriate diffusion model. Various models* have been developed for atmospheric

---

*See for example: 9.1 Meteorology and Atomic Energy, AECU 3066, U. S. Gov't. Printing Office, pp. 38-58, (1955).

9.2 Barad, M. L., et al., A Diffusion-Deposition Model for In-Flight Release of Fission Fragments, AFCRC-TN-60-400 (June 1960).

9.3 Jones, S. P. and S. C. Stern, The Dissemination of Antipersonnel Agents by Means of an Elevated Line Source, GMI Report, (Aug. 1957) (Secret).

DECLASSIFIED IN FULL
Authority: EO 13526
Chief, Records & Declass Div, WHS
Date: JUL 19 2013

diffusion of particulate matter and in general these agree within a factor of two. Since the variation of ground level dosage varies over many orders of magnitude, this can be considered good agreement. The model used in this investigation will be that developed by K. Calder, which was recently discussed with Mr. Felix Craw at Fort Detrick. The refinements to be made are:

1) It will be assumed that infection is proportional to the number of particles (with at least one viable agent) that the lung retains rather than the total number of viable agents;

2) It will be assumed that the decay rate is proportional to the surface area of the particle;

3) The decay rate will be assumed to decrease with increasing time.

These refinements seem reasonable after a discussion with Mr. Bourland of Ft. Detrick concerning recent experimental results. The diffusion model with these modifications is being programmed on a digital computer. The results of this computation will be plots of probability of infection as a function of downwind distance for various weather conditions and particle sizes.

DECLASSIFIED IN FULL
Authority: EO 13526
Chief, Records & Declass Div, WHS
Date: JUL 19 2013

10. WORK ON LIQUID AGENT DISSEMINATING STORE

At the time Phase II of this project was negotiated, General Mills, Inc. was requested to consider the potential external store-carrying capabilities of the AN/USD-5 Drone, before selecting the final configuration of the research prototype liquid agent disseminating store to be designed and manufactured under this contract. For this reason the design phase was not initiated at the beginning of Phase II. An alternate approach was selected, which included subcontracted studies to be conducted by North American Aviation, Inc. and Fairchild Aircraft and Missiles Division. These studies were scheduled to precede the detailed design of the research store and were planned so as to provide data necessary to determine the feasibility of designing a store which was near-optimum for use on several manned aircraft and also the AN/USD-5 Drone.

The two studies mentioned above were considered necessary since the AN/USD-5 does not currently have provisions for external stores. Modification of the wing design was considered necessary to provide this capability.

The work statements for these two studies follow:

10.1 Work Statement - Study at North American Aviation, Inc.

Complete the design requirements for a prototype external store liquid agent dissemination system. The results already obtained under this contract with General Mills, Inc. shall be used. The design requirements to be established shall apply insofar as possible to a universal store: however, detailed design shall consider installation of the store on the AN/USD-5 Drone and also the F-100D airplane, which is anticipated as a test vehicle.

DECLASSIFIED IN FULL
Authority: EO 13526
Chief, Records & Declass Div, WHS
Date: JUL 19 2013

(a) As part of this work, data shall be submitted to General Mills, Inc. for purposes of evaluating compatability with the drone. These data shall consist of preliminary aerodynamic, weight and inertia characteristics.

(b) Coordinate with General Mills, Inc., the Army Chemical Corps, and the Drone Manufacturer in establishing a mutually acceptable store configuration at General Mills, Inc. direction.

(c) Preparation of Layout Drawings. - Layout drawings of the external store shall be prepared, which shall include external geometry, definition of components (such as turbine, generator, valves, pumps, nozzle assembly and actuators), controls and control sequencing, jettison provisions, agent capacity, insulation, agitation and heating and maintenance provisions.

10.2 Work Statement - Study at Fairchild Aircraft and Missiles Division

10.2.1 Conduct a study to provide data required for selection of external store size, weight and location on the drone wing. Data shall be prepared, showing the relationship between the critical parameters. These data shall be presented as graphs, which shall include but not be limited to the following:

(a) Drone incremental structural weight versus tank and pylon total loaded weight at a minimum of three spanwise locations.

(b) Incremental drag of the installed stores versus tank capacity.

(c) Nautical Miles per pound of fuel versus external tank capacity at a selected Mach number with gross weight as a parameter.

(d) Radius of action versus external tank capacity at a minimum of three spanwise locations.

DECLASSIFIED IN FULL
Authority: EO 13526
Chief, Records & Declass Div, WHS
Date: JUL 19 2013

A brief stability and control analysis shall be made for each configuration studied. This analysis shall be held to the minimum required to insure feasibility.

10.2.2 An investigation of the overall performance of the AN/USD-5 Drone and one tank size, shape, and weight located at one wing station shall be conducted. The selection of the store and the wing location for mounting it shall be mutually agreed upon between General Mills, Inc. and Fairchild Aircraft and Missiles Division. The performance data will be presented in the form of a mission profile.

A three-view drawing of the AN/USD-5 with the selected store installation shall be prepared.

Load factors and air loads on the external store shall be provided for the selected store size, shape, weight, and wing station location.

10.2.3 Compile the information outlined below for the AN/USD-5 Drone.

(a) An investigation shall be made of the electrical power available on the AN/USD-5 (on a time sharing basis) for furnishing the required power to the external stores.

(b) A drawing of the AN/USD-5 on the launcher showing the launcher clearances shall be prepared.

10.2.4 Furnish engine exhaust temperature profiles at the flight conditions which apply to the dissemination run.

During this reporting period, the information required under item (a) of the work statement to North American Aviation, Inc. was received by General Mills, Inc. for release to Fairchild. It is anticipated that all of the effort covered by both of the work statements presented above will be completed during the next reporting period.

DECLASSIFIED IN FULL
Authority: EO 13526
Chief, Records & Declass Div, WHS
Date: JUL 19 2013

11. SUMMARY AND CONCLUSIONS

During this reporting period, Phase II of this program was initiated. This phase includes continuation of research in several areas related to solid agent dissemination (such as delivery, metering, dissemination and deagglomeration) and also includes completion of the design requirements for a liquid agent store, design of a research model and manufacture of one unit for future field experiments.

Experiments have been initiated to evaluate the effect of exposure to heated air streams on the viability of Sm aerosols. Preliminary work indicates approximately 80 percent kill of the organisms when exposed to 80°C for 1.2 seconds. Future experiments will be conducted with a more refined apparatus to obtain more detailed data (Section 2).

An experimental apparatus for the measurement of frictional forces between powder beds and channel walls has been developed. Measurements have been made with finely divided talc. It has been possible to isolate a powder characteristic which is directly proportional to the coefficient of friction. Measurements of the dynamic angle of repose for Sm powder have been made under controlled humidity conditions. Correlations with the moisture content have been obtained, which show a slight dependency on moisture content (Section 3).

Theoretical studies of load transmission in particulate materials have been advanced during this reporting period. As a result, a promising experimental technique for measurement of shear strength and compactibility characteristics of particulate materials was conceived. A triaxial shear test fixture is described and several specific cases of force transmission have been analyzed (Section 4).

DECLASSIFIED IN FULL
Authority: EO 13526
Chief, Records & Declass Div, WHS
Date: JUL 19 2013

Experiments have been conducted to further explore results from our earlier studies of force transmission in specific arrays of material. Photographs of slip-lines in these arrays illustrate the effects of packing geometry (Section 5).

The properties of slurries of two types have been investigated in considerable detail during this reporting period. These types are (1) egg slurries and (2) slurries made with Sm in a fluorochemical liquid. The work on egg slurries has yielded detailed information on specific heat of four egg slurry samples furnished by Fort Detrick. Apparatus for evaluation of the thermal conductivity of egg slurries has been developed and calibrated. The rheological behavior of Sm slurries, made with Minnesota Mining fluorochemical liquid FC-75 has been studied in detail, using a rotating coaxial cylindrical viscometer. Curves of shear rate versus shear stress have been obtained, as a function of temperature and concentration (Section 6).

Progress has been made in connection with the studies of the use of slipstream energy for deagglomeration of finely divided materials. The characteristics of a high velocity isokinetic sampling probe have been studied by disseminating finely divided talc into the wind tunnel. Studies of the effects of off-design operation of the probe show that incorrect flow rate and operation at an angle of attack cause biased sampling. Proper control of both of these factors is provided for in our system. Modifications to permit use of Sm in the wind tunnel have been designed (Section 7).

DECLASSIFIED IN FULL
Authority: EO 13526
Chief, Records & Declass Div, WHS
Date: JUL 19 2013

The influence of the effective filling density on the aerodynamic drag of a solid agent store has been analysed. Penalties in systems where the effective filling density is less than 0.20 gm/cm^3 were found to be substantial. The advantages of increasing this density above 0.40 gm/cm^3 are quite minor, and may be outweighed by other problems incurred (Section 8).

A systems study has been initiated. Mathematical models for aerosol diffusion have been reviewed and an approach for future studies outlined (Section 9).

During the reporting period, work on the liquid agent disseminator included initiation of two studies dealing with (1) completion of the design requirements and preparation of layout drawings, and (2) study of compatibility of stores designed for manned aircraft with the AN/USD-5 Drone (Section 10).

DECLASSIFIED IN FULL
Authority: EO 13526
Chief, Records & Declass Div, WHS
Date: JUL 19 2013

DEPARTMENT OF DEFENSE
WASHINGTON HEADQUARTERS SERVICES
1155 DEFENSE PENTAGON
WASHINGTON, DC 20301-1155

MEMORANDUM FOR DEFENSE TECHNICAL INFORMATION CENTER
(ATTN: WILLIAM B. BUSH)
8725 JOHN J. KINGMAN ROAD, STE 0944
FT. BELVIOR, VA 22060-6218

AUG 1 2013

SUBJECT: OSD MDR Cases 12-M-3144 through 12-M-3156

At the request of [redacted], we have conducted a Mandatory Declassification Review of the documents in the above referenced cases on the attached Compact Disc (CD) under the provisions of Executive Order 13526, section 3.5, for public release. We have declassified the documents in full. We have attached a copy of our response to the requester. If you have any questions, please contact Ms. Luz Ortiz by phone at 571-372-0478 or by e-mail at luz.ortiz@whs.mil, luz.ortiz@osd.smil.mil, or luz.ortiz@osdj.ic.gov.

Robert Storer

Robert Storer
Chief, Records and Declassification Division

Attachments:
1. MDR request w/ document list
2. OSD response letter
3. CD (U)

April 26, 2012

[redacted]

Department of Defense
Directorate for Freedom of Information and Security Review
Room 2C757
1155 Defense Pentagon
Washington, D.C. 20301-1155

Sir:

I am requesting under the Mandatory Declassification Review provisions of Executive Order 13291, copies of the following documents. I have tried several times to acquire them through DTIC, but the sites stated they are not available.

I am conducting research into the previous methods used to disseminate biological agents. Many source I use to have access to have been deleted from the internet. On numerous occasions I have been informed that formerly classified information that was declassified, have now become classified again (since 911). My attempts to locate such Executive Orders, regulations, laws, or other changes to this question have not successful nor revealed a specific source. As such I would appreciate any information you can shed on this question.

Documents requested.

AD 348405, Dissemination of Solid and Liquid BW (Biological Warfare)Agents Quarterly 12-M-3144
Progress Report Number 14, 4 Sept - 4 Dec 1963, G. R. Whitnah, February 1964, General Mills Report number 2512, General Mills, Inc., Minneapolis, MN, Contract number DA 18064 CML 2745,102pages. Prepared for U.S. Army Biological Laboratories, Fort Detrick, Maryland. Approved by S.P. Jones, Director of Aerospace Research at General Mills. Project No. 82408. General Mills Aerospace Research Division, 2295 Walnut Street, St. Paul 13,Minnesota.
AD 346751, Dissemination of Solid and Liquid BW (Biological Warfare) Agents, Quarterly 12-M-3145
Progress Report Number 12, March 4 - June 4, 1963, G. R. Whitnah, July 1963, General Mills Report number 2411, General Mills, Inc., Minneapolis, MN, Contract number DA 18064 CML 2745. 184 pages. Approved by S.P. Jones, Director of Aerospace Research at General Mills. Project No. 82408. General Mills Aerospace Research Division, 2295 Walnut Street, St. Paul 13, Minnesota.
AD 346750, Dissemination of Solid and Liquid BW (Biological Warfare) Agents, Quarterly 12-M-3146
Progress Report Number 13, 4 June - 4 Sept 1962, G.R. Whitnah, October 1963, General Mills

Report number 2451, General Mills, Inc., Minneapolis, MN, Contract Number DA 18064 CML 2745. 19 pages (?)

AD 332404, Dissemination of Solid and Liquid BW (Biological Warfare) Agents, Quarterly 12-M-3147
Progress Report Number 7, Dec. 4, 1961 - March 4, 1962, by G.R.Whitnah, February 1963, General Mills Report Number 2373, General Mills, Inc., Minneapolis, MN, Contract Number DA 18064 CML 2745. 123 pages.

AD 333298, Dissemination of Solid and Liquid BW (Biological Warfare)Agents, Quarterly 12-M-3148
Progress Report Number 9, June 4, 1962 - Sept. 4, 1962. by G.R. Whitnah, October 1962, General Mills Report Number 2344, General Mills, Inc., Minneapolis, MN, Contract Number DA 18064 CML 2745. 130 (or 150) pages.

AD 332405, Dissemination of Solid and Liquid BW (Biological Warfare) Agents, Quarterly 12-M-3149
Progress Report Number 8, Period March 4, 1962 - June 4, 1962. G.R. Whitnah, August 1962, General Mills Report Number 2322, General Mills, Inc., Minneapolis, MN, Contract Number DA 18064 CML 2745. 198 pages.

AD 329067, Dissemination of Solid and Liquid BW (Biological Warfare) Agents, Quarterly 12-M-3150
Progress Report Number Six, G.R. Whitnah, February 1962, General Mills Report Number 2264, General Mills, Inc., Minneapolis, MN, Contract Number DA 18064 CML 2745. 103 pages. Approved by S.P. Jones, Manager, Materials and Mechanics Research, General Mills Research and Development Office, 2003 East Hennepin Avenue, Minneapolis 13, Minnesota.

AD 327072, Dissemination of Solid and Liquid BW (Biological Warfare) Agents, Quarterly 12-M-3151
Progress Report Number Five, 4 June - 4 Sept 1961. by G.R.Whitnah, November 1961, General Mills Report Number 2249, General Mills, Inc., Minneapolis, MN, Contract Number DA 18064 CML 2745.

AD 325247, Dissemination of Solid and Liquid BW (Biological Warfare) Agents, Quarterly 12-M-3152
Progress Report Number 4, 4 March - 4 June 1961, by J.E. Upton for G.R. Whitnah, Project Manager. February 1963, General Mills Report Number 2216, General Mills, Inc., Minneapolis, MN, Contract Number DA 18064 CML 2745. General Mills Electronics Group, Research Dept., 2003 East Hennepin Avenue, Minneapolis 13, Minnesota. 225 pages.

AD 324746, Dissemination of Solid and Liquid BW (Biological Warfare) Agents, Progress 12-M-3153
Report 3 Juen - 3 Sept. 1960. by G.R. Whitnah, October 1960, General Mills Report Number 2125, General Mills, Inc., Minneapolis, MN, Contract Number DA 18064 CML 2745. 78 pages

AD 323599, Dissemination of Solid and Liquid BW (Biological Warfare) Agents, Quarterly 12-M-3154
Progress Report Number 2, for period 4 Sept - 4 Dec 1960, by G.R. Whitnah, February 1961, General Mills Report Number 2161, General Mills, Inc., Minneapolis, MN, Contract Number DA 18064 CML 2745. 90 pages? Mechanical Division of General Mills, Inc., Research Department, 2003 East Hennepin Avenue, Minneapolis 13, Minnesota.

AD 323598, Dissemination of Solid and Liquid BW (Biological Warfare) Agents, Quarterly 12-M-3155
Progress Report, for period 4 Dec. 1960 - 4 March 1961, by G.R. Whitnah, May 1961, General Mills Report Number 2200, General Mills, Inc., Minneapolis, MN, Contract Number DA 18064 CML 2745. 95 pages.

AD 337635, Dissemination of Solid and Liquid BW (Biological Warfare) Agents, Quarterly 12-M-3156
Progress Report No. 10, period Sept. 4, 1962 - Dec. 4, 1962. G.R. Whitnah, Project Manager, Approved by S.P. Jones, Aerospace Research, February 1963. 247 pages.

Sincerely